U.PORTO
FEUP FACULDADE DE ENGENHARIA
UNIVERSIDADE DO PORTO

FFT-based Homogenization Methods

Professor:
Francisco Manuel Andrade Pires

Student:
José Luís Passos Vila-Chã

Report presented under the scope of the
Doctoral Program in Mechanical Engineering

Porto, September 2021

Page intentionally left blank.

Contents

List of Figures

List of Tables

Page intentionally left blank.

Chapter 1

Continuum Mechanics and Finite Element Method

This chapter deals with the concepts needed to described the behavior of a solid undergoing large deformation, as well as, the conservation principles that ensure its mechanical equilibrium. It also presents a succint overview of the Finite Element Method as a tool to solve mechanical initial value equilibrium problem. These topics are broadly covered in the literature and here the approach used follows **?**,

1.1 Kinematics of Deformation

1.1.1 Motion

Let a deformable body $\mathscr{B}$ occupy an open region Ω_0 of the tridimensional Euclidean space $\mathscr{E}$ with a regular boundary $\partial\Omega_0$ in its reference configuration. Its motion, depicted in Figure **??**, is defined by a smooth one-to-one function

$$\boldsymbol{\varphi}\colon \Omega \times \mathscr{R} \to \mathscr{E}, \tag{1.1}$$

mapping each material particle of coordinates $\boldsymbol{X}$ in the reference configuration to its position $\boldsymbol{x}$ in the deformed configuration, for a given instant of time t, as

$$\boldsymbol{x} = \boldsymbol{\varphi}(\boldsymbol{X}, t) = \boldsymbol{\varphi}_t(\boldsymbol{X}). \tag{1.2}$$

Thus, the displacement field is defined as

$$\boldsymbol{u}(\boldsymbol{X}, t) = \boldsymbol{\varphi}(\boldsymbol{X}, t) - \boldsymbol{X}, \tag{1.3}$$

and, since the function that defines the motion is one-to-one, the reference configuration can be recovered as

$$\boldsymbol{X} = \boldsymbol{\varphi}^{-1}(\boldsymbol{x}, t) = \boldsymbol{x} - \boldsymbol{u}(\boldsymbol{\varphi}^{-1}(\boldsymbol{x}, t), t), \tag{1.4}$$

where $\boldsymbol{\varphi}^{-1}$ is the reference mapping function.

1.1.2 Material and spatial descriptions

Dealing with finite deformations, the behavior of the body under analysis can be described with respect to the reference configuration, using the so-called material or Lagrangian description, or to the deformed configuration, using the so-called spatial or Eulerian description.

In the Lagrangian description any field, be it scalar, vectorial or tensorial defined over the body is expressed as a function of the reference configuration, $\boldsymbol{X} \in \Omega_0$. On the other hand, the Eulerian descritpion of same field is done using the deformed configuration, $\boldsymbol{x} \in \Omega$.

As such let $\alpha(\boldsymbol{x}, t)$ be a spatial field and $\beta(\boldsymbol{X}, t)$ a material field. Their material α_m and spatial β_s desctiptions are given by

$$\alpha_m(\boldsymbol{X}, t) = \alpha(\boldsymbol{\varphi}(\boldsymbol{X}, t), t), \tag{1.5}$$

$$\beta_s(\boldsymbol{x}, t) = \beta(\boldsymbol{\varphi}^{-1}(\boldsymbol{x}, t), t), \tag{1.6}$$

noting that any field associated with a motion of $\mathscr{B}$ can be expressed as a function of time and material or spatial position.

The same distinction between material and spatial descriptions applies to operators such as the divergence and the gradient. The spatial and material gradients, ∇ and ∇_0, respectively, are defined as

$$\nabla\alpha = \frac{\partial}{\partial \boldsymbol{x}}\alpha(\boldsymbol{x}, t), \quad \nabla_0\beta = \frac{\partial}{\partial \boldsymbol{X}}\beta(\boldsymbol{X}, t), \tag{1.7}$$

where the derivatives are taken with respect to the spatial and reference configuration accordingly.

1.1.3 Deformation gradient

The deformation gradient, a second order tensor denoted by $\boldsymbol{F}$, is defined as

$$\boldsymbol{F}(\boldsymbol{X}, t) \equiv \nabla_0\boldsymbol{\varphi}(\boldsymbol{X}, t) = \frac{\partial \boldsymbol{x}}{\partial \boldsymbol{X}}, \tag{1.8}$$

or, taking into account that

$$\boldsymbol{x} = \boldsymbol{X} + \boldsymbol{u}(\boldsymbol{X}, t), \tag{1.9}$$

it can be expressed as

$$\boldsymbol{F}(\boldsymbol{X}, t) = \boldsymbol{I} + \nabla_0\boldsymbol{u}. \tag{1.10}$$

The deformation gradient relates the relative position between two neighboring material particles before and after deformation. To see this let $\boldsymbol{X}$ be the coordinates of some material prickle in the reference configuration and $\boldsymbol{X} + d\boldsymbol{X}$ the coordinates of some material particle in its neighborhood, their corresponding coordinates in the deformed configuration are given by

$$\boldsymbol{X} = \boldsymbol{x} - \boldsymbol{u}(\boldsymbol{X}, t), \tag{1.11}$$

$$\boldsymbol{X} + d\boldsymbol{X} = \boldsymbol{x} + d\boldsymbol{x} - \boldsymbol{u}(\boldsymbol{X} + d\boldsymbol{X}, t). \tag{1.12}$$

Subtracting Equation (1.11) to Equation (1.12), it is found that

$$d\boldsymbol{X} = d\boldsymbol{x} + \boldsymbol{u}(\boldsymbol{X}, t) - \boldsymbol{u}(\boldsymbol{X} + d\boldsymbol{X}, t) \tag{1.13}$$
$$= (\boldsymbol{I} + \nabla_0 \boldsymbol{u}(\boldsymbol{X}, t))\, d\boldsymbol{x} \tag{1.14}$$
$$= \boldsymbol{F}\, d\boldsymbol{x}. \tag{1.15}$$

Due to this relation, it can be shown that the determinat of the deformation gradient has a physical meaning. It is the local unit volume change, that is,

$$J \equiv \det \boldsymbol{F} = \frac{dv}{dv_0}, \tag{1.16}$$

where dv_0 is an infinitesimal volume of the body in its reference configuration and dv the infinitesimal volume after deformation.

Isochoric/Volumetric decomposition

Any deformation can be locally decomposed in volumetric and isochoric (or distortional) components. From Equation (1.16) it can be gathered that an isochoric deformation is characterized by $J = 1$. As such, the deformation gradient can be decomposed as

$$\boldsymbol{F} = \boldsymbol{F}_{\text{iso}} \boldsymbol{F}_{\text{vol}} = \boldsymbol{F}_{\text{vol}} \boldsymbol{F}_{\text{iso}}, \tag{1.17}$$

where the isochoric and columetric components are defined by

$$\boldsymbol{F}_{\text{iso}} = (\det \boldsymbol{F})^{-\frac{1}{3}}, \quad \boldsymbol{F}_{\text{vol}} = (\det \boldsymbol{F})^{\frac{1}{3}} \boldsymbol{I}. \tag{1.18}$$

Polar decomposition

The deformation gradient can also be decomposed in rotation and stretch components, the so-called polar decomposition, defined as

$$\boldsymbol{F} = \boldsymbol{R}\boldsymbol{U} = \boldsymbol{V}\boldsymbol{R}, \tag{1.19}$$

where $\boldsymbol{R}$ is the proper orthogonal rotation tensor and $\boldsymbol{U}$ and $\boldsymbol{V}$ are the symmetric positive right and left stretch tensors, respectively.

Equation (1.19) has a physical interpretation with the right polar decomposition ($\boldsymbol{F} = \boldsymbol{R}\boldsymbol{U}$) corresponding to a stretch mapping followed by a rotation, and the left polar decomposition ($\boldsymbol{F} = \boldsymbol{V}\boldsymbol{R}$) corresponding to a rotation followed by a stretch mapping. The right $\boldsymbol{U}$ and left $\boldsymbol{V}$ stretch tensors are related through the rotation matrix $\boldsymbol{R}$ as

$$\boldsymbol{V} = \boldsymbol{R}\boldsymbol{U}\boldsymbol{R}^T, \tag{1.20}$$

and can be obtained from deformation gradient by

$$\boldsymbol{C} \equiv \boldsymbol{U}^2 = \boldsymbol{F}^T\boldsymbol{F}, \quad \boldsymbol{B} \equiv \boldsymbol{V}^2 = \boldsymbol{F}\boldsymbol{F}^T., \tag{1.21}$$

where $\boldsymbol{C}$ and $\boldsymbol{B}$ are the right and left Cauchy-Green strain tensors.

Since $\boldsymbol{U}$ and $\boldsymbol{V}$ are symmetric tensors, they admit the spectral decomposition

$$\boldsymbol{U} = \sum_{i=1}^{3} \lambda_i \boldsymbol{E}_i^* \otimes \boldsymbol{E}_i^*, \quad \boldsymbol{V} = \sum_{i=1}^{3} \lambda_i \boldsymbol{e}_i^* \otimes \boldsymbol{e}_i^*, \tag{1.22}$$

where λ_i, $i = 1,2,3$, are the eigenvalues of both $\boldsymbol{U}$ and $\boldsymbol{V}$ and $\boldsymbol{E}_i^*$ and $\boldsymbol{e}_i^*$ are the respective eigenvectors.

The eigenvectors of left $\boldsymbol{V}$ and right $\boldsymbol{U}$ stretch tensors are related through

$$\boldsymbol{e}_i^* = \boldsymbol{R}\boldsymbol{E}_i^*. \tag{1.23}$$

forming two orthogonal bases. These vectors define the Lagrangian and Eulerian principal directions, respectively, allowing for the expression of the local stretching from a material particle, associated with any deformation, as a superposition of stretches along the three mutual orthogonal directions.,

1.2 Strain tensors

In Continuum Mechanics there are two main families of strain tensors derived from the deformation gradient and used to describe the body deformation. The Lagrange family strain tensors are defined as

$$\boldsymbol{E}^{(m)} = \begin{cases} \dfrac{1}{m}(\boldsymbol{U}^m - \boldsymbol{I}), & m \neq 0, \\ \ln(\boldsymbol{U}), & m = 0, \end{cases} \tag{1.24}$$

where m is a real number, and likewise, the Euler family strain tensors are defined as

$$\boldsymbol{\varepsilon}^{(m)} = \begin{cases} \dfrac{1}{m}(\boldsymbol{V}^m - \boldsymbol{I}), & m \neq 0, \\ \ln(\boldsymbol{V}), & m = 0, \end{cases} \tag{1.25}$$

where m is also real number.

In particular, choosing $m = 0$, one obtains the so-called material and spatial logarithmic strain tensors

$$\boldsymbol{E}^{(0)} \equiv \ln[\boldsymbol{U}] = \sum_{i=1}^{3} \ln\lambda_i \boldsymbol{E}_i^* \otimes \boldsymbol{E}_i^*, \tag{1.26}$$

$$\boldsymbol{e}^{(0)} \equiv \ln[\boldsymbol{V}] = \sum_{i=1}^{3} \ln\lambda_i \boldsymbol{e}_i^* \otimes \boldsymbol{e}_i^*. \tag{1.27}$$

1.3 Forces and stress measures

The deformation of a body is intrinsically related to the forces acting on it. These forces can be divided in two classes, from a purely mechanical point of view: volume (or body) forces, proportional to the mass contained in a volume element, as such measured in force per unit volume, and surface forces, acting on the surface of a volume element, measured as force per unit area. Related to the latter is the concept of stress, that can be described mathematically by second order tensors with different definitions.

Cauchy stress tensor

According to Cauchy's theorem the relation between the so-called Cauchy stress vector, $\boldsymbol{t}(\boldsymbol{x},\boldsymbol{n})$, and the unitary outward vector normal to the deformed surface under analysis, $\boldsymbol{n}$, is linear and given by

$$\boldsymbol{t}(\boldsymbol{x},\boldsymbol{n}) \equiv \boldsymbol{\sigma}(\boldsymbol{x})\boldsymbol{n}, \tag{1.28}$$

where $\boldsymbol{\sigma}$ is the second order Cauchy stress tensor.

The Cauchy stress vector is naturally associated with the deformed configured and thus, expressed in a spatial description and measured in force per unit deformed area. It must also be noted that as a consequence of the balance of angular momentum, the Cauchy stress tensor is symmetric.

First Piola-Kirchhoff stress tensor

The First Piola-Kirchhoff stress tensor, $\boldsymbol{P}$, can be regarded as the material counterpart of the Cauchy stress tensor, as it establishes a linear dependence between the stress vector $\boldsymbol{t}_0(\boldsymbol{X},\boldsymbol{m})$, measured in force per unit reference area, and the unitary outward vector normal to the undeformed surface under analysis, $\boldsymbol{m}$,

$$\boldsymbol{t}_0 = \boldsymbol{P}\boldsymbol{m}, \tag{1.29}$$

which must related to the Cauchy stress vector by

$$\boldsymbol{t}_0 = \frac{\mathrm{d}a}{\mathrm{d}a_0}\boldsymbol{t} = \frac{\mathrm{d}a}{\mathrm{d}a_0}\boldsymbol{\sigma}\boldsymbol{n}, \tag{1.30}$$

where $\mathrm{d}a$ is the infinitesimal deformed area normal to the unitary vector $\boldsymbol{n}$ and $\mathrm{d}a_0$ the corresponding undeformed are normal to $\boldsymbol{m}$. It can be shown that the relation between da and da_0 is

$$\frac{da}{da_0}\boldsymbol{n} = J\boldsymbol{F}^{-T}\boldsymbol{m}, \tag{1.31}$$

and substituting on the equation above motivates the following definition

$$\boldsymbol{P} \equiv J\boldsymbol{\sigma}\boldsymbol{F}^{-T}, \tag{1.32}$$

where J is the determinant of the deformation gradient $\boldsymbol{F}$ and $\boldsymbol{\sigma}$ is the Cauchy stress tensor. From Equation (1.32), one gathers that, in general, the First Piola-Kirchhoff stress tensor is not symmetric.

Kirchhoff stress tensor

The Kirchhoff stress tensor, $\boldsymbol{\tau}$, is a widely used symmetric tensor, defined as

$$\boldsymbol{\tau} \equiv J\boldsymbol{\sigma}. \tag{1.33}$$

Deviatoric/Hydrostatic decomposition

The Cauchy stress tensor, $\boldsymbol{\sigma}$, can split as

$$\boldsymbol{\sigma} = \boldsymbol{\sigma}_d - p\boldsymbol{I}, \tag{1.34}$$

where p is the hydrostatic pressure defined as

$$p \equiv -\frac{1}{3}\text{tr}\,[\boldsymbol{\sigma}], \tag{1.35}$$

and $\boldsymbol{\sigma}_d$ is the deviatoric stress defined as

$$\sigma_d \equiv \boldsymbol{\sigma} - p\boldsymbol{I}. \tag{1.36}$$

1.4 Heat

Changes in temperature of a body are very often related to heat flowing inside, entering or leaving it. In continuum mechanics, heat is measured in power per unit surface.

Heat flux vector

According to Cauchy's theorem the relation between the heat flux across a surface, $h(\boldsymbol{x}, \boldsymbol{n})$, and the unitary outward normal to the deformed surface under analysis, $\boldsymbol{n}$, is linear and given by

$$h(\boldsymbol{x}, \boldsymbol{n}) = -\boldsymbol{q}(\boldsymbol{x}) \cdot \boldsymbol{n}. \tag{1.37}$$

where $\boldsymbol{q}$ is the heat flux vector.

1.5 Fundamental conservation principles

In Continuum Mechanics. there is a set of conservation principles and thermodynamic laws, that irrespective of the quantities used to describe the mechanical behavior of a body undergoing large deformations must always be satisfied.

1.5.1 Principle of mass conservation

The principle of mass conservation can be stated as

$$\dot{\rho} + \rho\,\text{div}\,\dot{\boldsymbol{u}} = 0, \tag{1.38}$$

where ρ is the material density measured in mass per unit deformed volume.

1.5.2 Principle of linear momentum conservation

The principle of linear momentum conservation can be stated in both material and spatial description. In a spatial description it reads

$$\begin{cases} \operatorname{div}\boldsymbol{\sigma} + \boldsymbol{b} = \rho\ddot{\boldsymbol{u}}, & \forall \boldsymbol{x} \in \Omega, \\ \\ \boldsymbol{t} = \boldsymbol{\sigma}\boldsymbol{n}, & \forall \boldsymbol{x} \in \partial\Omega, \end{cases} \tag{1.39}$$

where $\boldsymbol{b}$ is the body forces field measured as per unit deformed volume.

One can also write the principle of linear momentum conservation in material coordinates, as

$$\begin{cases} \operatorname{div}_0 \boldsymbol{P} + \boldsymbol{b}_0 = \rho_0\ddot{\boldsymbol{u}}, & \forall \boldsymbol{X} \in \Omega_0, \\ \\ \boldsymbol{t}_0 = \boldsymbol{P}\boldsymbol{m}, & \forall \boldsymbol{X} \in \partial\Omega_0, \end{cases} \tag{1.40}$$

where $\boldsymbol{b}_0$ is the body forces field, measured in force per unit undeformed volume, and ρ_0 is the material density, measured in mass per unit undeformed volume. Both these quantities can be found from their spatial counterparts as

$$\boldsymbol{b}_0 = J\boldsymbol{b}, \quad \rho_0 = J\rho. \tag{1.41}$$

Take notice of the abuse of language regarding functions defined on the referece configuration Ω_0 and on the deformed configuration Ω. The same symbol, f, is used for a function f defined on Ω and the function $f \circ \boldsymbol{\varphi}$ defined on Ω_0.

Equations (1.39) and (1.40) are the so-called strong, point-wise or local equilibrium equations, as they enforce the mechanical equilibrium at every material particle of the body.

1.5.3 First principle of thermodynamics

Let e be the internal energy per unit mass, r the heat supply per unit mass and $\boldsymbol{q}$ the heat flux, then the first principle of thermodynamics pertaining to the balance of energy can be written in the spatial description as

$$\begin{cases} \rho\dot{e} = \boldsymbol{\sigma} : \boldsymbol{D} + \rho r - \operatorname{div}\boldsymbol{q}, & \forall \boldsymbol{x} \in \Omega, \\ \boldsymbol{t} = \boldsymbol{\sigma}\boldsymbol{n}, & \forall \boldsymbol{x} \in \partial\Omega, \\ h = \boldsymbol{q} \cdot \boldsymbol{n}, & \forall \boldsymbol{x} \in \partial\Omega. \end{cases} \tag{1.42}$$

The second order tensor $\boldsymbol{D}$ denotes a strain rate measure, such that the double contraction $\boldsymbol{\sigma} : \boldsymbol{D}$ represents the stress power per unit volume in the deformed configuration of body. In material coordinates, it reads

$$\begin{cases} \rho_0\dot{e} = \boldsymbol{P} : \dot{\boldsymbol{F}} + \rho_0 r - \operatorname{div}_0 \boldsymbol{q}_0, & \forall \boldsymbol{X} \in \Omega_0, \\ \boldsymbol{t}_0 = \boldsymbol{P}\boldsymbol{m}, & \forall \boldsymbol{X} \in \partial\Omega_0, \\ h_0 = \boldsymbol{q}_0 \cdot \boldsymbol{m}, & \forall \boldsymbol{X} \in \partial\Omega_0, \end{cases} \tag{1.43}$$

where $\boldsymbol{q}_0$ is the Piola transformation of $\boldsymbol{q}$, i.e.,

$$\boldsymbol{q}_0 = J\boldsymbol{F}^{-T}\boldsymbol{q}, \tag{1.44}$$

and

$$h_0 = Jh. \tag{1.45}$$

1.5.4 Second principle of thermodynamics

The local entropy balance can written as

$$\rho \dot{s} = -\operatorname{div}\left[\frac{\boldsymbol{q}}{\theta}\right] + \frac{\rho r}{\theta} + \hat{s}, \tag{1.46}$$

where $\hat{s}$ is the entropy production. The second principle of thermodynamics postulates that the changes in the entropy in the universe can never be negative, which is mathematically expressed by

$$\hat{s} \geq 0, \tag{1.47}$$

yielding

$$\rho \dot{s} + \operatorname{div}\left[\frac{\boldsymbol{q}}{\theta}\right] - \frac{\rho r}{\theta} \geq 0, \tag{1.48}$$

where θ and s are the temperature and specific entropy fields respectively. In a material description, it reads

$$\rho_0 \dot{s} + \operatorname{div}_0\left[\frac{\boldsymbol{q}_0}{\theta}\right] - \frac{\rho_0 r}{\theta} \geq 0. \tag{1.49}$$

1.5.5 Clausius-Duhem inequality

Combining the first and second thermodynamic principles yields

$$\rho \dot{s} + \operatorname{div}\left[\frac{\boldsymbol{q}}{\theta}\right] - \frac{1}{\theta}(\rho \dot{e} - \boldsymbol{\sigma} : \boldsymbol{D} + \operatorname{div} \boldsymbol{q}) \geq 0, \tag{1.50}$$

From the definition of the specific Helmholtz free energy

$$\psi \equiv e - \theta s, \tag{1.51}$$

and defining the temperature field gradient as $\boldsymbol{g} = \nabla\theta$, it is possible to establish the so-called Clausius-Duhem inequality in the spatial description as

$$\underbrace{\boldsymbol{\sigma} : \boldsymbol{D} - \rho\left(\dot{\psi} + s\dot{\theta}\right)}_{\mathcal{D}_{\text{mech}}} \underbrace{- \frac{1}{\theta}\boldsymbol{q} \cdot \boldsymbol{g}}_{\mathcal{D}_{\text{cond}}} \geq 0, \tag{1.52}$$

where the identity

$$\operatorname{div}\left[\frac{\boldsymbol{q}}{\theta}\right] = \frac{1}{\theta}\operatorname{div} \boldsymbol{q} - \frac{1}{\theta^2}\boldsymbol{q} \cdot \nabla\theta. \tag{1.53}$$

is used.

From a physical point of view, the Clausius-Duhem inequality states that the energy dissipation per unit deformed volume is always non-negative. Moreover the terms in the inequalitiy can be splited between the mechanical internal dissipation $\mathcal{D}_{\text{mech}}$ and the dissipation due to heat conduction $\mathcal{D}_{\text{cond}}$. From

$$\hat{s} = \boldsymbol{\sigma} : \boldsymbol{D} - \rho\left(\dot{\psi} + s\dot{\theta}\right) - \frac{1}{\theta}\boldsymbol{q} \cdot \boldsymbol{g}, \tag{1.54}$$

assuming that the process leads to an uniform temperature distribution, yields for the mechanical dissipation $\mathcal{D}_{\text{mech}}$,

$$\mathcal{D}_{\text{mech}} = \hat{s}|_{\theta \text{ uniform}} = \boldsymbol{\sigma} : \boldsymbol{D} - \rho\left(\dot{\psi} + s\dot{\theta}\right), \tag{1.55}$$

since conduction is excluded and only mechanical and temperature transient effects remain. If on the other hand, only conduction effects are retained, i.e., assuming the process to be isothermic, isochoric and isovolumetric, the dissipation due to conduction, $\mathcal{D}_{\text{cond}}$, is obtained as

$$\mathcal{D}_{\text{cond}} = -\frac{1}{\theta}\boldsymbol{q}\cdot\boldsymbol{g}. \tag{1.56}$$

Equation (1.52) can also be written as

$$\boldsymbol{P}:\dot{\boldsymbol{F}} - \rho_0(\dot{\psi} + s\dot{\theta}) - \frac{1}{\theta}\boldsymbol{q}_0\cdot\boldsymbol{g}_0 \geq 0, \tag{1.57}$$

where $\boldsymbol{g}_0 = \nabla_0\theta$, aplying the Piola transformation, and as

$$\boldsymbol{\tau} : \boldsymbol{D} - \rho_0\left(\dot{\psi} + s\dot{\theta}\right) - \frac{J}{\theta}\boldsymbol{q}\cdot\boldsymbol{g} \geq 0, \tag{1.58}$$

multiplying it by J and attending to the definition of the Kirchhoff stress tensor, where the left hand side represents now the energy dissipation per unit reference volume.

1.6 Mechanical constitutive initial value problem

In Continuum Mechanics, a constitutive model is a set of equations, also called constitutive equations, establishing the stress-strain relation for some material. Before going further, it is important to define a thermokinetic process of a body $\mathscr{B}$ as

$$\text{thermokinetic process:} \quad \{\boldsymbol{\varphi}(\boldsymbol{X},t), \theta(\boldsymbol{X},t)\}, \tag{1.59}$$

ans a calordynamic process of $\mathscr{B}$ as

$$\text{calorodynamic process:} \quad \{\boldsymbol{\sigma}(\boldsymbol{X},t), e(\boldsymbol{X},t), s(\boldsymbol{X},t), r(\boldsymbol{X},t), \boldsymbol{b}(\boldsymbol{X},t), \boldsymbol{q}(\boldsymbol{X},t)\}, \tag{1.60}$$

which satisfies the fundamental conservation principles previously introduced.

It is also important to note that any constitutive model must satisfy a set of constitutive axioms, explained in detail by **?**. As these are too general to be used directly in practice, a particular case of the general history functional-based constitutive theory based on the thermodynamics with internal variables approach is used.

1.6.1 Thermodynamics with internal variables

The values of $\boldsymbol{\sigma}$, ψ, s and $\boldsymbol{q}$ at a material particle define its thermodynamic state, assuming $\boldsymbol{b}$ follows from the balance of linear momentum and r from the energy

balance equation. In thermodynamics with interval variables approach, that thermodynamic state is assumed to be completely defined by the instantaneous values of a finite number of state variables

$$\{\boldsymbol{F}, \theta, \boldsymbol{g}, \boldsymbol{\alpha}\}. \tag{1.61}$$

at a given instant of the calorodynamic process, where

$$\boldsymbol{\alpha} = \{\alpha_k\} \tag{1.62}$$

is a set of internal variables, scalar or tensorial in nature, associated with dissipative mechanisms. As such, the accuracy of the constitutive model depends strongly on the appropriate choice of internal variables, as these contain the relevant information about the thermodynamical history of the material.

Accordingly, the specific Helmholtz free energy is postulated to follow

$$\psi = \psi(\boldsymbol{F}, \theta, \boldsymbol{\alpha}). \tag{1.63}$$

To find the constitutive equations for the stress tensor and the entropy, one can substitute

$$\dot{\psi} = \frac{\partial \psi}{\partial \boldsymbol{F}} : \dot{\boldsymbol{F}} + \frac{\partial \psi}{\partial \theta}\dot{\theta} + \frac{\partial \psi}{\partial \alpha_k}\dot{\alpha}_k, \tag{1.64}$$

found from the chain rule, on the Clausius-Duhem equation, Equation (1.52), obtaining

$$\left(\boldsymbol{\sigma}\boldsymbol{F}^{-T} - \rho\frac{\partial \psi}{\partial \boldsymbol{F}}\right) : \dot{\boldsymbol{F}} - \rho\left(s + \frac{\partial \psi}{\partial \theta}\right)\dot{\theta} - \rho\frac{\partial \psi}{\partial \alpha_k}\dot{\alpha}_k - \frac{1}{\theta}\boldsymbol{q}\cdot\boldsymbol{g} \geq 0, \tag{1.65}$$

where the velocity gradient was adopted to set the work conjugacy as

$$\boldsymbol{\sigma} : \boldsymbol{D} = \boldsymbol{\sigma} : \boldsymbol{L} = \boldsymbol{\sigma} : \dot{\boldsymbol{F}}\boldsymbol{F}^{-1} = \boldsymbol{\sigma}\boldsymbol{F}^{-T} : \boldsymbol{F}. \tag{1.66}$$

Since the Clausius-Duhem inequality must hold for any thermokinetic process and so remain valid for any set $\{\dot{\boldsymbol{F}}(t), \dot{\theta}(t)\}$, the Cauchy stress and entropy constitutive equations must be

$$\boldsymbol{\sigma} = \rho\frac{\partial \psi}{\partial \boldsymbol{F}}\boldsymbol{F}^T, \tag{1.67}$$

$$s = -\frac{\partial \psi}{\partial \theta}. \tag{1.68}$$

It is also possible to write the constitutive equations for the Kirchhoff stress tensor as

$$\boldsymbol{\tau} = J\rho\frac{\partial \psi}{\partial \boldsymbol{F}}\boldsymbol{F}^T, \tag{1.69}$$

multiplying Equation (1.67) by J, and the first Piola-Kirchhoff stress tensor as

$$\boldsymbol{P} = \rho_0\frac{\partial \psi}{\partial \boldsymbol{F}} \tag{1.70}$$

multiplying Equation (1.65) also by J.

For each internal variable α_k of the set α of internal variables, the conjugate thermodynamical forces are defined to be

$$A_k \equiv \rho_0 \frac{\partial \psi}{\partial \alpha_k}, \tag{1.71}$$

so that the Clausius-Duhem equation can be written in a reduced form as

$$-\boldsymbol{A} * \dot{\boldsymbol{\alpha}} - \frac{J}{\theta} \boldsymbol{q} \cdot \boldsymbol{g} \geq 0, \tag{1.72}$$

where $\boldsymbol{A}$ is the set of conjugate thermodynamical forces and $*$ denotes the appropriate product operation.

To completely define the constitutive model, one still needs to postulate the constitutive equations for the flux variables $\dot{\boldsymbol{\alpha}}$ and $\frac{1}{\theta}\boldsymbol{q}$. These are given by

$$\dot{\boldsymbol{\alpha}} = f(\boldsymbol{F}, \theta, \boldsymbol{g}, \boldsymbol{\alpha}), \tag{1.73}$$

$$\frac{1}{\theta}\boldsymbol{q} = g(\boldsymbol{F}, \theta, \boldsymbol{g}, \boldsymbol{\alpha}). \tag{1.74}$$

A sufficient condition for the previous constitutive functions to satisfy the Clausius-Duhem inequality is the hypothesis of normal dissipativity, whereby one defines the constitutive functions for the flux variables as

$$\dot{\alpha}_k = -\frac{\partial \Xi}{\partial A_k}, \quad \frac{1}{\theta}\boldsymbol{q} = -\frac{\partial \Xi}{\partial \boldsymbol{g}}, \tag{1.75}$$

where the dissipation potential is

$$\Xi = \Xi(\boldsymbol{A}, \boldsymbol{g}; \boldsymbol{F}, \theta, \boldsymbol{\alpha}), \tag{1.76}$$

a convex function with respect to each A_k and $\boldsymbol{g}$, and zero valued at the origin, $\{\boldsymbol{A}, \boldsymbol{g}\} = \{\boldsymbol{0}, \boldsymbol{0}\}$. Note that in the previous definition the state variables appear only as parameters.

Chapter 2

Mechanical problem

In the following chapter, the general framework presented in the previous chapter is applied to a purely mechanical analysis, neglecting the thermal terms.

2.0.1 Mechanical constitutive initial value problem

In the purely mechanical case, with all the quantities related to the thermal domain removed, a constitutive model based on internal variables is established by the following set of equations

$$\boldsymbol{P} = \rho_0 \frac{\partial \psi}{\partial \boldsymbol{F}}, \tag{2.1}$$

$$\psi = \psi(\boldsymbol{F}, \boldsymbol{\alpha}), \tag{2.2}$$

$$\dot{\boldsymbol{\alpha}} = f(\boldsymbol{F}, \boldsymbol{\alpha}). \tag{2.3}$$

Thus, the spatial mechanical constitutive initial value problem can be stated as follows

Problem 2.1 | Spatial mechanical constitutive initial value problem.

Given the initial values of the internal variables, $\boldsymbol{\alpha}(t_0)$, and the history of the deformation gradient

$$\boldsymbol{F}(t), \quad t \in [t_0, t_{\text{end}}], \tag{2.4}$$

find the functions for $\boldsymbol{\sigma}(t)$ and $\boldsymbol{\alpha}(t)$ such that the constitutive equations

$$\boldsymbol{\sigma} = \rho \frac{\partial \psi}{\partial \boldsymbol{F}} \boldsymbol{F}^T, \tag{2.5}$$

$$\psi = \psi(\boldsymbol{F}, \boldsymbol{\alpha}), \tag{2.6}$$

$$\dot{\boldsymbol{\alpha}} = f(\boldsymbol{F}, \boldsymbol{\alpha}). \tag{2.7}$$

are satisfied for every $t \in [t_0, t_{\text{end}}]$.

Likewise, in a material description it can be stated as

Problem 2.2 | Material mechanical constitutive intial value problem.

Given the initial values of the internal variables, $\boldsymbol{\alpha}(t_0)$, and the history of the deformation gradient

$$\boldsymbol{F}(t), \quad t \in [t_0, t_{\text{end}}], \tag{2.8}$$

find the functions for $\boldsymbol{P}(t)$ and $\boldsymbol{\alpha}(t)$ such that the constitutive equations

$$\boldsymbol{P} = \rho_0 \frac{\partial \psi}{\partial \boldsymbol{F}}, \tag{2.9}$$

$$\psi = \psi(\boldsymbol{F}, \boldsymbol{\alpha}), \tag{2.10}$$

$$\dot{\boldsymbol{\alpha}} = f(\boldsymbol{F}, \boldsymbol{\alpha}). \tag{2.11}$$

are satisfied for every $t \in [t_0, t_{\text{end}}]$.

2.0.2 Weak equilibrium. The principle of virtual work

The strong equations that enforce the equilirium of a body can be writen using the spatial description as

$$\rho \ddot{\boldsymbol{u}} = \operatorname{div} \boldsymbol{\sigma} + \boldsymbol{b} \quad \text{in } \Omega, \tag{2.12}$$

and the material description as

$$\rho_0 \ddot{\boldsymbol{u}} = \operatorname{div}_0 \boldsymbol{P} + \boldsymbol{b}_0 \quad \text{in } \Omega_0. \tag{2.13}$$

From a practical standpoint, finding the exact solution to the strong equilibrium equations in the context of real engineering problems is most often nearly or entirely impossible. Most numerical methods obtain only approximate solutions to the so-called weak equilibrium equations to circumvent this problem. These result from relaxing the strong equilibrium equations so that the solutions need only satisfy the equilibrium equations in an average sense instead of satisfying them pointwise. This is achieved through an integration over the body volume. The weak equilibrium equations can be found making use of several energetic and weighted residual methods, such as the Virtual Work Principle used here.

Problem 2.3 | Principle of virtual work (spatial version).

The Virtual Work Principle states, in a spatial description, that the body is in equilibrium if and only if the Cauchy stress field satisfies

$$\int_\Omega [\boldsymbol{\sigma} : \nabla \boldsymbol{\eta} - (\boldsymbol{b} - \rho \ddot{\boldsymbol{u}}) \cdot \boldsymbol{\eta}] \, \mathrm{d}v - \int_{\partial\Omega} \boldsymbol{t} \cdot \boldsymbol{\eta} \, \mathrm{d}a = 0, \quad \forall \boldsymbol{\eta} \in \mathscr{V}_u, \tag{2.14}$$

where $\mathscr{V}_u$ is the space of virtual displacement of the body, defined by the space of sufficiently regular arbitrary displacements

$$\boldsymbol{\eta} \colon \Omega \to \mathscr{U} \tag{2.15}$$

where $\mathscr{U}$ is the n-dimension vector associated with $\mathscr{E}$.

The principle of virtual work can be expressed in a completly equivalent way using a material description.

Problem 2.4 | Principle of virtual work (material version).

The Virtual Work Principle states, in a material description, that the body is in equilibrium if and only if the First Piola-Kirchhoff stress field satisfies

$$\int_{\Omega_0} [\boldsymbol{P} : \nabla_0 \boldsymbol{\eta} - (\boldsymbol{b}_0 - \rho_0 \ddot{\boldsymbol{u}}) \cdot \boldsymbol{\eta}] \, \mathrm{d}v - \int_{\partial\Omega_0} \boldsymbol{t}_0 \cdot \boldsymbol{\eta} \, \mathrm{d}da = 0, \quad \forall \boldsymbol{\eta} \in \mathscr{V}_{u,0}, \tag{2.16}$$

where $\mathscr{V}_{u,0}$ is the space of virtual displacement of the body, defined by the space of sufficiently regular arbitrary displacements

$$\boldsymbol{\eta} : \Omega_0 \to \mathscr{U}. \tag{2.17}$$

2.0.3 Mechanical constitutive initial boundary value problem

It is now possible to pose the mechanical constitutive initial value problem in its weak form. Assume that a body $\mathscr{B}$ is made from a generic material, characterized by a given constitutive model, whose internal variables are known at the initial time, as presented in Figure **??**. In addition, it is assumed that the interior of the body was subjected to a prescribed history of body forces, $\boldsymbol{b}(\boldsymbol{X}, t)$, $t \in [t_0, t_{\text{end}}]$, and to the following boundary conditions:

- **Natural (or Neumann) boundary condition:** The boundary portion $\Omega_{\text{traction, 0}}$ of $\mathscr{B}$ is subjected to a prescribed history of traction forces, $\boldsymbol{t}_{\text{presc}}(\boldsymbol{X}, t)$, $\boldsymbol{X} \in \partial\Omega_{\text{traction,0}}$, $t \in [t_0, t_{\text{end}}]$,

- **Essential (or Dirichlet) boundary condition:** The boundary portion $\Omega_{\text{motion, 0}}$ of $\mathscr{B}$ is subjected to a prescribed displacement field history, $\boldsymbol{u}_{\text{presc}}(\boldsymbol{X}, t)$, such that

$$\boldsymbol{\varphi}(\boldsymbol{X}, t) = \boldsymbol{X} + \boldsymbol{u}_{\text{presc}}(\boldsymbol{X}, t), \quad \boldsymbol{X} \in \partial\Omega_{\text{motion, 0}}, \quad t \in [t_0, t_{\text{end}}].$$

It is also convenient to define the set of kinematically admissible displacements of $\mathscr{B}$ as the set of all sufficiently regular displacement functions tha satisfy the essential boundary condition (**?**),

$$\mathscr{K}_u \equiv \{\boldsymbol{u} : \Omega_0 \times \mathscr{R} \to \mathscr{U} \mid \boldsymbol{u}(\boldsymbol{X}, t) = \boldsymbol{u}_{\text{presc}}(\boldsymbol{X}, t), \quad \boldsymbol{X} \in \partial\Omega_{\text{motion,0}}, \quad t \in [t_0, t_{\text{end}}]\}. \tag{2.18}$$

So the weak form of the quasi-static mechanical constitutive initial boundary value problem can be stated in a spatial description as follows

Problem 2.5 | Spatial mechanical initial BVP.

Find a kinematically admissible displacement function, $\boldsymbol{u} \in \mathscr{K}_u$, such that for every $t \in [t_0, t_{\text{end}}]$, the body $\mathscr{B}$ is in equilibrium as stated by the Virtual Work Principle

$$\int_{\Omega} [\boldsymbol{\sigma} : \nabla \boldsymbol{\eta} - (\boldsymbol{b} - \rho \ddot{\boldsymbol{u}}) \cdot \boldsymbol{\eta}] \, \mathrm{d}v - \int_{\partial\Omega} \boldsymbol{t} \cdot \boldsymbol{\eta} \, \mathrm{d}a = 0, \quad \forall \boldsymbol{\eta} \in \mathscr{V}_u, \tag{2.19}$$

where the space of virtual displacements at time t is defined by

$$\mathscr{V}_u \equiv \left\{ \boldsymbol{\eta} : \Omega \to \mathscr{U} \mid \boldsymbol{\eta} = \mathbf{0} \quad \text{in} \quad \boldsymbol{\varphi}(\partial\Omega_{\text{motion},0}, t) \right\}, \tag{2.20}$$

and at each point of $\mathscr{B}$, the Cauchy stress tensor is the solution of spatial mechanical constitutive initial values problem.

and in the material description as

Problem 2.6 | Material mechanical initial BVP.

Find a kinematically admissible displacement function, $\boldsymbol{u} \in \mathscr{K}_u$, such that for every $t \in [t_0, t_{\text{end}}]$, the body $\mathscr{B}$ is in equilibrium as stated by the Virtual Work Principle

$$\int_{\Omega_0} [\boldsymbol{P} : \nabla_0 \boldsymbol{\eta} - (\boldsymbol{b}_0 - \rho_0 \ddot{\boldsymbol{u}}) \cdot \boldsymbol{\eta}] \, \mathrm{d}v - \int_{\partial\Omega_0} \boldsymbol{t}_0 \cdot \boldsymbol{\eta} \, \mathrm{d}a = 0, \quad \forall \boldsymbol{\eta} \in \mathscr{V}_{u,0}, \tag{2.21}$$

where the space of virtual displacements at time t is defined by

$$\mathscr{V}_{u,0} \equiv \left\{ \boldsymbol{\eta} : \Omega_0 \to \mathscr{U} \mid \boldsymbol{\eta} = \mathbf{0} \quad \text{in} \quad \partial\Omega_{\text{motion},0} \right\}, \tag{2.22}$$

and at each point of $\mathscr{B}$, the First Piola-Kirchhoff stress tensor is the solution of material mechanical constitutive initial values problem.

2.1 Time descretization

Given a generic path-dependent model, i.e., a model in which the stress state does not depend only on the instantaneous deformation state but also on the deformation history, the solution of the constitutive initial value problem for a given set of initial conditions is usually not known for complex strain paths $\boldsymbol{F}(t)$. Thus, there is a need to use an appropriate numerical algorithm to integrate the rate constitutive equations.

In general, the algorithms for integrating rate constitutive equations are obtained adopting some time (or pseudo-time) discretization and some hypothesis on the deformation path between adjacent time stations. In the present document, an algorithm is adopted based on approximated incremental constitutive functions. Attending to the mechanical constitutive initial boundary value problem and considering the time increment $[t_n, t_{n+1}]$, this approach is comprised by the following two requirements:

- **Cauchy and First Piola-Kirchhoff stress tensors.** Considering a time increment $[t_n, t_{n+1}]$ and given the set $\boldsymbol{\alpha}_n$ of internal variables at t_n, the deformation gradient $\boldsymbol{F}_{n+1}$ at time t_{n+1} determines the stress $\boldsymbol{\sigma}_{n+1}$ uniquely through

  $$\boldsymbol{\sigma}_{n+1} = \hat{\boldsymbol{\sigma}}(\boldsymbol{\alpha}_n, \boldsymbol{F}_{n+1}), \tag{2.23}$$

  where $\hat{\boldsymbol{\sigma}}$ is the incremental constitutive function for the Cauchy stress tensor.

  Similarly, the First Piola-Kirchhoff stress tensor $\boldsymbol{P}_{n+1}$ must be uniquely determined by the prescribed deformation gradient $\boldsymbol{F}_{n+1}$ prescribed at t_{n+1} as

  $$\boldsymbol{P}_{n+1} = \hat{\boldsymbol{P}}(\boldsymbol{\alpha}_n, \boldsymbol{F}_{n+1}), \tag{2.24}$$

where $\hat{\boldsymbol{P}}$ is the incremental constitutive function for the First Piola-Kirchhoff stress tensor.

- **Set of internal variables.** Assuming that the set of internal variables $\boldsymbol{\alpha}_n$ is known at t_n, the set of internal variables must be uniquely determined by the prescribed deformationgradient $\boldsymbol{F}_{n+1}$ prescribed at t_{n+1} as

$$\boldsymbol{\alpha}_{n+1} = \hat{\boldsymbol{\alpha}}(\boldsymbol{\alpha}_n, \boldsymbol{F}_{n+1}), \tag{2.25}$$

where $\hat{\boldsymbol{\alpha}}$ is the incremental constitutive function for the set of internal variables.

Generally, the numerical constitutive laws are nonlinear and path-independent within one increment. In other words, within each increment, $\boldsymbol{\sigma}_{n+1}$ and $\boldsymbol{\alpha}_{n+1}$, they are functions of $\boldsymbol{F}_{n+1}$ alone with the argument $\boldsymbol{\alpha}_n$ constant within the same time interval.

Making use of the aforementioned time discretization, one can state the weak form of the mechanical constitutive initial boundary value problem in the spatial description as

Problem 2.7 | Spatial incremental mechanical initial BVP.

Given the set of internal variables $\boldsymbol{\alpha}_n$ at t_n, the prescribed body and traction force fields $\boldsymbol{b}_{n+1}$ and $\boldsymbol{t}_{n+1}$ at t_{n+1}, and the prescribed deformating gradient $\boldsymbol{F}_{n+1}$ at t_{n+1}, find the kinematically admissible displacement field $\boldsymbol{u}_{n+1} \in \mathscr{K}_{u,n+1}$ such that the body $\mathscr{B}$ is in equilibrium as stated by the virtual Work Principle

$$\int_{\Omega_{n+1}} [\hat{\boldsymbol{\sigma}}(\boldsymbol{F}_{n+1}, \boldsymbol{\alpha}_n) : \nabla \boldsymbol{\eta} - (\boldsymbol{b}_{n+1} - \rho \ddot{\boldsymbol{u}}_{n+1}) \cdot \boldsymbol{\eta}] \, \mathrm{d}v - \int_{\partial\Omega_{n+1}} \boldsymbol{t}_{n+1} \cdot \boldsymbol{\eta} \, \mathrm{d}a = 0, \quad \forall \boldsymbol{\eta} \in \mathscr{V}_u, \tag{2.26}$$

where the space of kinematically admissible displacement fields $\mathscr{K}_{n+1}$ is defined by

$$\mathscr{K}_{u,n+1} \equiv \{\boldsymbol{u} : \Omega_0 \times \mathscr{R} \to \mathscr{U} \mid \boldsymbol{u}_{n+1}(\boldsymbol{X}) = \boldsymbol{u}_{\mathrm{presc},n+1}(\boldsymbol{X}),\ \boldsymbol{X} \in \partial\Omega_{\mathrm{motion},0}\}. \tag{2.27}$$

and in the material description as

Problem 2.8 | Material incremental mechanical initial BVP.

Given the set of internal variables $\boldsymbol{\alpha}_n$ at t_n, the prescribed body and traction force fields $\boldsymbol{b}_{0,n+1}$ and $\boldsymbol{t}_{0,n+1}$ at t_{n+1}, and the prescribed deformating gradient $\boldsymbol{F}_{n+1}$ at t_{n+1}, find the kinematically admissible displacement field $\boldsymbol{u}_{n+1} \in \mathscr{K}_{u,n+1}$ such that the body $\mathscr{B}$ is in equilibrium as stated by the virtual Work Principle

$$\int_{\Omega_0} [\hat{\boldsymbol{P}}(\boldsymbol{F}_{n+1}, \boldsymbol{\alpha}_n) : \nabla_0 \boldsymbol{\eta} - (\boldsymbol{b}_{0,n+1} - \rho_0 \ddot{\boldsymbol{u}}_{n+1}) \cdot \boldsymbol{\eta}] \, \mathrm{d}v - \int_{\partial\Omega_{0,n+1}} \boldsymbol{t}_{0,n+1} \cdot \boldsymbol{\eta} \, \mathrm{d}a = 0, \quad \forall \boldsymbol{\eta} \in \mathscr{V}_{u,0}, \tag{2.28}$$

where the space of kinematically admissible displacement fields $\mathscr{K}_{n+1}$ is defined by

$$\mathscr{K}_{u,n+1} \equiv \{\boldsymbol{u} : \Omega_0 \times \mathscr{R} \to \mathscr{U} \mid \boldsymbol{u}_{n+1}(\boldsymbol{X}) = \boldsymbol{u}_{\mathrm{presc},n+1}(\boldsymbol{X}),\ \boldsymbol{X} \in \partial\Omega_{\mathrm{motion},0}\}. \tag{2.29}$$

2.2 Finite Element Method

With the incremental weak form of the mechanical constitutive initial boundary value problem now established, an approximated solution can be found using the Finite Element Method.

2.2.1 Finite element concept

The first in the Finite Element method is to discretize the continuum domain Ω in a finite set of n_{elem} mutually exclusive subdomains called finite elements $\Omega^{(e)}$. The discretized domain, ${}^{h}\Omega$, is therefore an approximation to the continuum domain expressed by

$$\Omega \approx {}^{h}\Omega \equiv \bigcup_{e=1}^{n_{\text{elem}}} \Omega^{(e)}. \tag{2.30}$$

The spaces of virtual displacements $\mathscr{V}_u$ and $\mathscr{V}_{u,0}$ as well as the space of kinematically admissible displacement fields $\mathscr{K}_u$ are also discretized in the same way, with their discretized forms denoted by ${}^{h}\mathscr{V}_u$, ${}^{h}\mathscr{V}_{u,0}$ and ${}^{h}\mathscr{K}_u$.

2.2.2 Interpolation functions

Let e be a generic finite element with n_{nodes} nodes, where each node i of coordinates $\boldsymbol{x}^i$ is associated with an interpolation function $N_i^{(e)}$. These interpolation functions are often called shape functions and perform the required filed interpolations inside the element domain $\Omega^{(e)}$.

Letting $a(\boldsymbol{x})$ be a generic field defined over $\Omega^{(e)}$, its interpolation at any point $\boldsymbol{x}$ inside the element is defined by the element shape functions as

$$a(\boldsymbol{x}) \approx {}^{h}a(\boldsymbol{x}) \equiv \sum_{i=1}^{n_{\text{nodes}}} a(\boldsymbol{x}_i) N_i^{(e)}(\boldsymbol{x}). \tag{2.31}$$

If instead $a(\boldsymbol{x})$ is instead a generic field defined over the global domain Ω, the interpolation of $a(\boldsymbol{x})$ at any point $\boldsymbol{x}$ is defined by the global shape functions as

$$a(\boldsymbol{x}) \approx {}^{h}a(\boldsymbol{x}) \equiv \sum_{i=1}^{n_{\text{points}}} a(\boldsymbol{x}_i) N_i^{g}(\boldsymbol{x}), \tag{2.32}$$

where n_{points} is the total number of nodes of the finite element mesh. The discretized spaces ${}^{h}\mathscr{V}_u$ and ${}^{h}\mathscr{K}_u$ can now be defined as

$${}^{h}\mathscr{K}_u \equiv \left\{ {}^{h}\boldsymbol{u}(\boldsymbol{x}) = \sum_{i=1}^{n_{\text{points}}} \boldsymbol{u}(\boldsymbol{x}_i) N_i^{g}(\boldsymbol{x}) \mid \boldsymbol{u}(\boldsymbol{x}_i) = \boldsymbol{u}_{\text{presc}}(\boldsymbol{x}_i) \quad \text{if } \boldsymbol{x}_i \in \partial\Omega_{\text{motion},0} \right\}, \tag{2.33}$$

$${}^{h}\mathscr{V}_u \equiv \left\{ {}^{h}\boldsymbol{\eta}(\boldsymbol{x}) = \sum_{i=1}^{n_{\text{points}}} \boldsymbol{\eta}(\boldsymbol{x}_i) N_i^{g}(\boldsymbol{x}) \mid \boldsymbol{\eta}(\boldsymbol{x}_i) = \boldsymbol{0} \quad \text{if } \boldsymbol{x}_i \in \partial\Omega_{\text{motion},0} \right\} \tag{2.34}$$

Quantities defined on the reference configuration Ω_0 accepted a treatment entirely similar to the one described above, and thus is omitted.

2.2.3 Interpolation matrix and discrete gradient operators

The global shape functions can be conveniently assembled in the so-called global interpolation matrix as

$$\mathbf{N}^g(\boldsymbol{x}) \equiv \left[\mathrm{diag}[N_1^g(\boldsymbol{x})]\ \mathrm{diag}[N_2^g(\boldsymbol{x})]\ \cdots\ \mathrm{diag}[N_{n_{\mathrm{points}}}^g(\boldsymbol{x})]\right], \tag{2.35}$$

where $\mathrm{diag}[N_i^g]$ is a diagonal matrix $n_{\mathrm{dim}} \times n_{\mathrm{dim}}$

$$\mathrm{diag}[N_i^g(\boldsymbol{x})] \equiv \begin{bmatrix} N_i^g & 0 & \cdots & 0 \\ 0 & N_i^g & \cdots & 0 \\ \vdots & \vdots & \ddots & \vdots \\ 0 & 0 & \cdots & N_i^g \end{bmatrix} \tag{2.36}$$

where n_{dim} is the number of degrees of freedom per node.

Defining the global vector of nodal displacements as

$$\mathbf{u} = \left[u_1^1, \ldots, u_{n_{\mathrm{dim}}}^1, \ldots, u_1^{n_{\mathrm{points}}}, \ldots, u_{n_{\mathrm{dim}}}^{n_{\mathrm{points}}}\right]^T, \tag{2.37}$$

the displacement field $\boldsymbol{u}(\boldsymbol{x})$ defined over the global domain Ω, can be found from Equation (2.32) at any point $\boldsymbol{x}$ as

$$^h\boldsymbol{u}(\boldsymbol{x}) \equiv \mathbf{N}^g(\boldsymbol{x})\mathbf{u}, \quad ^h\boldsymbol{u} \in {}^h\mathscr{K}_u. \tag{2.38}$$

2.2.4 Spatial discretization

Applying the aforementioned finite element discretization to the incremental mechanical constitutive initial boundary value problem, we can then write in the spatial description

$$\int_{^h\Omega} \left[\hat{\boldsymbol{\sigma}}^T \mathbf{B}^g \boldsymbol{\eta} - (\mathbf{b}_{n+1} - \rho\ddot{\mathbf{u}}_{n+1}) \cdot \mathbf{N}^g \boldsymbol{\eta}\right] \mathrm{d}v - \int_{\partial^h\Omega_{\mathrm{traction}}} \mathbf{t}_{n+1} \cdot \mathbf{N}^g \boldsymbol{\eta}\, \mathrm{d}a = 0, \quad \forall \boldsymbol{\eta} \in {}^h\mathscr{V}_u, \tag{2.39}$$

where $\mathbf{B}^g$ is the discrete symmetric global gradient operator, defined for a 2D problem in cartesian coordinates as

$$\mathbf{B}^g \equiv \begin{bmatrix} \frac{\partial N_1^g}{\partial x} & 0 & \frac{\partial N_2^g}{\partial x} & 0 & \cdots & \frac{\partial N_{n_{\mathrm{points}}}^g}{\partial x} & 0 \\ 0 & \frac{\partial N_1^g}{\partial y} & 0 & \frac{\partial N_2^g}{\partial y} & \cdots & 0 & \frac{\partial N_{n_{\mathrm{points}}}^g}{\partial y} \\ \frac{\partial N_1^g}{\partial y} & \frac{\partial N_1^g}{\partial x} & \frac{\partial N_2^g}{\partial y} & \frac{\partial N_2^g}{\partial x} & \cdots & \frac{\partial N_{n_{\mathrm{points}}}^g}{\partial y} & \frac{\partial N_{n_{\mathrm{points}}}^g}{\partial x} \end{bmatrix}. \tag{2.40}$$

Equation (2.39) can be rewritten as

$$\left\{\int_{^h\Omega} \left[\mathbf{B}^{gT} \hat{\boldsymbol{\sigma}}(\boldsymbol{\alpha}_n, \boldsymbol{F}_{n+1}) - \mathbf{N}^{gT}\mathbf{b}_{n+1} + \mathbf{N}^{gT}\rho\ddot{\mathbf{u}}_{n+1}\right] \mathrm{d}v - \int_{\partial^h\Omega_{\mathrm{traction}}} \mathbf{N}^{gT}\mathbf{t}_{n+1}\, \mathrm{d}a\right\}^T \boldsymbol{\eta} = 0, \quad \forall \boldsymbol{\eta} \in {}^h\mathscr{V}_u, \tag{2.41}$$

and, since it must be satisfied for any $\boldsymbol{\eta} \in {}^{h}\mathscr{V}_{u}$, the incremental quasi-static discretized mechanical constitutive initial boundary value problem can thus be stated in the spatial description as

Problem 2.9 | Spatial incremental discretized mechanical initial BVP.

Given the set of internal variables $\boldsymbol{\alpha}_n$ at t_n, the prescribed body and traction force fields $\boldsymbol{b}_{n+1}$ and $\boldsymbol{t}_{n+1}$, and the prescribed deformation gradient $\boldsymbol{F}_{n+1}$ at t_{n+1}, find the kinematically admissible nodal displacement field $\boldsymbol{u}_{n+1} \in {}^{h}\mathscr{K}_{u,n+1}$ such that the body $\mathscr{B}$ is in equilibrium as stated by the Virtual Work Principle

$$\mathbf{M}\ddot{\mathbf{u}}_{n+1} + \mathbf{f}^{\text{int}}(\mathbf{u}_{n+1}) - \mathbf{f}^{\text{ext}}_{n+1} = \mathbf{0}, \tag{2.42}$$

where $\mathbf{f}^{\text{int}}$ e $\mathbf{f}^{\text{ext}}_{n+1}$ are the global vectors of internal and external forces defined as

$$\mathbf{f}^{\text{int}} \equiv \int_{{}^{h}\Omega} \mathbf{B}^{g\,T}\hat{\boldsymbol{\sigma}}(\boldsymbol{F}_{n+1}, \boldsymbol{\alpha}_n)\,\mathrm{d}v, \tag{2.43}$$

$$\mathbf{f}^{\text{ext}}_{n+1} \equiv \int_{{}^{h}\Omega} \mathbf{N}^{g\,T}\mathbf{b}_{n+1}\,\mathrm{d}v + \int_{\partial {}^{h}\Omega_{\text{traction}}} \mathbf{N}^{g\,T}\mathbf{t}_{n+1}\,\mathrm{d}a, \tag{2.44}$$

and $\mathbf{M}$ is the mass matrix defined as

$$\mathbf{M} = \int_{{}^{h}\Omega} \rho \mathbf{N}^{g\,T}\mathbf{N}^{g}\,\mathrm{d}v. \tag{2.45}$$

In a material description, Equation (2.41) is written as

$$\left\{ \int_{{}^{h}\Omega_0} \left[\mathbf{G}^{g\,T}\hat{\boldsymbol{P}}(\boldsymbol{\alpha}_n, \boldsymbol{F}_{n+1}) - \mathbf{N}^{g\,T}\mathbf{b}_{0,n+1} + \mathbf{N}^{g\,T}\rho_0\ddot{\mathbf{u}}_{n+1} \right] \mathrm{d}v \right.$$
$$\left. - \int_{\partial {}^{h}\Omega_{\text{traction},0}} \mathbf{N}^{g\,T}\mathbf{t}_{0,n+1}\,\mathrm{d}a \right\}^{T} \boldsymbol{\eta} = 0, \quad \forall \boldsymbol{\eta} \in {}^{h}\mathscr{V}_{u,0}, \tag{2.46}$$

where $\mathbf{G}^{g}$ is the discrete global gradient operator, defined for a 2D problem in cartesian coordinates as

$$\mathbf{G}^{g} \equiv \begin{bmatrix} \dfrac{\partial N^{g}_{1}}{\partial x} & 0 & \dfrac{\partial N^{g}_{2}}{\partial x} & 0 & \cdots & \dfrac{\partial N^{g}_{n_{\text{points}}}}{\partial x} & 0 \\ 0 & \dfrac{\partial N^{g}_{1}}{\partial x} & 0 & \dfrac{\partial N^{g}_{2}}{\partial x} & 0 & \cdots & \dfrac{\partial N^{g}_{n_{\text{points}}}}{\partial x} \\ \dfrac{\partial N^{g}_{1}}{\partial y} & 0 & \dfrac{\partial N^{g}_{2}}{\partial y} & \cdots & 0 & \dfrac{\partial N^{g}_{n_{\text{points}}}}{\partial y} & 0 \\ 0 & \dfrac{\partial N^{g}_{1}}{\partial y} & 0 & \dfrac{\partial N^{g}_{2}}{\partial y} & \cdots & 0 & \dfrac{\partial N^{g}_{n_{\text{points}}}}{\partial y} \end{bmatrix}, \tag{2.47}$$

and, as for the spatial description, it must be satisfied for any $\boldsymbol{\eta} \in {}^{h}\mathscr{V}_{u,0}$, the incremental quasi-static discretized mechanical constitutive initial boundary value problem can thus be stated in the material description as

Problem 2.10 | Material incremental discretized mechanical initial BVP.

Given the set of internal variables $\boldsymbol{\alpha}_n$ at t_n, the prescribed body and traction force fields $\boldsymbol{b}_{0,n+1}$ and $\boldsymbol{t}_{0,n+1}$, and the prescribed deformation gradient $\boldsymbol{F}_{n+1}$ at t_{n+1}, find the kinematically admissible nodal displacement field $\boldsymbol{u}_{n+1} \in {}^h\mathscr{K}_{u,n+1}$ such that the body $\mathscr{B}$ is in equilibrium as stated by the Virtual Work Principle

$$\mathbf{M}\ddot{\mathbf{u}}_{n+1} + \mathbf{f}^{\text{int}}(\mathbf{u}_{n+1}) - \mathbf{f}^{\text{ext}}_{n+1} = \mathbf{0}, \tag{2.48}$$

where $\mathbf{f}^{\text{int}}$ e $\mathbf{f}^{\text{ext}}_{n+1}$ are the global vectors of internal and external forces defined as

$$\mathbf{f}^{\text{int}} \equiv \int_{{}^h\Omega_0} \mathbf{G}^{g\,T}\hat{\boldsymbol{P}}(\boldsymbol{F}_{n+1}, \boldsymbol{\alpha}_n)\,\mathrm{d}v, \tag{2.49}$$

$$\mathbf{f}^{\text{ext}}_{n+1} \equiv \int_{{}^h\Omega_0} \mathbf{N}^{g\,T}\mathbf{b}_{0,n+1}\,\mathrm{d}v + \int_{\partial^h\Omega_{\text{traction},0}} \mathbf{N}^{g\,T}\mathbf{t}_{0,n+1}\,\mathrm{d}a. \tag{2.50}$$

and $\mathbf{M}$ is the mass matrix defined as

$$\mathbf{M} = \int_{{}^h\Omega_0} \rho_0 \mathbf{N}^{g\,T}\mathbf{N}^g\,\mathrm{d}v. \tag{2.51}$$

The global vectors for the internal and external forces are usually obtained by assemblage of their elemental counterparts as

$$\mathbf{f}^{\text{int}} = \mathop{\mathsf{A}}_{e=1}^{n_{\text{elem}}} \left(\mathbf{f}^{\text{int}}\right)^{(e)}, \tag{2.52}$$

$$\mathbf{f}^{\text{ext}} = \mathop{\mathsf{A}}_{e=1}^{n_{\text{elem}}} \left(\mathbf{f}^{\text{ext}}\right)^{(e)}, \tag{2.53}$$

where the elemental vectors in the spatial description are defined as

$$\left(\mathbf{f}^{\text{int}}\right)^{(e)} \equiv \int_{{}^h\Omega^{(e)}} \mathbf{B}^T\hat{\boldsymbol{\sigma}}(\boldsymbol{F}_{n+1}, \boldsymbol{\alpha}_n)\,\mathrm{d}v, \tag{2.54}$$

$$\left(\mathbf{f}^{\text{ext}}_{n+1}\right)^{(e)} \equiv \int_{{}^h\Omega^{(e)}} \mathbf{N}^T\mathbf{b}_{n+1}\,\mathrm{d}v + \int_{\partial^h\Omega^{(e)}_{\text{traction}}} \mathbf{N}^T\mathbf{t}_{n+1}\,\mathrm{d}a, \tag{2.55}$$

and in material description as

$$\left(\mathbf{f}^{\text{int}}\right)^{(e)} \equiv \int_{{}^h\Omega_0^{(e)}} \mathbf{G}^T\hat{\boldsymbol{P}}(\boldsymbol{F}_{n+1}, \boldsymbol{\alpha}_n)\,\mathrm{d}v, \tag{2.56}$$

$$\left(\mathbf{f}^{\text{ext}}_{n+1}\right)^{(e)} \equiv \int_{{}^h\Omega_0^{(e)}} \mathbf{N}^T\mathbf{b}_{0,n+1}\,\mathrm{d}v + \int_{\partial^h\Omega^{(e)}_{0,\text{ traction}}} \mathbf{N}^T\mathbf{t}_{0,n+1}\,\mathrm{d}a, \tag{2.57}$$

The matrices $\mathbf{N}$, $\mathbf{B}$, and $\mathbf{G}$ are the elemental interpolation matrix, the symmetric elemental gradient operator, and the discrete elemental gradient operator.

In a similar manner, the global mass matrix is also usually obtained by assemblage of their elemental counterparts as

$$\mathbf{M} \equiv \mathop{\mathsf{A}}_{e=1}^{n_{\text{elem}}} \mathbf{M}^{(e)}, \tag{2.58}$$

where the elemental mass matrices in the spatial description are defined as

$$\mathbf{M}^{(e)} = \int_{h\Omega^{(e)}} \rho \mathbf{N}^T \mathbf{N} \, \mathrm{d}v, \tag{2.59}$$

and the material descriptrion

$$\mathbf{M}^{(e)} = \int_{h\Omega_0^{(e)}} \rho_0 \mathbf{N}^T \mathbf{N} \, \mathrm{d}v. \tag{2.60}$$

2.2.5 Numerical integration

In the Finite Element Method, the integrations over the element domain are generally performed numerically using the Gaussian Quadrature Method. Stating it's application succinctly, let $a(\boldsymbol{x})$ be a generic field, if there is a coordinate transformation from a local (or natural) normalized domain Υ to the element domain $\Omega^{(e)}$, $\boldsymbol{x}\colon \Upsilon \to \Omega^{(e)}$, the integral of $a(\boldsymbol{x})$ over the domain $\Omega^{(e)}$ can be numerically determined as

$$\int_{\Omega^{(e)}} a(\boldsymbol{x}) \, \mathrm{d}\boldsymbol{x} = \int_{\Upsilon} a(\boldsymbol{x}(\boldsymbol{\zeta})) \, j(\boldsymbol{\zeta}) \, \mathrm{d}\boldsymbol{\zeta} \approx \sum_{i=1}^{n_{\mathrm{GP}}} w_i \, a(\boldsymbol{x}(\boldsymbol{\zeta}_i)) \, j(\boldsymbol{\zeta}_i), \tag{2.61}$$

where $\boldsymbol{\zeta}_i$ and w_i, $i = 1, \ldots, n_{\mathrm{GP}}$ are the positions and weigths of the Gauss sampling points in the domain Υ and $j(\boldsymbol{\zeta})$ is the determinant of the coordinate trasnformation's Jacobian defined as

$$j(\boldsymbol{\zeta}) = \det\left(\frac{\partial \boldsymbol{x}}{\partial \boldsymbol{\zeta}}\right). \tag{2.62}$$

2.3 Linearisation

The equilibrium equation, Equation (2.42) in a spatial description and Equation (3.25) in a material description, is generally nonlinear due to geometrical and/or material nonlinearities. The Newton-Raphson Method is an efficient and robust iterative scheme with a quadratic convergence rate often used to solve the equilibrium equation at each time increment, t_n. The residual of the fully discretized balance of linear momentum is defined for an iteration step i of the Newton-Raphson method as

$$\mathbf{r}(\mathbf{u}_{n+1}^i) = \mathbf{M}\ddot{\mathbf{u}}_{n+1}^i + \mathbf{f}^{\mathrm{int}}(\mathbf{u}_{n+1}^i) - \mathbf{f}_{n+1}^{\mathrm{ext}}. \tag{2.63}$$

A Taylor expansion about the current solution $\mathbf{u}_{n+1}^i$ is performed, discarding all terms of higher order than one, yielding the linearised form

$$\mathrm{Lin}\,\mathbf{r}(\mathbf{u}_{n+1}^i) = \mathbf{r}(\mathbf{u}_{n+1}^i) + \underbrace{\left.\frac{\partial \mathbf{r}(\mathbf{u}_{n+1})}{\partial \mathbf{u}_{n+1}}\right|^i}_{\mathbf{K}(\mathbf{u}_{n+1}^i)} \delta\mathbf{u}. \tag{2.64}$$

with the dynamic effective tangential stiffness matrix $\mathbf{K}(\mathbf{u}_{n+1}^i)$. The linearisation of the internal forces included in $\mathbf{K}$ is known as the tangential stiffness matrix $\mathbf{K}_T$, which is defined as

$$\mathbf{K}_T^i = \left.\frac{\partial \mathbf{f}^{\mathrm{int}}}{\partial \mathbf{u}_{n+1}}\right|^i. \tag{2.65}$$

Equilibrium is achieved if

$$\mathrm{Lin}\,\mathbf{r}(\mathbf{u}_{n+1}^{i}) = \mathbf{0}, \tag{2.66}$$

so that a linear system of equation is given by

$$\mathbf{K}(\mathbf{u}_{n+1}^{i})\delta\mathbf{u} = -\mathbf{r}\left(\mathbf{u}_{n+1}^{i}\right). \tag{2.67}$$

Thus, a new solution of the displacement increment $\delta\mathbf{u}$ for current iteration step $i+1$ is determined, and the final displacement solution of time step $n+1$ is obtained via updating

$$\mathbf{u}_{n+1}^{i+1} = \mathbf{u}_{n+1}^{i} + \delta\mathbf{u}. \tag{2.68}$$

A solution of t_{n+1} is found, i.e. an equilibrium state is reached and $\mathbf{u}_{n+1} = \mathbf{u}_{n+1}^{i+1}$, if prescribed, user-defined convergence criteria are fulfilled.

2.4 Constitutive laws

Chapter 3

Thermo field

For the development of the thermomechanical models, the temperature field needs to be considered. This section provides an overview of the governing equations required to describe a temperature field with the finite element method (FEM). The procedure to establish a fully discrete system of equations for the themal field is comparable to the one for the structural field in chapter **??**. Furthermore, the basics of nonlinear continuum thermodynamics have already been featured in chapter **??**. Consequently, the detailed derivation are skipped in this chapter.

3.1 Governing equations

Based on the general model presented in Section **??**, the balance equations for the temperature field are obtained as a special case by neglecting all mechanical terms. Hence, the energy balance equation (Equation (1.42)), now in material description, reduces to

$$\rho_0 \; e = -\operatorname{div}_0 \boldsymbol{q}_0 + \rho_0 r \quad \text{in } \Omega_0, \tag{3.1}$$

where all mechanical terms are neglected. The target application of the present work are coupled generally nonlinear thermomechanical interaction problems, where the initial and the current domains are not equal, i.e. $\Omega_0 \neq \Omega$. Thus, for the sake of simplicity and in view of the later coupled problem, all following relations are expressed in material quantities. A purely thermal analysis is independent of the deformation, so that reference and current configuration are identical and the domain remains constant, i.e. $\Omega_0 \equiv \Omega$.

3.2 Thermal constitutive initial value problem

From Section **??**, discarding all variables related to the mechanical problem, the general thermal constitutive initial value problem is

Problem 3.1 | General thermal constitutive intial value problem.

Given the initial value of the internal variables $\boldsymbol{\alpha}(t_0)$ and the history of the

temperature distribution

$$\theta(t), \quad t \in [t_0, t_{\text{end}}],$$

find the function for $\boldsymbol{q}_0(t)$, $s(t)$ and $\boldsymbol{\alpha}(t)$ such that the constitutive equations

$$s = -\frac{\partial \psi}{\partial \theta}, \tag{3.2}$$

$$\psi = \psi(\theta), \tag{3.3}$$

$$\dot{\boldsymbol{\alpha}} = f(\theta, \boldsymbol{g}_0, \boldsymbol{\alpha}), \tag{3.4}$$

$$\frac{1}{\theta}\boldsymbol{q}_0 = g(\theta, \boldsymbol{g}_0, \boldsymbol{\alpha}). \tag{3.5}$$

are satisfied for every $t \in [t_0, t_{\text{end}}]$.

No distinction between spatial and material configurations applies as $\Omega = \Omega_0$. Next, a standard set of assumptions are introduced.

Helmholtz free energy As a first step, the specific heat C_V is established and defined according to the thermodynamical principles to be the amount of heat required to change a unit mass of a substance by one degree in temperature, i.e.

$$C_{\text{V}} = \frac{\partial e}{\partial \theta}. \tag{3.6}$$

The index $(\cdot)_{\text{V}}$ denotes that C_{V} is measured at constant volume. Its dimensions are energy over temperature, i.e., [E/Θ], and using the International System of Units (SI), C_V is expressed in joule per kelvin. Using Equation 1.51, the specific heat at constant volume can be written as

$$C_{\text{V}} = -\frac{\partial^2 \psi}{\partial \theta^2}\theta = \frac{\partial s}{\partial \theta}\theta. \tag{3.7}$$

In general, the heat capacity depends on the deformation and on the temperature. A substance whose specific volume (or density) is constant is called an incompressible substance. This incompressibilty or constant-volume assumption should be taken to imply that the energy associated with the volume change is negligible compared with other forms of energy. For the application to elastomers, see for instance Netz [96], the heat capacity C_V can be assumed to depend only on the temperature, and the partial derivatives in Equation (3.7) turn into exact derivatives, yielding

$$C_{\text{V}} = \frac{\mathrm{d}s}{\mathrm{d}\theta}\theta. \tag{3.8}$$

Furthermore, for the application to metals, a constant specific heat capacity (i.e. $C_{\text{V}} = \text{const.}$) is a valid assumption, utilised e.g. in Adam and Ponthot [1], Ghadiani [48], Ibrahimbegovic and Chorfi [61], and Simo and Miehe [122]. Accordingly, the heat capacity is also assumed to be constant (i.e. $C_{\text{V}} = \text{const.}$), since focus in this work is on the application to metals. Thus, the entropy can be written as

$$s(\theta) = C_{\text{V}} \ln\left(\frac{\theta}{\theta_0}\right), \tag{3.9}$$

after integration, where θ_0 and C_V denote the constant initial temperature and the constant specific heat, respectively.

Given the constituive relation for the entropy (Equation (3.2)), the Helmholtz free energy per unit reference volume is found to be

$$\psi(\theta) = -C_V \left[(\theta - \theta_0) - \theta \ln\left(\frac{\theta}{\theta_0}\right) \right], \tag{3.10}$$

Subsequently, the time derivative of the entropy is

$$\dot{s}(\theta) = \frac{\partial s}{\partial \theta}\dot{\theta} = -\frac{\partial^2 \psi}{\partial \theta^2}\dot{\theta} = C_V \frac{1}{\theta}\dot{\theta}. \tag{3.11}$$

Law for the heat flux As previously mentioned, in a purely thermal analysis the deformation is neglected, consequently the material and spatial heat flux coincide, that is $\boldsymbol{q}_0 \equiv \boldsymbol{q}$, which is also valid for the material and spatial gradient, hence $\nabla_0 \theta = \nabla \theta$. To satisfy the dissipation inequality due to conduction (Equation (**??**)), a constitutive law for the heat flux has to be chosen associating the heat flux $\boldsymbol{q}_0$ with its dual variable $\boldsymbol{g}_0$ and the temperature θ. Accordingly, so-called Fourier's law, which is linear and isotropic is utilised, which is defined as

$$\boldsymbol{q}_0 = -k\boldsymbol{g}_0. \tag{3.12}$$

Herein, the thermal conductivity k is assumed constant and positive that is $k \geq 0$. Thus, heat is conducted in the direction of decreasing temperatures. Apart from Fourier's law, different constitutive laws for the heat flux are available in the literature, as e.g. Duhamel's law of heat conduction (see e.g. Holzapfel [58]) which uses a positive semi-definite second-order tensor k instead of the constant conductivity k. If Duhamel's law is restricted to thermally isotropic behaviour (i.e. no preferred direction), the conductivity tensor reduces to $k = k\boldsymbol{I}$. If a constant heat conductivity $k = \text{const.}$ is assumed, Fourier's law is recovered as a special form of Duhamel's law. Moreover, e.g. in Holzapfel and Simo [59] and Sherief and Abd El-Latief [117], a variable conductivity ($k \neq \text{const}$ is assumed in the context of elastomers). In Bargmann and Steinmann [13] and Bargmann et al. [14], three different constitutive laws for the heat flux $\boldsymbol{q}$ are proposed based on the Green-Naghdi's non-classical theory. Nevertheless, for the present work Fourier's law yields physical results and hence is exclusively considered in this work.

"Standard" thermal constitutive description No extra internal variables $\boldsymbol{\alpha}$ are considered in the present description of the thermal problem. Thus, the thermal constitutive initial value problem given the standard assumptions laid out above accepts a closed form solution, i.e., the functions for $\boldsymbol{q}$ and s are known from the outset.

Problem 3.2 | "Standard" thermal constitutive description

Given the history of the temperature distribution

$$\theta(t), \quad t \in [t_0, t_{\text{end}}],$$

compute the functions for $\boldsymbol{q}_0(t)$ and $s(t)$ at every $t \in [t_0, t_{\text{end}}]$ using the constitutive equations

$$s = C_{\text{V}} \ln\left(\frac{\theta}{\theta_0}\right), \tag{3.13}$$

$$\boldsymbol{q}_0 = -k\boldsymbol{g}_0. \tag{3.14}$$

3.3 Weak energy balance equation

The solution of the thermal problem using the FEM requires the use of the weak form of the energy balance equation. Applying to the governing equation (Equation (3.1)) in the strong form, a variational approach, multiplying it by the virtual temperatures ξ followed by integration by parts, one can find the energy balance equation in its weak form.

Problem 3.3 | Weak energy balance equation

There is energy balance in the body if and only if the temperature distribution satisfies

$$\int_{\Omega_0} \left[\left(\dot{e} - \rho_0 r\right)\xi - \boldsymbol{q}_0 \cdot \nabla_0 \xi \right] \mathrm{d}v - \int_{\partial\Omega_0} h_0 \xi \, \mathrm{d}a = 0, \quad \forall \xi \in \mathscr{V}_{\theta,0}, \tag{3.15}$$

where $\mathscr{V}_{\theta,0}$ is the space of virtual temperature distributions on the body, defined by the space of sufficiently regular arbitrary temperature distributions.

3.4 The thermal initial boundary value problem

Following the same approach as in Section **??**, it is now possible to introduce the the thermal initial boundary value problem. Assume that the internal variables governing the body $\mathscr{B}$ are known at the initial time t_0. In addition, assume that the heat generated in the interior of the body is prescribed, $r(\boldsymbol{X}, t)$, $t \in [t_0, t_{\text{end}}]$, as well as,

- **Natural (or Neumann) boundary condition.** The boundary portion $\partial\Omega_{\text{heat},0}$ of $\mathscr{B}$ is subject to a prescribed history of heat flux, $h_{\text{presc},0}(\boldsymbol{X}, t) = \boldsymbol{q}_{\text{presc},0}(\boldsymbol{X}, t) \cdot \boldsymbol{m}(\boldsymbol{X})$, $\boldsymbol{X} \in \partial\Omega_{\text{heat},0}$, $t \in [t_0, t_{\text{end}}]$.

- **Essential (or Dirichlet) boundary condition.** The boundary portion $\partial\Omega_{\text{temperature},0}$ of $\mathscr{B}$ is subject to a prescribed temperature history, $\theta_{\text{presc}}(\boldsymbol{X}, t)$, $\boldsymbol{X} \in \partial\Omega_{\text{temperature},0}$, $t \in [t_0, t_{\text{end}}]$.

As before the admissible temperature distributions for the body $\mathscr{B}$ are all sufficiently regular temperature fields that satisfy the essential boundary condition,

$$\mathscr{K}_\theta = \{\theta : \Omega_0 \times \mathbb{R} \to \mathbb{R} \,|\, \theta(\boldsymbol{X}, t) = \theta_{\text{presc}}(\boldsymbol{X}, t), \quad \boldsymbol{X} \in \partial\Omega_{\text{temperature},0}, \quad t \in [t_0, t_{\text{end}}]\}. \tag{3.16}$$

Combining the weak energy balance equations with the "standard" thermal constitutive description, the weak form of the "standard" thermal constitutive initial boundary value problem can be stated as follows

Problem 3.4 | "Standard" thermal initial BVP.

Find an admissible temperature distribution, $\theta \in \mathscr{K}_\theta$, such that for every $t \in [t_0, t_{\text{end}}]$, the body $\mathscr{B}$ is in energetic equilibrium

$$\int_{\Omega_0} \left[\left(C_V \dot{\theta} - \rho_0 r \right) \xi + k \boldsymbol{g}_0 \cdot \nabla_0 \xi \right] \mathrm{d}v - \int_{\partial\Omega_0} h_0 \xi \, \mathrm{d}a = 0, \quad \forall \xi \in \mathscr{V}_{\theta,0}, \tag{3.17}$$

where the space of virtual temperature distributions at time t is defined by

$$\mathscr{V}_{\theta,0} \equiv \left\{ \xi : \Omega_0 \to \mathbb{R} \mid \xi = 0 \quad \text{in} \quad \partial\Omega_{\text{temperature},0} \right\}. \tag{3.18}$$

3.5 Finite Element Method

Following a procedure entirely similar to the one described in Section **??**, the global shape functions can be conveniently assembled in the so-called global interpolation matrix as

$$\mathbf{N}^g(\boldsymbol{X}) \equiv \left[N_1^g(\boldsymbol{X}), N_2^g(\boldsymbol{X}), \ldots, N_{n_{\text{points}}}^g(\boldsymbol{X}) \right]. \tag{3.19}$$

The vector containg the nodal values of the temperature is denoted by Θ and defined as

$$\Theta(t) = \left[\theta^1(t), \ldots, \theta^{n_{\text{points}}}(t) \right]^T, \tag{3.20}$$

such that the value of the temperature inside the descretized domain ${}^h\Omega_0$ can be found from

$${}^h\theta(\boldsymbol{X}, t) \equiv \mathbf{N}^g(\boldsymbol{X}) \Theta(t), \quad {}^h\theta \in {}^h\mathscr{K}_\theta. \tag{3.21}$$

It is also convenient to defined the discrete gloabal gradient operator $\mathbf{H}^g$. For instance, in a 2D problem, where cartesian coordinates are employed, this discrete operator is defined as

$$\mathbf{H}^g \equiv \begin{bmatrix} \dfrac{\partial N_1^g}{\partial X} & \dfrac{\partial N_2^g}{\partial X} & \cdots & \dfrac{\partial N_{n_{\text{points}}}^g}{\partial X} \\ \dfrac{\partial N_1^g}{\partial Y} & \dfrac{\partial N_2^g}{\partial Y} & \cdots & \dfrac{\partial N_{n_{\text{points}}}^g}{\partial Y} \end{bmatrix}. \tag{3.22}$$

Applying the aforementioned finite element discretization to the "standard" thermal initial BVP yields

$$\int_{{}^h\Omega_0} \left[\left(C_V \dot{\theta} - \rho_0 r \right) \mathbf{N}^g \xi + k \boldsymbol{g}_0 \cdot \mathbf{H}^g \xi \right] \mathrm{d}v - \int_{{}^h\partial\Omega_0} h_0 \mathbf{N}^g \xi \, \mathrm{d}a = 0, \quad \forall \xi \in {}^h\mathscr{V}_{\theta,0}, \tag{3.23}$$

which can be rewritten

$$\left\{ \int_{{}^h\Omega_0} \left[(\mathbf{N}^g)^T \left(C_V \dot{\theta} - \rho_0 r \right) + k (\mathbf{H}^g)^T \mathbf{H}^g \boldsymbol{\theta} \right] \mathrm{d}v - \int_{{}^h\partial\Omega_0} (\mathbf{N}^g)^T h_0 \, \mathrm{d}a \right\}^T \boldsymbol{\xi} = 0, \quad \forall \boldsymbol{\xi} \in {}^h\mathscr{V}_{\theta,0}, \tag{3.24}$$

where the relation $\boldsymbol{g}_0 = \mathbf{H}^g \boldsymbol{\theta}$ is employed. Since Equation (3.24) must be satisfied for any $\boldsymbol{\xi} \in {}^h\mathscr{V}_{\theta,0}$, the discretized "standard" thermal initial boundary value problem can be statted as

Problem 3.5 | Discretized "standard" thermal initial BVP.

Given the prescribed heat sources and heat fluxes $r(\boldsymbol{X}, t)$ and $h_0(\boldsymbol{X}, t)$ find the admissible nodal temperatures $\theta(t) \in {}^h\mathscr{K}_\theta$ such that the body $\mathscr{B}$ is in energetic equilibrium

$$\mathbf{C}\dot{\boldsymbol{\theta}}(t) + \mathbf{K}\boldsymbol{\theta}(t) - \mathbf{f}^{\mathrm{ext}}(t) = \mathbf{0}, \tag{3.25}$$

where $\mathbf{C}$ and $\mathbf{K}$ are the temperature damping and stiffness matrix defined as

$$\mathbf{C} = \int_{{}^h\Omega_0} C_V \mathbf{N}^{g\,T} \mathbf{N}^g \, \mathrm{d}v., \tag{3.26}$$

$$\mathbf{K} = \int_{{}^h\Omega_0} k \mathbf{H}^{g\,T} \mathbf{H}^g \, \mathrm{d}v. \tag{3.27}$$

and $\mathbf{f}^{\mathrm{ext}}(t)$ is the global vector of external forces defined as

$$\mathbf{f}^{\mathrm{ext}}(t) \equiv \int_{{}^h\Omega_0} \rho \mathbf{N}^{g\,T} r(\boldsymbol{X}, t) \, \mathrm{d}v + \int_{\partial^h\Omega_{\mathrm{heat},0}} \mathbf{N}^{g\,T} h_0(\boldsymbol{X}, t) \, \mathrm{d}a. \tag{3.28}$$

Chapter 4

Thermo-mechanical problem

In the following chapter, the general framework presented in chapter **??** is applied to the complete thermo-mechanical analysis. Chapters **??** and **??** concerning the standalone mechanical and thermal problems provide a guide for the developments that follow. This coupling is a so-called volume coupling, as in each point of the domain, the two fields are coupled. In contrast, surface-coupled problems, e.g., fluid-structure interactions problems, include problems where there is coupling only at the interface between the fluid and the structural domain.

The standard approach to finite deformation thermomechanical analysis is the thermomechanical potential . It is already included in the description of continuum thermodynamics in Chapter **??**, where the Helmholtz free-energy is allowed to depend on the temperature θ. Thus, the temperature is directly included in the constitutive law. Following the setup of finite strain plasticity in the general non-isothermal case, in addition to the plastic intermediate configuration, a thermal intermediate configuration has to be considered , i.e.,

$$\boldsymbol{F} = \boldsymbol{F}^t \, \boldsymbol{F}^e \, \boldsymbol{F}^p. \tag{4.1}$$

In contrast to thermal deformations, which are solely volumetric, the volume remains constant during plastic deformations for most metals. Hence, plastic deformations are assumed isochoric, $J^p = \det \boldsymbol{F}^p = 1$, yielding the following split for the jacobian of the deformation

$$J = J^t J^e. \tag{4.2}$$

Following Danowski (2014), the thermal expansion is assumed to be

$$J^t = \frac{\mathrm{d}v}{\mathrm{d}v_0} = \exp(3\alpha_T \Delta\theta). \tag{4.3}$$

Combining the last two equations, the elastic volumetric deformation J^e, can be expressed as

$$J^e = J^e(\theta) = J / J^t. \tag{4.4}$$

Consequently, the additional thermal intermediate configuration can be omitted and volumetric deformations are described only J^e. Thus, if thermal stresses arise due to a temperature change, elastic strains balance the body which implicitly correspond to the thermal strains according to Equation (4.4).

4.0.1 Thermo-mechanical constitutive initial value problem

In the full thermo-mechanical case, considering all quantities related to both the mechanical and the thermal domain, a constitutive model based on internal variables is established by the following set of equations

$$\boldsymbol{P} = \rho_0 \frac{\partial \psi}{\partial \boldsymbol{F}}, \tag{4.5}$$

$$s = -\frac{\partial \psi}{\partial \theta}, \tag{4.6}$$

$$\psi = \psi(\boldsymbol{F}, \theta, \boldsymbol{g}_0, \boldsymbol{\alpha}), \tag{4.7}$$

$$\dot{\boldsymbol{\alpha}} = f(\boldsymbol{F}, \theta, \boldsymbol{g}_0, \boldsymbol{\alpha}), \tag{4.8}$$

$$\frac{1}{\theta}\boldsymbol{q}_0 = g(\boldsymbol{F}, \theta, \boldsymbol{\alpha}). \tag{4.9}$$

The Helmholtz free energy ψ in Equation 4.7 is expressed with respect to the reference volume, so that ψ is reformulated using potential functions,to emphasize this additive decomposition, as follows

$$\rho_0 \psi\left(\boldsymbol{F}, \theta, \boldsymbol{\alpha}\right) := \hat{\mathbb{U}}\left(J^e, \theta\right) + \hat{\mathbb{W}}(\boldsymbol{F}_{\text{iso}}, \theta) + \hat{\mathbb{M}}\left(J^e, \theta\right) + \hat{\mathbb{T}}(\theta) + \hat{\mathbb{K}}\left(\boldsymbol{\alpha}, \theta\right), \tag{4.10}$$

where in contrast to the deformation gradient $\boldsymbol{F}$, the Jacobi-determinant J^e and the isochoric deformation gradient $\boldsymbol{F}_{\text{iso}}$ are applied. $\hat{\mathbb{U}}$ and $\hat{\mathbb{W}}$ can be identified with the standard hyperelastic materials potentials, with the caveat that now the material parameters can depend on the temperature, whereas $\hat{\mathbb{M}}$ describes the thermomechanical coupling potential. The potential $\hat{\mathbb{T}}$ represents the purely thermal potential and is assumed identical to Equation (**??**). Finally, $\hat{\mathbb{K}}$ is the convex plastic potential.

Based on the potential functions, the coupling of the two fields, mechanical and thermal, can be explained:

- the temperature enters the structural field via additional thermal stresses and possibly via temperature-dependent material parameters. Herein, $\hat{\mathbb{M}}$ characterizes the thermomechanical coupling potential, leading to thermal stresses and thermal expansion and dilatation, whereas $\hat{\mathbb{K}}$ being temperature-dependent and therefore enables exemplarily von Mises plasticity combined with temperature-dependent isotropic hardening and thermal softening.
- the structure enters the thermal field via coupling terms, arising from $\hat{\mathbb{M}}$ and $\hat{\mathbb{K}}$, in addition to the purely thermal energy $\hat{\mathbb{T}}$, and thus, coupling terms as the internal or mechanical dissipation $\mathcal{D}_{\text{mech}}$ may emerge in the thermal balance equation. Furthermore, for finite deformation thermomechanical problems, where the initial domain Ω_0 deforms to Ω, so that $\Omega \neq \Omega_0$, and a Lagrangian formulation is used, the deformation enters the thermal field additionally due to the mapping of all quantities in the balance equations to the reference configuration.

The constitutive relations found for the first Piola-Kirchhoff stress tensor (Equation (**??**)) and the entropy (Equation (**??**)) are the same. The expression for the entropy in full can be written as

$$s = C_V \ln\left(\frac{\theta}{\theta_0}\right) - \frac{1}{\rho_0}\left(\frac{\partial \hat{\mathbb{U}}\left(J^e,\theta\right)}{\partial\theta} + \frac{\partial \hat{\mathbb{W}}(\boldsymbol{F}_{\text{iso}},\theta)}{\partial\theta} + \frac{\partial \hat{\mathbb{M}}\left(J^e,\theta\right)}{\partial\theta} + \frac{\partial \hat{\mathbb{K}}\left(\boldsymbol{\alpha},\theta\right)}{\partial\theta}\right). \tag{4.11}$$

As in Chapter **??**, the heat conduction law is chosen to be the Fourier heat conduction law, repeated here for the sake of clarity in the spatial description

$$\boldsymbol{q} = -k\boldsymbol{g}. \tag{4.12}$$

Applying the Piola transformation yields for the material description of the heat flux vector,

$$\boldsymbol{q}_0 = -k_0 \boldsymbol{C}^{-1}\boldsymbol{g}_0. \tag{4.13}$$

Thus, the material thermo-mechanical constitutive initial value problem can be stated as

Problem 4.1 | Material thermomechanical constitutive initial value problem.

Given the initial values of the internal variables, $\boldsymbol{\alpha}(t_0)$, the history of the deformation gradient

$$\boldsymbol{F}(t), \quad t \in [t_0, t_{\text{end}}], \tag{4.14}$$

and the history of the temperature distribution

$$\theta(t), \quad t \in [t_0, t_{\text{end}}], \tag{4.15}$$

find the functions for $\boldsymbol{P}(t)$, $s(t)$, $\boldsymbol{q}_0(t)$ and $\boldsymbol{\alpha}(t)$ such that the constitutive equations

$$\boldsymbol{P} = \rho_0 \frac{\partial \psi}{\partial \boldsymbol{F}}, \tag{4.16}$$

$$s = C_V \ln\left(\frac{\theta}{\theta_0}\right) - \frac{1}{\rho_0}\left(\frac{\partial \hat{\mathbb{U}}\left(J^e,\theta\right)}{\partial\theta} + \frac{\partial \hat{\mathbb{W}}(\boldsymbol{F}_{\text{iso}},\theta)}{\partial\theta} + \frac{\partial \hat{\mathbb{M}}\left(J^e,\theta\right)}{\partial\theta} + \frac{\partial \hat{\mathbb{K}}\left(\boldsymbol{\alpha},\theta\right)}{\partial\theta}\right), \tag{4.17}$$

$$\psi = \frac{1}{\rho_0}\left(\hat{\mathbb{U}}\left(J^e\right) + \hat{\mathbb{W}}(\boldsymbol{F}_{\text{iso}}) + \hat{\mathbb{M}}\left(J^e,\theta\right) + \hat{\mathbb{T}}(\theta) + \hat{\mathbb{K}}\left(\boldsymbol{\alpha},\theta\right)\right), \tag{4.18}$$

$$\boldsymbol{q}_0 = -k_0 \boldsymbol{C}^{-1}\boldsymbol{g}_0, \tag{4.19}$$

$$\dot{\boldsymbol{\alpha}} = f(\boldsymbol{F},\theta,\boldsymbol{g}_0,\boldsymbol{\alpha}), \tag{4.20}$$

are satisfied for every $t \in [t_0, t_{\text{end}}]$, where

$$\hat{\mathbb{T}}(\theta) = -C_{\text{V}}\left[\left(\theta-\theta_0\right) - \theta\ln\left(\frac{\theta}{\theta_0}\right)\right]. \tag{4.21}$$

4.0.2 Weak equilibrium. The principle of virtual work

The strong equations that enforce the equilibrium of a body can be writen using the material description as

$$\rho_0 \ddot{\boldsymbol{u}} = \mathrm{div}_0 \boldsymbol{P} + \boldsymbol{b}_0, \quad \text{in } \Omega_0, \tag{4.22}$$

$$\rho_0 \dot{e} = \boldsymbol{P} : \dot{\boldsymbol{F}} + \rho_0 r - \mathrm{div}_0 \boldsymbol{q}_0, \quad \text{in } \Omega_0. \tag{4.23}$$

Following an approach entirely similar to the ones presented in Chapters **??** and **??**, the weak form of the linear momentum and energy balance equations can be found to be

Problem 4.2 | Weak form of the linear momentum and energy balance equations (material version).

In a material description, the body is in mechanical and energetic equilibrium if and only if the First Piola-Kirchhoff stress field, $\boldsymbol{P}(t)$, the heat flux vector $\boldsymbol{q}_0(t)$, satisfy

$$\int_{\Omega_0} [\boldsymbol{P}(t) : \nabla_0 \boldsymbol{\eta} - (\boldsymbol{b}_0(t) - \rho_0 \ddot{\boldsymbol{u}}(t)) \cdot \boldsymbol{\eta}] \, \mathrm{d}v - \int_{\partial\Omega_0} \boldsymbol{t}_0(t) \cdot \boldsymbol{\eta} \, \mathrm{d}a = 0, \quad \forall \boldsymbol{\eta} \in \mathscr{V}_{u,0}, \tag{4.24}$$

$$\int_{\Omega_0} \left[\left(\rho_0 \dot{e}(t) - \boldsymbol{P}(t) : \dot{\boldsymbol{F}}(t) - \rho_0 r(t) \right) \xi - \boldsymbol{q}_0(t) \cdot \nabla_0 \xi \right] \mathrm{d}v - \int_{\partial\Omega_0} h_0(t) \xi \, \mathrm{d}a = 0, \quad \forall \xi \in \mathscr{V}_{\theta,0}, \tag{4.25}$$

where $\mathscr{V}_{u,0}$ is the space of virtual displacement of the body, defined by the space of sufficiently regular arbitrary displacements

$$\boldsymbol{\eta} : \Omega_0 \to \mathscr{U}. \tag{4.26}$$

and $\mathscr{V}_{\theta,0}$ is the space of virtual temperature distributions of the body, defined by the space of sufficiently regular arbitrary temperature distributions

$$\xi : \Omega_0 \to \mathscr{R}. \tag{4.27}$$

4.0.3 Mechanical constitutive initial boundary value problem

It is now possible to pose the thermo-mechanical constitutive initial value problem in its weak form. Assume that a body $\mathscr{B}$ is made from a generic material, characterized by a given constitutive model, whose internal variables are known at the initial time, as presented in Figure **??**. In addition, it is assumed that the interior of the body was subjected to a prescribed history of body forces, $\boldsymbol{b}(\boldsymbol{X}, t)$, and a prescribed history of heat sources, $r(\boldsymbol{X}, t)$, $t \in [t_0, t_{\text{end}}]$, and to the following boundary conditions:

- **Natural (or Neumann) boundary condition:**
  - **Mechanical field:** The boundary portion $\Omega_{\text{traction, 0}}$ of $\mathscr{B}$ is subjected to a prescribed history of traction forces, $\boldsymbol{t}_{\text{presc,0}}(\boldsymbol{X}, t)$, $\boldsymbol{X} \in \partial\Omega_{\text{traction,0}}$, $t \in [t_0, t_{\text{end}}]$,
  - **Thermal field:** The boundary portion $\partial\Omega_{\text{heat,0}}$ of $\mathscr{B}$ is subject to a prescribed history of heat flux, $h_{\text{presc,0}}(\boldsymbol{X}, t) = \boldsymbol{q}_{\text{presc,0}}(\boldsymbol{X}, t) \cdot \boldsymbol{m}(\boldsymbol{X})$, $\boldsymbol{X} \in \partial\Omega_{\text{heat,0}}$, $t \in [t_0, t_{\text{end}}]$.

- **Essential (or Dirichlet) boundary condition:**
  - **Mechanical field:** The boundary portion $\Omega_{\text{motion, 0}}$ of $\mathscr{B}$ is subjected to a prescribed displacement field history, $\boldsymbol{u}_{\text{presc}}(\boldsymbol{X}, t)$, such that
  $$\boldsymbol{\varphi}(\boldsymbol{X}, t) = \boldsymbol{X} + \boldsymbol{u}_{\text{presc}}(\boldsymbol{X}, t), \quad \boldsymbol{X} \in \partial\Omega_{\text{motion, 0}}, \quad t \in [t_0, t_{\text{end}}].$$
  - **Thermal field:** The boundary portion $\partial\Omega_{\text{temperature,0}}$ of $\mathscr{B}$ is subject to a prescribed temperature history, $\theta_{\text{presc}}(\boldsymbol{X}, t)$, $\boldsymbol{X} \in \partial\Omega_{\text{temperature,0}}$, $t \in [t_0, t_{\text{end}}]$.

It is also convenient to define the set of kinematically admissible displacements and admissible temperature distributions of $\mathscr{B}$ as the set of all sufficiently regular displacement and temperature functions that satisfy the correspondin essential boundary conditions (**?**),

$$\mathscr{K}_u \equiv \{\boldsymbol{u} : \Omega_0 \times \mathscr{R} \to \mathscr{U} \mid \boldsymbol{u}(\boldsymbol{X}, t) = \boldsymbol{u}_{\text{presc}}(\boldsymbol{X}, t), \quad \boldsymbol{X} \in \partial\Omega_{\text{motion,0}}, \quad t \in [t_0, t_{\text{end}}]\}. \tag{4.28}$$

$$\mathscr{K}_\theta \equiv \{\theta : \Omega_0 \times \mathscr{R} \to \mathscr{R} \mid \theta(\boldsymbol{X}, t) = \theta_{\text{presc}}(\boldsymbol{X}, t), \quad \boldsymbol{X} \in \partial\Omega_{\text{temperature,0}}, \quad t \in [t_0, t_{\text{end}}]\}. \tag{4.29}$$

To obtain the thermo-mechanical initial boundary value problem, express the internal specific energy of the system using its specific Helmholtz free energy, yielding

$$\dot{e} \equiv \dot{\psi} + s\dot{\theta} + \dot{s}\theta. \tag{4.30}$$

Considering Equation (**??**) for the entropy, its time derivative is

$$\dot{s} = C_{\text{V}} \frac{1}{\theta}\dot{\theta} - \frac{1}{\rho_0 \theta}\mathcal{H}^{\text{ep}}, \tag{4.31}$$

where the definition of $\hat{\mathbb{T}}$ (Equation (**??**)) and the Gough-Joule effect, $\mathcal{H}^{\text{ep}}$ is defined to be

$$\begin{aligned}\mathcal{H}^{\text{ep}} = \theta \Bigg(& \frac{\partial^2 \hat{\mathbb{U}}\left(J^e, \theta\right)}{\partial\theta \partial J^e}\dot{J}^e + \frac{\partial^2 \hat{\mathbb{U}}\left(J^e, \theta\right)}{\partial\theta^2}\dot{\theta} + \; + \frac{\partial^2 \hat{\mathbb{W}}\left(\boldsymbol{F}_{\text{iso}}, \theta\right)}{\partial\theta^2}\dot{\theta} + \frac{\partial^2 \hat{\mathbb{W}}\left(\boldsymbol{F}_{\text{iso}}, \theta\right)}{\partial\theta \partial \boldsymbol{F}_{\text{iso}}} : \dot{\boldsymbol{F}}_{\text{iso}} \\ & + \frac{\partial^2 \hat{\mathbb{M}}\left(J^e, \theta\right)}{\partial\theta \partial J^e}\dot{J}^e + \frac{\partial^2 \hat{\mathbb{M}}\left(J^e, \theta\right)}{\partial\theta^2}\dot{\theta} + \; + \frac{\partial^2 \hat{\mathbb{K}}\left(\boldsymbol{\alpha}_k, \theta\right)}{\partial\theta^2}\dot{\theta} + \frac{\partial^2 \hat{\mathbb{K}}\left(\boldsymbol{\alpha}_k, \theta\right)}{\partial\theta \partial \boldsymbol{\alpha}_k} * \dot{\boldsymbol{\alpha}}_k \Bigg).\end{aligned} \tag{4.32}$$

Applying the chain-rule, one finds for $\dot{\psi}$

$$\dot{\psi} = \frac{\partial \psi}{\partial \boldsymbol{F}} : \dot{\boldsymbol{F}} + \frac{\partial \psi}{\partial \theta}\dot{\theta} + \frac{\partial \psi}{\partial \boldsymbol{\alpha}} * \dot{\boldsymbol{\alpha}}, \tag{4.33}$$

which can be rewritten considering the constitutive relations for the first Piola-Kirchhoff stress tensor (Equation (**??**)) and the entropy (Equation (**??**)), and the definition of the thermodynamical forces (Equation (**??**)) as

$$\dot{\psi} = \frac{1}{\rho_0}\boldsymbol{P} : \dot{\boldsymbol{F}} - s\dot{\theta} - \boldsymbol{A} * \boldsymbol{\alpha}. \tag{4.34}$$

Combining Equation (4.34) and the expression found for the mechanical dissipation $\mathcal{D}_{\text{mech}}$ in Equation (**??**) yields

$$\mathcal{D}_{\text{mech}} = \rho_0 \boldsymbol{A} * \boldsymbol{\alpha}, \tag{4.35}$$

and thus $\dot{\psi}$ can be expressed as

$$\dot{\psi} = \frac{1}{\rho_0} \boldsymbol{P} : \dot{\boldsymbol{F}} - s\dot{\theta} - \frac{1}{\rho_0} \mathcal{D}_{\text{mech}}. \tag{4.36}$$

Combining Equations (**??**), Equation (4.31) and Equation (4.36) yields

$$\dot{e} = \frac{1}{\rho_0} \boldsymbol{P} : \dot{\boldsymbol{F}} - \frac{1}{\rho_0} \mathcal{D}_{\text{mech}} - C_{\text{V}} \dot{\theta} - \frac{1}{\rho_0} \mathcal{H}^{\text{ep}}. \tag{4.37}$$

So the weak form of the thermo-mechanical constitutive initial boundary value problem can be stated in a spatial description as follows and in the material description as

Problem 4.3 | Material thermo-mechanical initial BVP.

Find a kinematically admissible displacement function, $\boldsymbol{u} \in \mathscr{K}_u$, and an admissible temperature distribution, $\theta \in \mathscr{K}_\theta$, such that for every $t \in [t_0, t_{\text{end}}]$, the body $\mathscr{B}$ is in mechanical and energetic equilibrium

$$\int_{\Omega_0} [\boldsymbol{P}(t) : \nabla_0 \boldsymbol{\eta} - (\boldsymbol{b}_0(t) - \rho_0 \ddot{\boldsymbol{u}}(t)) \cdot \boldsymbol{\eta}] \, \mathrm{d}v - \int_{\partial\Omega_0} \boldsymbol{t}_0(t) \cdot \boldsymbol{\eta} \, \mathrm{d}a = 0, \quad \forall \boldsymbol{\eta} \in \mathscr{V}_{u,0}, \tag{4.38}$$

$$\int_{\Omega_0} \left[\left(\rho_0 C_{\text{V}} \dot{\theta}(t) - \mathcal{D}_{\text{mech}}(t) - \mathcal{H}^{\text{ep}}(t) - \rho_0 r(t) \right) \xi - \boldsymbol{q}_0(t) \cdot \nabla_0 \xi \right] \mathrm{d}v - \int_{\partial\Omega_0} h_0(t) \xi \, \mathrm{d}a = 0, \quad \forall \xi \in \mathscr{V}_{\theta,0}, \tag{4.39}$$

where the space of virtual displacements at time t is defined by

$$\mathscr{V}_{u,0} \equiv \{ \boldsymbol{\eta} : \Omega_0 \to \mathscr{U} \mid \boldsymbol{\eta} = \boldsymbol{0} \quad \text{in} \quad \partial\Omega_{\text{motion},0} \}, \tag{4.40}$$

the space of virtual temperatures at time t is defined by

$$\mathscr{V}_{\theta,0} \equiv \left\{ \xi : \Omega_0 \to \mathscr{R} \mid \xi = 0 \quad \text{in} \quad \partial\Omega_{\text{temperature},0} \right\}, \tag{4.41}$$

and at each point of $\mathscr{B}$, the First Piola-Kirchhoff stress tensor is the solution of material mechanical constitutive initial value problem.

4.1 Time descretization

In the context of thermo-mechanical problems, a generic path-dependent model is a model in which the thermodynamical state does not depend only on the instantaneous deformation and temperature states but also on their history. Under these conditions, the solution of the constitutive initial value problem for a given set of initial conditions

is usually not known for complex strain, $\boldsymbol{F}(t)$, or temperature paths, $\theta(t)$, paths. Thus, as in the domain of a strictly mechanical problem, there is a need to use an appropriate numerical algorithm to integrate the rate constitutive equations.

Attending to the thermo-mechanical constitutive initial boundary value problem and considering the time increment $[t_n, t_{n+1}]$, this approach is comprised by the following requirements:

- **First Piola-Kirchhoff stress tensors.** Considering a time increment $[t_n, t_{n+1}]$ and given the set $\boldsymbol{\alpha}_n$ of internal variables at t_n, the deformation gradient $\boldsymbol{F}_{n+1}$ and the temperature distribution θ_{n+1} at time t_{n+1} determines the First Piola-Kirchhoff stress tensor $\boldsymbol{P}_{n+1}$ uniquely as

$$\boldsymbol{P}_{n+1} = \hat{\boldsymbol{P}}(\boldsymbol{F}_{n+1}, \theta_{n+1}, \boldsymbol{\alpha}_n), \tag{4.42}$$

  where $\hat{\boldsymbol{P}}$ is the incremental constitutive function for the First Piola-Kirchhoff stress tensor.

- **Set of internal variables.** Assuming that the set of internal variables $\boldsymbol{\alpha}_n$ is known at t_n, the set of internal variables must be uniquely determined by the prescribed deformation gradient $\boldsymbol{F}_{n+1}$ and temperature distribution θ_{n+1} prescribed at t_{n+1} as

$$\boldsymbol{\alpha}_{n+1} = \hat{\boldsymbol{\alpha}}(\boldsymbol{F}_{n+1}, \theta_{n+1}, \boldsymbol{\alpha}_n), \tag{4.43}$$

  where $\hat{\boldsymbol{\alpha}}$ is the incremental constitutive function for the set of internal variables.

- **Mechanical dissipation.** Considering a time increment $[t_n, t_{n+1}]$ and given the set $\boldsymbol{\alpha}_n$ of internal variables at t_n, the deformation gradient $\boldsymbol{F}_{n+1}$ and the temperature distribution θ_{n+1} at time t_{n+1} determines the mechanical dissipation $\mathcal{D}_{\text{mech}}$ as

$$\mathcal{D}_{\text{mech},n+1} = \hat{\mathcal{D}}_{\text{mech}}(\boldsymbol{F}_{n+1}, \theta_{n+1}, \boldsymbol{\alpha}_n). \tag{4.44}$$

- **Gough-Joule effect.** Considering a time increment $[t_n, t_{n+1}]$ and given the set $\boldsymbol{\alpha}_n$ of internal variables at t_n, the deformation gradient $\boldsymbol{F}_{n+1}$ and the temperature distribution θ_{n+1} at time t_{n+1} determines the Gough-Joule effect $\mathcal{H}^{\text{ep}}$ as

$$\mathcal{H}^{\text{ep}}_{n+1} = \hat{\mathcal{H}}^{\text{ep}}(\boldsymbol{F}_{n+1}, \theta_{n+1}, \boldsymbol{\alpha}_n). \tag{4.45}$$

Generally, the numerical constitutive laws are nonlinear and path-independent within one increment.

Making use of the aforementioned time discretization, one can state the weak form of the mechanical constitutive initial boundary value problem in the material description as

Problem 4.4 | Material incremental thermo-mechanical initial BVP.

Given the set of internal variables $\boldsymbol{\alpha}_n$ at t_n, the prescribed body and traction force fields $\boldsymbol{b}_{0,n+1}$ and $\boldsymbol{t}_{0,n+1}$, as well as, the prescribed heat sources, $\boldsymbol{r}_{n+1}$ and heat fluxes, $h_{0,n+1}$, at t_{n+1}, and the prescribed deformation gradient $\boldsymbol{F}_{n+1}$ and temperature distribution θ_{n+1} at t_{n+1}, find the kinematically admissible displacement field $\boldsymbol{u}_{n+1} \in \mathscr{K}_{u,n+1}$ and the admissible temperature distribution $\theta_{n+1} \in \mathscr{K}_{\theta,n+1}$ such that the body $\mathscr{B}$ is in mechanical and energetic equilibrium

$$\int_{\Omega_0} [\hat{\boldsymbol{P}}(\boldsymbol{F}(\boldsymbol{u}_{n+1}), \theta_{n+1}, \boldsymbol{\alpha}_n) : \nabla_0 \boldsymbol{\eta} - (\boldsymbol{b}_{0,n+1} - \rho_0 \ddot{\boldsymbol{u}}_{n+1}) \cdot \boldsymbol{\eta}] \, \mathrm{d}v - \int_{\partial\Omega_0} \boldsymbol{t}_{0,n+1} \cdot \boldsymbol{\eta} \, \mathrm{d}a = 0, \quad \forall \boldsymbol{\eta} \in \mathscr{V}_{u,n+1}, \tag{4.46}$$

$$\int_{\Omega_0} \left[\left(\rho_0 C_\mathrm{V} \dot{\theta}_{n+1} - \hat{\mathcal{D}}_\mathrm{mech}(\boldsymbol{F}(\boldsymbol{u}_{n+1}), \theta_{n+1}, \boldsymbol{\alpha}_n) - \hat{\mathcal{H}}^\mathrm{ep}(\boldsymbol{F}(\boldsymbol{u}_{n+1}), \theta_{n+1}, \boldsymbol{\alpha}_n) - \rho_0 r_{n+1} \right) \xi - \boldsymbol{q}_{0,n+1} \cdot \nabla_0 \xi \right] \mathrm{d}v - \int_{\partial\Omega_0} \hat{h}_{0,n+1} \xi \, \mathrm{d}a = 0, \quad \forall \xi \in \mathscr{V}_{\theta,n+1}, \tag{4.47}$$

where

$$\mathscr{K}_{u,n+1} \equiv \{\boldsymbol{u} : \Omega \times \mathscr{R} \to \mathscr{U} \mid \boldsymbol{u}_{n+1}(\boldsymbol{X}) = \boldsymbol{u}_{\mathrm{presc},n+1}(\boldsymbol{X}),\ \boldsymbol{X} \in \partial\Omega_{\mathrm{motion},0}\}, \tag{4.48}$$

$$\mathscr{K}_{\theta,n+1} \equiv \{\boldsymbol{u} : \Omega \times \mathscr{R} \to \mathscr{R} \mid \theta_{n+1}(\boldsymbol{X}) = \theta_{\mathrm{presc},n+1}(\boldsymbol{X}),\ \boldsymbol{X} \in \partial\Omega_{\mathrm{temperature},0}\}. \tag{4.49}$$

4.2 Finite Element Method

It is now possible to apply the finite element method to discretize spatial the incremental thermo-mechanical initial boundary value problem. The approach is entirely similar to the one present in the context of the strictly mechanical (see Section **??**) and strictly thermal (see Section **??**) problems. As such, some details are omitted.

4.2.1 Interpolation

Defining the global vector of nodal displacements $\mathbf{u}$ and the global vector of nodal temperatures Θ, like before, as

$$\mathbf{u}(t) = \left[u_1^1(t), \ldots, u_{n_\mathrm{dim}}^1(t), \ldots, u_1^{n_\mathrm{points}}(t), \ldots, u_{n_\mathrm{dim}}^{n_\mathrm{points}}(t) \right]^T, \tag{4.50}$$

$$\Theta(t) = \left[\theta^1(t), \theta^2(t), \ldots, \theta^{n_\mathrm{points}}(t) \right]^T, \tag{4.51}$$

the displacement $\boldsymbol{u}(\boldsymbol{X}, t)$ and temperature $\theta(\boldsymbol{X}, t)$ fields defined over the global domain Ω_0, can be found at any point $\boldsymbol{X}$ as

$$^h\boldsymbol{u}(\boldsymbol{X}, t) \equiv \mathbf{N}^{g,u}(\boldsymbol{X})\mathbf{u}(t), \quad {}^h\boldsymbol{u} \in {}^h\mathscr{K}_u, \tag{4.52}$$

$$^h\theta(\boldsymbol{X}, t) \equiv \mathbf{N}^{g,\theta}(\boldsymbol{X})\Theta(t), \quad {}^h\boldsymbol{\theta} \in {}^h\mathscr{K}_\theta, \tag{4.53}$$

where $\mathbf{N}^{g,u}$ and $\mathbf{N}^{g,\theta}$ are the global interpolation matrices with appropriate dimensions given the dimensions of $\mathbf{u}$ and θ. The global shape functions used to interpolate between the nodal values of the displacement and the temperature can even be different if need be.

4.2.2 Spatial discretization

The application of finite element discretization to the mechanical part of the incremental thermo-mechanical constitutive initial boundary value problem is exactly the same as the one presented in Section **??** for the strictly mechanical problem, as the the equation to be discretized is the same On the other hand, applying the discretization to the thermal part of the incremental thermo-mechanical constitutive initial boundary value problem, yields

$$\int_{{}^h\Omega_0} \left[\left(\rho_0 C_V \mathbf{N}^{g,\theta} \dot{\theta}_{n+1} - \hat{\mathcal{D}}_{\text{mech}} - \hat{\mathcal{H}}^{\text{ep}} - \rho_0 r_{n+1} \right) \cdot \mathbf{N}^{g,\theta} \xi - \boldsymbol{q}_{0,n+1} \cdot \mathbf{H}^{g,\theta} \xi \right] \mathrm{d}v - \int_{{}^h\partial\Omega_0} h_{0,n+1} \mathbf{N}^{g,\theta} \xi \, \mathrm{d}a = 0, \quad \forall \xi \in {}^h\mathcal{V}_\theta, \tag{4.54}$$

where $\mathbf{H}^{g,\theta}$ is the discrete global gradient operator for scalars, defined in Equation (**??**).

Equation (4.55) can be rewritten as

$$\left\{ \int_{{}^h\Omega_0} \left[\mathbf{N}^{g,\theta\,T} \left(\rho_0 C_V \mathbf{N}^{g,\theta} \dot{\theta}_{n+1} - \hat{\mathcal{D}}_{\text{mech}} - \hat{\mathcal{H}}^{\text{ep}} - \rho_0 r_{n+1} \right) - \mathbf{H}^{g,\theta\,T} \boldsymbol{q}_{0,n+1} \right] \mathrm{d}v - \int_{\partial^h\Omega_0} \mathbf{N}^{g,\theta\,T} h_{0,n+1} \, \mathrm{d}a \right\}^T \xi = 0, \quad \forall \xi \in {}^h\mathcal{V}_\theta, \tag{4.55}$$

and, since it must be satisfied for any $\xi \in {}^h\mathcal{V}_\theta$, the incremental discretized thermo-mechanical constitutive initial boundary value problem can thus be stated in the material description as

Problem 4.5 | Material incremental discretized thermo-mechanical initial BVP.

Given the set of internal variables $\boldsymbol{\alpha}_n$ at t_n, the prescribed body and traction force fields $\boldsymbol{b}_{0,n+1}$ and $\boldsymbol{t}_{0,n+1}$, as well as, the prescribed heat sources and heat flux fields $\boldsymbol{r}_{0,n+1}$ and $h_{0,n+1}$, and both the prescribed deformation gradient $\boldsymbol{F}_{n+1}$ and the prescribed temperature θ_{n+1} at t_{n+1}, find the kinematically admissible nodal displacement field $\boldsymbol{u}_{n+1} \in {}^h\mathcal{K}_{u,n+1}$ and the admissible nodal temperature field $\theta_{n+1} \in {}^h\mathcal{K}_{\theta,n+1}$ such that the body $\mathcal{B}$ is in mechanical and energetic equilibrium

$$\mathbf{M}\ddot{\mathbf{u}}_{n+1} + \mathbf{f}_u^{\text{int}}(\theta_{n+1}, \mathbf{u}_{n+1}) - \mathbf{f}_{u,n+1}^{\text{ext}} = \mathbf{0}, \tag{4.56}$$

$$\mathbf{C}\dot{\theta}_{n+1} + \mathbf{f}_\theta^{\text{int}}(\theta_{n+1}, \mathbf{u}_{n+1}) - \mathbf{f}_{\theta,n+1}^{\text{ext}} = \mathbf{0}, \tag{4.57}$$

where $\mathbf{f}_u^{\text{int}}$ e $\mathbf{f}_{u,n+1}^{\text{ext}}$ are the mechanical global vectors of internal and external forces

defined as

$$\mathbf{f}_u^{\text{int}} \equiv \int_{h\Omega_0} \mathbf{G}^{g,u\,T} \hat{\boldsymbol{P}}(\boldsymbol{F}(\boldsymbol{u}_{n+1}), \theta_{n+1}\boldsymbol{\alpha}_n)\,\mathrm{d}v, \tag{4.58}$$

$$\mathbf{f}_{u,n+1}^{\text{ext}} \equiv \int_{h\Omega_0} \mathbf{N}^{g,u\,T} \mathbf{b}_{0,n+1}\,\mathrm{d}v + \int_{\partial^h\Omega_{\text{traction},0}} \mathbf{N}^{g,u\,T} \mathbf{t}_{0,n+1}\,\mathrm{d}a, \tag{4.59}$$

and $\mathbf{f}_\theta^{\text{int}}$ e $\mathbf{f}_{\theta,n+1}^{\text{ext}}$ the thermal global vectors of internal and external forces defined as

$$\mathbf{f}_\theta^{\text{int}} \equiv \left[\int_{h\Omega_0} \mathbf{N}^{g,\theta\,T} \hat{\mathscr{D}}_{\text{mech}}(\boldsymbol{F}(\boldsymbol{u}_{n+1}), \theta_{n+1}\boldsymbol{\alpha}_n) + \mathbf{N}^{g,\theta\,T} \hat{\mathcal{H}}^{\text{ep}}(\boldsymbol{F}(\boldsymbol{u}_{n+1}), \theta_{n+1}\boldsymbol{\alpha}_n) \right.$$
$$\left. \mathbf{H}^{g,\theta\,T} \boldsymbol{q}_0(\boldsymbol{F}(\boldsymbol{u}_{n+1}), \theta_{n+1}) \right] \mathrm{d}v, \tag{4.60}$$

$$\mathbf{f}_{\theta,n+1}^{\text{ext}} \equiv \int_{h\Omega_0} \mathbf{N}^{g,\theta\,T} \mathbf{r}_{0,n+1}\,\mathrm{d}v + \int_{\partial^h\Omega_{\text{heat},0}} \mathbf{N}^{g,\theta\,T} h_{0,n+1}\,\mathrm{d}a. \tag{4.61}$$

The mass matrix $\mathbf{M}$ and the thermal capacitance matrix $\mathbf{C}$ are defined by

$$\mathbf{M} = \int_{h\Omega_0} \rho_0 \mathbf{N}^{g,u\,T} \mathbf{N}^{g,u}\,\mathrm{d}v, \tag{4.62}$$

$$\mathbf{C} = \int_{h\Omega_0} \rho_0 C_{\text{V}} \mathbf{N}^{g,\theta\,T} \mathbf{N}^{g,\theta}\,\mathrm{d}v. \tag{4.63}$$

The global vectors for the internal and external forces are usually obtained by assemblage of their elemental counterparts as

$$\mathbf{f}_u^{\text{int}} = \mathop{\mathsf{A}}_{e=1}^{n_{\text{elem}}} \left(\mathbf{f}_u^{\text{int}}\right)^{(e)}, \tag{4.64}$$

$$\mathbf{f}_u^{\text{ext}} = \mathop{\mathsf{A}}_{e=1}^{n_{\text{elem}}} \left(\mathbf{f}_u^{\text{ext}}\right)^{(e)}, \tag{4.65}$$

$$\mathbf{f}_\theta^{\text{int}} = \mathop{\mathsf{A}}_{e=1}^{n_{\text{elem}}} \left(\mathbf{f}_\theta^{\text{int}}\right)^{(e)}, \tag{4.66}$$

$$\mathbf{f}_\theta^{\text{ext}} = \mathop{\mathsf{A}}_{e=1}^{n_{\text{elem}}} \left(\mathbf{f}_\theta^{\text{ext}}\right)^{(e)}, \tag{4.67}$$

where the mechanical elemental vectors in the material description are defined as

$$\mathbf{f}_u^{\text{int}} \equiv \int_{h\Omega_0^{(e)}} \mathbf{G}^{u\,T} \hat{\boldsymbol{P}}(\boldsymbol{F}(\boldsymbol{u}_{n+1}), \theta_{n+1}\boldsymbol{\alpha}_n)\,\mathrm{d}v, \tag{4.68}$$

$$\mathbf{f}_{u,n+1}^{\text{ext}} \equiv \int_{h\Omega_0^{(e)}} \mathbf{N}^{u\,T} \mathbf{b}_{0,n+1}\,\mathrm{d}v + \int_{\partial^h\Omega_{\text{traction},0}^{(e)}} \mathbf{N}^{u\,T} \mathbf{t}_{0,n+1}\,\mathrm{d}a, \tag{4.69}$$

and the thermal vectors, also in the material description, are

$$\mathbf{f}_{\theta}^{\text{int}} \equiv \left[\int_{{}^{h}\Omega_0^{(e)}} \mathbf{N}^{\theta\,T} \hat{\mathscr{D}}_{\text{mech}}(\boldsymbol{F}(\boldsymbol{u}_{n+1}), \theta_{n+1}\boldsymbol{\alpha}_n) + \mathbf{N}^{\theta\,T} \hat{\mathcal{H}}^{\text{ep}}(\boldsymbol{F}(\boldsymbol{u}_{n+1}), \theta_{n+1}\boldsymbol{\alpha}_n) \right.$$
$$\left. \mathbf{H}^{\theta\,T} \boldsymbol{q}_0(\boldsymbol{F}(\boldsymbol{u}_{n+1}), \theta_{n+1}) \right] \mathrm{d}v, \tag{4.70}$$

$$\mathbf{f}_{\theta,n+1}^{\text{ext}} \equiv \int_{{}^{h}\Omega_0^{(e)}} \mathbf{N}^{\theta\,T} \mathbf{r}_{0,n+1}\,\mathrm{d}v + \int_{\partial {}^{h}\Omega_{\text{heat},0}^{(e)}} \mathbf{N}^{\theta\,T} h_{0,n+1}\,\mathrm{d}a. \tag{4.71}$$

The elemental mechanical interpolation of the matrices $\mathbf{N}^{u}$, $\mathbf{B}^{u}$, $\mathbf{N}^{\theta}$ and $\mathbf{H}^{\theta}$ are the elemental mechanical interpolation matrix, the mechanical discrete elemental gradient operator, the elemental thermal interpolation matrix, and the thermal discrete elemental gradient operator for scalars.

In a similar manner, the global mass and capacitance matrices are also usually obtained by assemblage of their elemental counterparts as

$$\mathbf{M} \equiv \mathop{\mathsf{A}}_{e=1}^{n_{\text{elem}}} \mathbf{M}^{(e)}, \tag{4.72}$$

$$\mathbf{C} \equiv \mathop{\mathsf{A}}_{e=1}^{n_{\text{elem}}} \mathbf{C}^{(e)}, \tag{4.73}$$

where the elemental mass matrices in the material description are defined as

$$\mathbf{M}^{(e)} = \int_{{}^{h}\Omega^{(e)}} \rho_0 \mathbf{N}^{u\,T} \mathbf{N}^{u}\,\mathrm{d}v, \tag{4.74}$$

and the elemental thermal capacitance matrices, also in the material description, are defined as

$$\mathbf{C}^{(e)} = \int_{{}^{h}\Omega^{(e)}} \rho_0 C_{\text{V}} \mathbf{N}^{\theta\,T} \mathbf{N}^{\theta}\,\mathrm{d}v, \tag{4.75}$$

4.3 Linearisation

The equilibrium equation, Equation (2.42) in a spatial description and Equation (3.25) in a material description, is generally nonlinear due to geometrical and/or material nonlinearities. The Newton-Raphson Method is an efficient and robust iterative scheme with a quadratic convergence rate often used to solve the equilibrium equation at each time increment, t_n. The residual of the fully discretized balance of linear momentum is defined for an iteration step i of the Newton-Raphson method as

$$\mathbf{r}(\mathbf{u}_{n+1}^{i}) = \mathbf{M}\ddot{\mathbf{u}}_{n+1}^{i} + \mathbf{f}^{\text{int}}(\mathbf{u}_{n+1}^{i}) - \mathbf{f}_{n+1}^{\text{ext}}. \tag{4.76}$$

A Taylor expansion about the current solution $\mathbf{u}_{n+1}^{i}$ is performed, discarding all terms of higher order than one, yielding the linearised form

$$\text{Lin}\,\mathbf{r}(\mathbf{u}_{n+1}^{i}) = \mathbf{r}(\mathbf{u}_{n+1}^{i}) + \underbrace{\left.\frac{\partial \mathbf{r}(\mathbf{u}_{n+1})}{\partial \mathbf{u}_{n+1}}\right|^{i}}_{\mathbf{K}(\mathbf{u}_{n+1}^{i})} \delta\mathbf{u}. \tag{4.77}$$

with the dynamic effective tangential stiffness matrix $\mathbf{K}(\mathbf{u}^i_{n+1})$. The linearisation of the internal forces included in $\mathbf{K}$ is known as the tangential stiffness matrix $\mathbf{K}_T$, which is defined as

$$\mathbf{K}^i_T = \left.\frac{\partial \mathbf{f}^{\text{int}}}{\partial \mathbf{u}_{n+1}}\right|^i . \tag{4.78}$$

Equilibrium is achieved if

$$\text{Lin}\,\mathbf{r}(\mathbf{u}^i_{n+1}) = \mathbf{0}, \tag{4.79}$$

so that a linear system of equation is given by

$$\mathbf{K}(\mathbf{u}^i_{n+1})\delta\mathbf{u} = -\mathbf{r}\left(\mathbf{u}^i_{n+1}\right). \tag{4.80}$$

Thus, a new solution of the displacement increment $\delta\mathbf{u}$ for current iteration step $i+1$ is determined, and the final displacement solution of time step $n+1$ is obtained via updating

$$\mathbf{u}^{i+1}_{n+1} = \mathbf{u}^i_{n+1} + \delta\mathbf{u}. \tag{4.81}$$

A solution of t_{n+1} is found, i.e. an equilibrium state is reached and $\mathbf{u}_{n+1} = \mathbf{u}^{i+1}_{n+1}$, if prescribed, user-defined convergence criteria are fulfilled.

Correção do TPC de DT

Chapter 5

Solution procedures for coupled fields

This chapter presents an overview of solution procedures for coupled fields. It includes techniques applied to various coupled field problems, such as thermomechanical coupling, fluid-structure interaction, and aeroelasticity. Its goal is to support the choice of solution techniques for thermo-plastic problems, which are accurate, stable, efficient, both in terms of memory and computational time, and easy to implement and extend later to further couplings, e.g., electro-thermomechanical problems.

5.1 Context field elimination

Field elimination achieves the solution of a coupled problem by eliminating the variables of the first field and introducing them into the second field. This second field is then solved.

The main advantage of this procedure is the reduction of the number of state variables. Which in turn, leads to smaller systems of equations, which are presumably easier to solve. Furthermore, the analyst can choose the remaining variables such that they are the variables of interest. In this way, the variables eliminated do not need to be recovered. (Felippa and Park, 1980)

On the other hand Felippa and Park (1980) cite as disadvantages

- only possible for problems allowing explicit (and well-conditioned) variable eliminations;
- sparseness and symmetry attributes of matrices associated with the original coupled system can be adversely affected by the eliminations process; and
- available software modules for the isolated fields are not likely to be of much use for processing the reduced system.

The remainder of the chapter disregards these procedures, including in Section **??** where the comparison of the different schemes is discussed.

5.2 Monolithic

Monolithic algorithms solve the coupled nonlinear multi-physics system simultaneously. Predominantly, implicit schemes are applied to achieve good stability properties. In turn, the nonlinear residual equations are often solved using the Newton-Raphson method. A particular challenge for monolithic algorithms is the efficient solution of the large system of equations, including potential nonlinearities or lack of symmetry. Even the units chosen can contribute to the ill-conditioning of the system matrix. One essential aspect for efficient solvers for large-scale problems is a good preconditioning technique.

5.2.1 Numerical considerations

For the solution of a large system of equations, iterative methods are preferable to direct methods, in part, due to memory footprint considerations. The Newton-Krylov methods such as GMRES and the BiCGStab are among the most commonly used in multi-physics problems (Hron and Turek, 2006). However, their use does not suffice for an efficient and robust solution procedure for a multi-physics problem. In addition, the use of preconditioners alleviates the possible large condition numbers of the system matrix. There are several preconditioning techniques for the solution of large systems of equations, e.g., ILU preconditioners, domain decomposition, including multigrid approaches; multilevel recursive Schur complements preconditioners (see Smith et al. (2004) and Chen (2005)).

Heil (2004) is concerned with the fully coupled solution of large-displacement fluid-structure interaction problems by Newton's method. They use block-triangular approximations of the Jacobian matrix, obtained by neglecting selected fluid-structure interaction blocks, and show that they provide suitable preconditioners for the solution of the linear systems with GMRES. A Schur complement approximation for the Navier-Stokes block and multigrid approximations for the solution of the computationally most expensive operations is the basis for the efficient approximate implementation of the preconditioners.

Hron and Turek (2006) propose a method based on a fully implicit, monolithic formulation of the problem in the arbitrary Lagrangian-Eulerian framework to solve the problem of fluid-structure interaction of an incompressible elastic object in laminar incompressible viscous flow They utilize the standard geometric multigrid approach based on a hierarchy of grids obtained by successive regular refinement of a given coarse mesh. The complete multigrid iteration is performed in the standard defect-correction setup with the V or F-type cycle.

Tezduyar et al. (2006) show how preconditioning techniques more sophisticated than diagonal preconditioning can be used in iterative solutions of the linear equation systems in fluid-structure interaction problems.

In Gee et al. (2011), the authors focus on the strong coupling fluid-structure interaction employing monolithic solution schemes. Therein, a Newton-Krylov method is applied to the monolithic set of nonlinear equations. They propose two preconditioners that apply algebraic multigrid techniques to the entire fluid-structure interaction system of equations. As the first option, the authors employ a standard block Gauss-Seidel approach, where approximate inverses of the individual field blocks are based on an algebraic multigrid hierarchy tailored for the type of the underlying physical problem. A monolithic coarsening scheme for the coupled system that uses prolongation and restriction projections constructed for the individual fields

provides the basis for the second preconditioner. The resulting nonsymmetric monolithic algebraic multigrid method involves coupling the fields on coarse approximations to the problem yielding significantly enhanced performance, claim the authors.

In the context of multi-physics problems, Lin et al. (2010) propose a fully coupled algebraic multilevel preconditioner for Newton-Krylov solution methods. A set of multi-physics partial differential equation (PDE) applications attests its performance: a drift-diffusion approximation for semiconductor devices, a low Mach number formulation for the simulation of coupled flow, transport, and non-equilibrium chemical reactions, a low Mach number formulation for visco-resistive magnetohydrodynamics (MHD) systems. An aggressive-coarsening graph-partitioning of the non-zero block structure of the Jacobian matrix provides the basis for the algebraic multilevel preconditioner. Using a different approach Badia et al. (2014) employ a new family of recursive block LU preconditioners to solve the thermally coupled induction less magnetohydrodynamics problem equations, which model the flow of an electrically charged fluid under the influence of an external electromagnetic field with thermal coupling.

Netz (2013) addresses a thermo-mechanically coupled problem of thermo-viscoelasticity at finite strains using a monolithic approach. The authors solve the system of nonlinear algebraic equations obtained from the spatial (FEM) and temporal (diagonally-implicit Runge-Kutta methods) discretization of the problem monolithically. They employ the Multilevel-Newton algorithm to obtain a high-order result in the space and the time domain. The numerical concept is applied to a constitutive model of finite strain thermo-viscoelasticity. Rothe et al. (2015) also employ in the context of thermo-viscoelasticity, the multilevel Newton algorithm to solve the system of algebraic equations describing the discretized problem.

Danowski et al. (2013) presents a monolithic solution scheme for thermo-structure interaction problem, using right preconditioning and a GMRES. The preconditioner "sub-problem" is solved using a Richardson iteration scheme and a relaxed block Gauss-Seidel method, which uncouples the mechanical and thermal problems. This procedure tackles each problem using an independent algebraic multigrid (AMG) preconditioner. Verdugo and Wall (2016) also considers the procedure just mentioned, as well as a preconditioner based on a semi-implicit method for pressure-linked equations, extended to deal with an arbitrary number of fields. This technique also results in uncoupled problems that can be solved with standard AMG. They also introduce a more sophisticated preconditioner that enforces the coupling at all AMG levels, unlike the other two techniques, which resolve the coupling only at the finest level. These techniques are applied successfully to three different coupled problems: thermo-structure interaction, fluid-structure interaction, and a complex model of the human lung.

Mayr et al. (2020) propose a hybrid interface preconditioner for the monolithic solution of surface-coupled problems. They combine physics-based block preconditioners with an additional additive Schwarz preconditioner, whose subdomains span across the interface on purpose. This approach is motivated by the error assessment of physics-based block preconditioners, revealing an accumulation of the error at the coupling surface, despite their overall efficiency.

5.2.2 Usage examples

Thermo-mechanical coupling In the following paragraph, a small overview of the literature is presented regarding the application of monolithic solvers to the thermo-mechanical coupled problem. Carter and Booker (1989) suggests a monolithic approach to the thermoelastic problem at small strains. The constitutive laws considered do not acknowledge the dependence of the mechanical properties on the temperature and are not deduced from a Helmholz energy function. Glaser (1992) uses monolithic algorithms for the calculation of thin-walled structures using shell elements and an arc-length method for the TSI solution. While all coupling terms were considered, only a simplified mechanical dissipation was included where the hardening power was neglected (according to Danowski (2014)). Ibrahimbegovic and Chorfi (2002) presents a thermoplasticity covariant formulation within the framework of the principal axis methodology, which the authors claim, leads to a very efficient numerical implementation. The paper contains several numerical simulations dealing with the fully coupled thermomechanical response at large viscoplastic strains, including strain localization and cyclic loading cases, to illustrate the performance of the proposed methodology. The authors consider the von Mises thermoplasticity yield criterion and strain energy depending on logarithmic stretches, a hardening variable, and temperature. A monolithic solver achieves the solution to the coupled problem, but no details about it are given. Danowski (2014) proposes a volume-coupled TSI model based on the finite element method for the structural and thermal field. Various temperature-dependent, isotropic, elastic, and elastoplastic material models for small and finite strains are employed, incorporating the effect of the highly elevated temperatures predominating in rocket nozzles, the practical application focused in the Ph.D. thesis. The author considers both monolithic and partitioned coupling algorithms to solve fully coupled thermomechanical systems. Regarding the former, a novel monolithic Newton-Krylov scheme with problem-specific block Gauss-Seidel preconditioner and algebraic multigrid methods is introduced. Concerning the latter, loosely and strongly coupled partitioned schemes are examined, possibly including acceleration techniques, as, e.g., the Aitken Δ^2 method. Netz (2013) and Rothe et al. (2015) both present monolithic approaches, based on the multilevel Newton method, for the solution of the thermo-mechanical problem. In both contributions, thermo-visco-plastic materials are successfully analyzed. Recently, Felder et al. (2021) have presented a finite strain thermo-mechanically coupled two-surface damage-plasticity theory. The authors obtain the solution for the three coupled fields, displacement, nonlocal damage variable, and temperature, employing an implicit and monolithic solution scheme.

The thermo-mechanical coupling has also been studied in the more specific domain of contact mechanics. Zavarise et al. (1992) present one of the earliest contributions in this direction. They propose a FEM formulation of frictionless contact, accounting for full thermo-elastic coupling. The penalty method is used to enforce the non-penetration conditions. Another contribution, Hansen (2011), advances a standard mortar discretization with Lagrange multipliers to solve the small strain thermo-elasticity problem. The authors consider the heat equation coupled to linear mechanics through a thermal expansion term in their formulation. The solution approach is based on a preconditioned Jacobian-free Newton Krylov solution method, and the use case under analysis is a light water reactor nuclear fuel rod. Dittmann et al. (2014) investigate thermomechanical mortar contact algorithms and their application to NURBS-based Isogeometric Analysis in the context of nonlinear

elasticity. Mortar methods are applied to both the mechanical and thermal fields to model frictional contact, the energy transfer between the surfaces, and frictional heating. A monolithic approach is pursued in solving the nonlinear algebraic equations found after the discretization in time and space. In the Ph.D. thesis by the same first author, Dittmann (2017), this approach is further pursued in multi-field contact problems. More recently, Seitz et al. (2018); Seitz (2019) tackles the numerical treatment of contact problems considering inelastic deformation and thermomechanical coupling. It accounts for plastic spin, visco-plasticity, and thermo-plastic coupling, as well as temperature-dependent material parameters. The authors also opt for a monolithic solver, although no further details are supplied. See also, in the context of contact mechanics, Oancea and Laursen (1997); Pantuso et al. (2000); Hüeber and Wohlmuth (2009); Hesch and Betsch (2011); Gitterle (2012) and Novascone et al. (2015).

Others In the context of fluid-structure interaction, the monolithic approach seems to be more widely used than in thermo-mechanically coupled problems. A few contributions in this domain using a monolith approach are Blom (1998); Heil (2004); Hübner et al. (2004); Michler et al. (2004); Zhang and Hisada (2004); Dettmer and Perić (2006); Hron and Turek (2006); Tezduyar et al. (2006); Küttler et al. (2010); Gee et al. (2011); Klöppel et al. (2011); Mayr et al. (2015) and Mayr et al. (2020). The use of a monolithic approach can also be found in the domain of saturated soils (e.g., Lewis and Sukirman (1993), Borja et al. (1998), Jha and Juanes (2007), White and Borja (2008)). Monolithic solvers are also used in the context of magnetohydrodynamics (e.g., Shadid et al. (2010) and Badia et al. (2014)).

5.3 Partitioned

The following Section presents the partitioned time-stepping algorithms. For a detailed comparison with the monolithic approach and between themselves, see Section **??**.

A field partition is a field-by-field decomposition of the space discretization. Partitioning may be algebraic or differential. In algebraic partitioning, the complete coupled system is spatially discretized first and then decomposed. In differential partitioning, the decomposition is done first, and each field is then discretized separately. Differential partitioning often leads to non-matched meshes, as typical of fluid-structure interaction. Algebraic partitioning was initially developed for matched meshes and substructuring (Felippa et al., 2001).

The earliest contributions regarding the partitioned treatment of coupled systems emerged in the mid 1970s, involving structure-structure interactions and fluid-structure interactions (see e.g. Belytschko and Mullen (1976), Park et al. (1977), Belytschko and Mullen (1978), Hughes and Liu (1978) and Belytschko et al. (1979)).

Given a complex system, there are usually many ways of partitioning it into subsystems or fields. Felippa and Park (1980) provide a very pragmatic and helpful criterion to select the fields to be considered. According to their definition, a field is characterized by computational considerations. It is a segment of the overall problem for which a separable software module is either available or readily prepared if the interaction terms are suppressed. As such, a partitioned approach to the solution of multi-physics problems employs field analyzers specific to each field separately stepped in time. The coupling between the fields is achieved through proper

communication between the individual components using prediction, substitution, and synchronization techniques.

Before moving on, it may be helpful to clear up the difference between partitioned schemes, staggered schemes, operator splits, and fractional-step methods. The first is probably the most general term and includes the others. Its definition has already been given. A staggered scheme is a term most often used for the partitioned schemes where the solution concerning each field is sequential and obtained only once per time step as in the loosely coupled schemes to be introduced. However, it may also include the strongly coupled schemes, as well. An operator split is obtained through the decomposition of the fully coupled problem into subproblems. The structure of the problem is the same, as well as the unknowns considered. The only difference between the subproblems is the physical effects considered. The equation terms concerning each physical effect must be divided exclusively and exhaustively between the subproblems. Finally, according to Armero and Simo (1992) staggered algorithms for coupled problems can be viewed as fractional steps methods, in the sense of Holt and Yanenko (2012), arising from an operator split of the coupled problem of evolution.

5.3.1 Operator splits

The most common operator splits into thermomechanical problems are the isothermic and adiabatic split.

Isothermic The isothermic split is perhaps the most straightforward and natural approach, as noted by Argyris and Doltsinis (1981), one of the earliest contributions on the topic. The scheme achieves the solution of the thermo-mechanical problem, first solving the mechanical problem at a constant temperature, then a purely thermal phase is considered at a fixed configuration.

Adiabatic The adiabatic split is proposed in Armero and Simo (1992). It consists of a first phase where constant entropy is enforced and a second phase of purely thermal conduction with a fixed reference. In terms of implementation complexity, it is comparable to the isothermal split. This is possible because the constant entropy phase can be cast as a mechanical phase, where the stiffness and the external force are adjusted as a function of an intermediate temperature. This temperature is computed considering the strong form of the temperature evolution equation to retain the computational efficiency of the isothermal split, despite the momentum equation being enforced in its weak form. The advantage of this split is that when used in a staggered scheme, it is unconditionally stable (see Section **??**).

5.3.2 Loosely vs. Strongly coupled schemes

According to Felippa et al. (2001) there are several basic techniques associated with partitioned schemes (see Figure 5.1). These are

- preditction;
- substitution;
- interfield iteration;

- full step correction;
- lockstep advancing;
- midpoint correction;
- subcycling;
- augmentation.

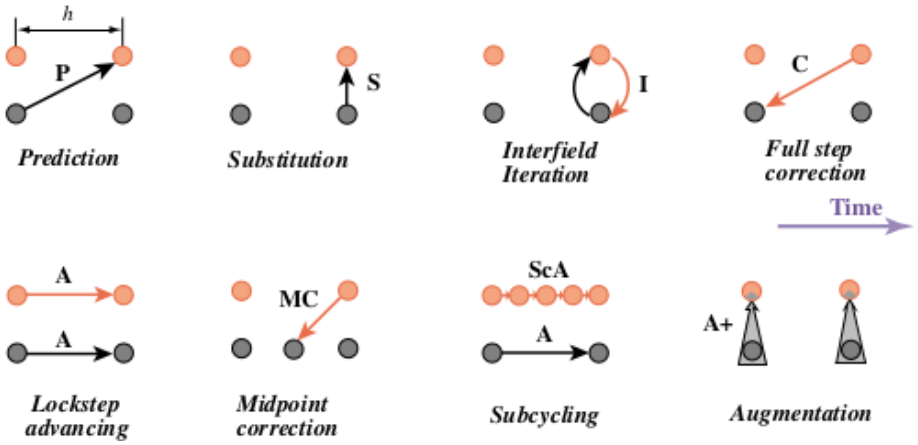

Figure 5.1: Devices of partitioned analysis time-stepping (Felippa et al., 2001).

Inter-field iterations are the primary criterion distinguishing loosely or one-way staggered coupled schemes and strongly or iterative staggered coupled schemes. In the loosely coupled schemes, the integration algorithm proceeds sequentially, solving the problem in each field only once per time step. On the other hand, for strongly coupled schemes, inter-field iterations are present, such that the problems are solved multiple times at the same time instant. This inner loop is repeated until a given tolerance is reached for the unknowns in each field.

The remainder of the techniques listed will be mentioned and explained in the discussion below.

5.3.3 Loosely coupled

The solution for the fully coupled problem is found in loosely coupled schemes by solving each field sequentially. For the thermomechanical problem, the two available schemes are the isothermal split (see e.g. Simo and Armero (1992), Agelet de Saracibar (1998)) and the adiabatic split (see e.g. Armero and Simo (1992) and Armero and Simo (1993)), as mentioned above.

According to Felippa et al. (2001), in linear problems, the first concern with partitioning is the degradation of time-stepping stability. After the analyst has ensured stability, an accuracy analysis of the method should be performed. In strongly nonlinear problems, such as fluid flow, stability and accuracy tend to be intertwined since numerical stability is harder to define. As such, they are usually considered together in method design. The expectation is for a method that operates well at a reasonable timestep.

Felippa and Geers (1988) present a detailed explanation about how to design from scratch a loosely coupled time-stepping algorithm applicable to linear systems of equations. It includes implementation details, such as the choice of the predictor formula, and the design steps, from the formulation of the original field equations and temporal discretization to the stability and accuracy analysis. Other contributions focused mainly on linear systems are Neishlos (1983), Zienkiewicz et al. (1988) and Combescure and Gravouil (2002),

Because the loosely coupled schemes are explicit, they are also often only conditionally stable. The isothermic split is such an example (Armero and Simo, 1992). On the other hand, the adiabatic split proposed in Armero and Simo (1992) is unconditionally stable, despite being explicit. Farhat et al. (1991) also propose a stable staggered scheme, achieved through semi-algebraic augmentation, which, however, is limited to linearized thermoelasticity. In the context of coupled flow and geomechanics, Kim et al. (2011b) show that when the mechanical problem is solved first, the drained split combined with a backward Euler discretization is conditionally stable, and the undrained split is unconditionally stable when combined with midpoint rule. When instead the flow problem is solved first, Kim et al. (2011a) show that the fixed-stress split is conditionally and the fixed-strain split is unconditionally stable for appropriate choices of the generalized midpoint rule.

Moreover, in the domain of fluid-structure interactions, it can be shown that staggered methods are inherently non-conservative. As time progresses in the simulation, these schemes introduce parasitic energy at the boundary, which contributes to their poor numerical stability (Michler et al., 2003). A further problem appears when solving these coupled physical problems, the so-called artificial added-mass effect, which leads to instability. It manifests itself when a slender structure and fluid have similar densities, and the latter is modeled as an incompressible fluid (Causin et al., 2005; Förster, 2007). It can even be shown that for every sequentially staggered scheme and spatial discretization of a problem, a mass ratio between the fluid and structural mass density can be found at which the coupled system becomes unstable (Förster et al., 2007).

Despite this, some contributions detail strategies allowing for the unconditional stability of these schemes. As part of the development loop of commercial tire designs, Gillard (2019) tackles the problem of tire hydroplaning. The author presents a robust explicit coupling scheme that relies on rigorous control of the energy artificially introduced at the interface by the staggering process through a dynamic adaptation of the coupling time step size. Regarding the artificial added-mass effect, Farhat et al. (2010) demonstrates that even for fluid-structure applications with strong added mass effects, a carefully designed staggered and sub-iteration-free time-integrator can achieve numerical stability and robustness concerning the slenderness of the structure, as long as the fluid is justifiably modeled as a compressible medium.

Another technique available to improve the stability of loosely coupled schemes is (algebraic) augmentation. It rests on the injection of one of the coupled equations into the other, after discretization in space, to 'soften' the system, either by reducing the large eigenvalues of the uncoupled stiff equation or by introducing some damping into it. Some examples of this approach include Park et al. (1977) and Park (1983).

Yet another technique to ensure stability in the context of fluid-structure interactions is presented in Fernández et al. (2006). Stability is achieved employing a semi-implicit coupling scheme, splitting the added-mass, viscous effects, and geometrical/convective nonlinearities, through a Chorin-Temam projection scheme

within the fluid.

Regarding accuracy, the loosely coupled schemes do not necessarily inherit the accuracy order of the schemes used in the integration of the separate fields, often being just of the first order in time (Farhat et al., 2006). However, some contributions detail approaches that are second-order time-accurate. In the context of thermo-elasticity, Armero and Simo (1992) show that a double-pass approach using the adiabatic split yields such a second-order accurate time-stepping algorithm. A few approaches yield similar results in the domain of fluid-structure interaction (see Piperno (1997), Farhat et al. (2006) and Farhat et al. (2010)). In any case, whatever the theoretical convergence order of the loosely coupled method, at a given time instant, the fully coupled discretized equations of the problem will never be exactly satisfied by the solutions found. There is a lag between the fields considered, e.g., the mechanical and thermal fields in a thermomechanical problem. In the context of strong coupling, this lag can be conceived as a numerical evaluation error. Solving approximately the exact (i.e., aggregated) equations can be reinterpreted as exactly solving a set of approximate (i.e., segregated) equations. Thus, one can construe loosely-coupled methods as solving a set of segregated equations instead of aggregated equations. Accordingly, the incurred numerical evaluation error can be reinterpreted as a discretization error. Loosely-coupled methods, therefore, satisfy conservation only in an asymptotic sense, i.e., for vanishing mesh width; this is a basic consistency requirement Michler (2005).

Prediction techniques can improve the order of the numerical evaluation error incurred by loosely-coupled partitioned methods. For the sake of explanation, consider the thermo-mechanical problem being solved using the isothermic split. When using predictors, instead of integrating the mechanical equations based on the structure's temperature in the previous time instant, a prediction can be used for the temperature of the structure boundary in the current time instant. Such predictions are generally based on an extrapolation of the solution from the previous time step. Prediction techniques improve the solution accuracy and stability of loosely-coupled methods (Piperno, 1997; Piperno and Farhat, 2001; Michler, 2005; Farhat et al., 2006).

Another technique available to improve the accuracy of the loosely coupled methods is subcycling. It involves solving each field's problems using different time steps since the fields present in a multi-physics problem often have different time scales. In the context of aeroelasticity, Piperno et al. (1995) claims that it can offer substantial computational advantages, including savings in the simulation CPU time because the structural field will be advanced fewer times. Farhat et al. (1997) and Piperno (1997) also argue for this technique along the same lines.

Usage examples The loosely coupled scheme has been used in the context of thermoelasticity (Argyris and Doltsinis, 1981; Armero and Simo, 1992; Johansson and Klarbring, 1993; Miehe, 1995a,b; Holzapfel and Simo, 1996), thermo-plasticity (Armero and Simo, 1992, 1993; Simo and Miehe, 1992; Wriggers et al., 1992; Agelet de Saracibar, 1998; Agelet de Saracibar et al., 1999) and thermo-viscoplasticity (Adam and Ponthot, 2002a,b).

For examples in aeroelasticity see e.g., Piperno et al. (1995); Farhat and Lesoinne (2000) and Farhat et al. (2003), and in fluid-structure interaction more broadly see e.g. Tezduyar et al. (2006) and Miller (2015) Other applications include fluid-soil interaction analysis (Saetta and Vitaliani, 1992; Armero, 1999; Mikelić and Wheeler, 2013).

5.3.4 Strongly coupled

In the strongly coupled scheme, inter-field iterations are performed until a given tolerance for the unknowns of each field is reached. They converge to the solution of the monolithic scheme and are thus able to satisfy discrete versions of the coupled problem exactly (Förster, 2007; Danowski, 2014). In principle, regarding thermomechanics, either the isothermal or the adiabatic slit can be used, but there seems to be no example of the latter. In contrast to the staggered schemes, there is no problem of conditional stability, but the scheme may converge very slowly or not at all. As an example coming from fluid-structure interactions, it has been shown that the number of coupling iterations increases when the time step decreases or when the structure becomes more flexible (Degroote et al., 2008). This can place a severe restriction on the use of these schemes. Several acceleration techniques are available in the literature to speed up convergence.

A straightforward way to improve the convergence behavior of the strongly coupled schemes is using predictors, in contrast to the values found in the last step. Thus, the initial guesses can be improved using well-chosen predictors Michler (2005). Along these lines, Erbts and Düster (2012) employs polynomial prediction methods, and Wendt et al. (2015) uses a line extrapolation method to improve the first guess of the unknown and thus decrease the number of iterations needed to achieve convergence.

Another approach that is well established for series acceleration is the Aitken delta-squared process. It uses previously computed values to obtain more accurate estimates for the unknown. Irons and Tuck (1969) is an early contribution detailing this low-memory convergence acceleration scheme. In the context of thermomechanics, Danowski (2014), Erbts et al. (2015) and Wendt et al. (2015) use this technique, with the last authors also employing a quasi-Newton least squares method. Some examples of contributions in the domain of fluid-structure interactions taking advantage of this approach are Degroote et al. (2008), Küttler and Wall (2008) and Küttler and Wall (2009). The last authors also introduce a vector extrapolation approach that includes more than three previous values of the iteration scheme in the improved estimate.

The strongly coupled approach lends itself to an interpretation as a nonlinear block Jacobi or Gauss-Seidel scheme, whose convergence is conditional and at most linear (Matthies and Steindorf, 2003b; Joosten et al., 2009). Cervera et al. (1996) provides an in-depth analysis of block Jacobi and Gauss-Seidel schemes applied to coupled problems, including considerations regarding efficiency, complexity, and parallelization. Matthies and Steindorf (2003a,b) suggests a block-Newton method instead, with the Jacobian of the system being approximate by a finite difference method. Under some assumptions on the subsystem solvers, this approach converges quadratically. Michler et al. (2005) propose a solution method based on the conjugation of sub-iterations via a Newton-Krylov method, which confines the GMRES acceleration to the interface degrees-of-freedom. The latter renders storage requirements for the Krylov space and computational cost of the least-squares problem low. The nesting of Newton and GMRES iterations lends itself to the reuse of Krylov vectors in subsequent linear system solutions. Küttler and Wall (2009) claims that the approach proposed by the last authors should not be regarded as a Newton-based solver but as a Krylov-based vector extrapolation scheme

One can also improve the convergence speed of the strongly coupled scheme using reduced-order models to produce a more accurate first guess and thus decrease the

number of iterations needed for the method to converge. Vierendeels et al. (2007) presents a technique that uses the Jacobian from reduced-order models that are built up during the coupling iterations. The reduced-order model is built for each step and approximates an arbitrary interface displacement fitting a linear regression to the previous displacement-stress points. Degroote et al. (2008) follows the same technique, coupling it with an Aitken delta-squared process.

Blom (2017) proposes a manifold mapping technique to decrease the number of sub-iterations of a high-fidelity fluid-structure interaction model. The idea is to perform many sub-iterations with a low-fidelity model instead of the high-fidelity flow and structure models.

Usage examples Regarding the use of strongly coupled schemes in the context of thermo-mechanics, there are a few contributions. Erbts and Düster (2012) present results concerning thermo-elasticity at finite strains, Netz (2013) concerning thermo-viscoelasticity, Danowski (2014) includes results on thermo-elasticity and thermo-elasto-plasticity. In field of fluid-structure interaction, a few examples of the use of strongly coupled schemes are Torii et al. (2006), Wall et al. (2007) and Blom (2017). Including more than two fields, Erbts et al. (2015) tackles electro-thermo-mechanical problems, as does Wendt et al. (2015), which also considers radiative heat transfer. In Lenarda and Paggi (2016), the strongly coupled scheme is used to solve coupled hygro-thermo-mechanical problems in photovoltaic laminates.

5.4 Comparison of solution techniques

According to Felippa and Geers (1988), the desirable properties of a time-stepping algorithm for solving coupled problems are:

- enjoys unconditional stability;
- is highly accurate;
- is easy to implement;
- is not memory intensive;
- requires low CPU time;
- satisfies software modularity constraints.

In the following, the time-stepping schemes presented above are compared with these criteria in mind. The application in view is thermomechanics.

Stability Regarding stability, the loosely coupled using an isothermal split is conditionally stable (Armero and Simo, 1992). Despite this, the limitation is not significant for metals plasticity, according to Simo and Miehe (1992). However, examples where the scheme diverges, can be found in Armero and Simo (1992). In this last contribution, the adiabatic split is introduced and shown to be unconditionally stable in the context of thermo-elasticity. Armero and Simo (1993) show that these properties extend to thermo-plasticity. The strongly coupled schemes are unconditionally stable because no critical time step leads to numerical instabilities in

the results. Despite this, the inner loop of the scheme may converge slowly or not at all Matthies and Steindorf (2003b). It depends on the spectral radius of the matrices involved (Cervera et al., 1996). There are, however, acceleration techniques that can mitigate this problem, including predictors and Aitken Δ^2 methods (see Section **??**). Danowski (2014) presents a numerical example concerning an internal pressurized thick-walled cylinder, whose material is viscoplastic, for which the strongly coupled scheme employed diverged, despite the use of an Aitken method. On the other hand, the monolithic scheme, as long as appropriately preconditioned, is unconditionally stable (Danowski, 2014).

Accuracy Regarding accuracy, the solution found from the loosely coupled method will never exactly satisfy the fully coupled discretized equations of the problem. There will be a time lag between the thermal and the mechanical field. Loosely-coupled methods, therefore, satisfy conservation only in an asymptotic sense, i.e., for vanishing mesh width (Michler, 2005). As long as it does not diverge, the monolithic and strongly coupled satisfy the coupled discretized equations exactly.

Ease of implementation The partitioned schemes are much easier to implement as most of them can work with the field analyzers as black boxes, concerning themselves only with communication between the solvers, initial guesses, and acceleration schemes using previously computed values. The monolithic scheme requires the computation of the full stiffness matrix, including the mixed terms and appropriate preconditioning that varies widely with the specific multi-physics problem to be solved.

Memory requirements When it comes to memory requirements, the partitioned schemes often require only the diagonal blocks of the stiffness matrix found in the linearization process. Previous values also need to be saved from one iteration to the next, increasing the memory cost for some acceleration techniques. In contrast, the fully coupled monolithic scheme requires the full stiffness matrix of the coupled problem.

CPU time According to Michler (2005), solving a fluid-structure interaction problem with the same accuracy using a loosely and strongly coupled scheme, the latter is more efficient than the former. For the same total number of iterations, the difference in the accuracy reached ranges from one to three orders of magnitude. These results run counter to a claim in Felippa et al. (2001). However, this is not supported by any numerical results from the last authors. In the numerical examples presented in Danowski (2014), the monolithic solver is in most cases faster than a strongly coupled scheme employing an Aitken method for problems in thermomechanics. The differences range from 120% to 140% in favor of the monolithic scheme. Supporting evidence for these conclusions can also be found in Novascone et al. (2015). The authors report CPU time ratios between the strongly coupled and monolithic approaches, ranging from 0.635 to 3.75 on the magnitude of the coupling.

Software modularity The partitioned approaches can take full advantage of software, including closed source commercial solvers. There is little to no software reuse for the monolithic approach, save for routines that solve linear systems and the like.

Conclusions Lastly, it may be helpful to reproduce the recommendations given in Felippa et al. (2001) regarding the choice between partitioned and monolithic approaches. According to the authors, the circumstances that favor the partitioned approach for tackling a coupled problem are a research environment with few delivery constraints, access to existing software, localized interaction effects (e.g., surface versus volume), and widespread spatial/temporal component characteristics. The opposite circumstances: commercial environment, rigid deliverable timetable, massive software development resources, global interaction effects, and comparable length/time scales favors a monolithic approach.

Putting it all together, the most appropriate choice for the present use case is the strongly coupled schemes with appropriate acceleration techniques. They can take advantage of already existing software, provide accurate results that agree with a monolithic approach, are not memory intensive, are easy to implement, and with the use of convergence acceleration techniques, are competitive from the computational efficiency standpoint. The only drawback seems to be the possibility of divergence in the inner loop, stalling the progress of the simulation.

Table 5.1: Summary of the comparison between the FFT-Galerkin method.

	Partitioned schemes		Monolithic
	Loosely coupled	Strongly coupled	
Stability	Isothermic split: conditionally stable Adiabatic split: unconditionally stable	unconditionally stable*	unconditionally stable
Accuracy	Coupled discretized equations not satisfied exactly	Coupled discretized equations satisfied	Coupled discretized equations satisfied
Ease of implementation	Only communication between field analyzers stricly needed		Full coupling needed: • Computation of mixed terms of the Jacobian • Preconditioning needed
Memory requirements	Only diagonal blocks of the full stiffness matrix needed		Full stiffness matrix needed
Software modularity constraints	Full software modularity		Poor or no software modularity

* The inner loop of the strongly coupled scheme may converge very slowly or even diverge.

Chapter 6

Validation results for the thermaal solver

This chapter provides validation results for the thermal solver implemented in this work. The appropriate examples are sourced from DIN EN 1991-1-2/NA:2010-12: Anhang CC - Prüfung und Validierung von Rechenprogramm für Brandschutznachweise mittels allgemeiner Rechenverfahren and the linear thermo-elastic test in the standard NAFEMS benchmarks . They include thermal effects such as variable conductivity, heat convection and radiation at the boundary. The numerical solutions are obtained using the thermal solver in LINKS, employing TRI3, TRI6, QUAD4, QUAD8 elements, in two-dimensions, and TETRA4 and TETRA10 elements in three-dimensions. No convergence study was performed, however the mesh size was chosen small enough so that assuming convergence of the FEM solution is reasonable. Moreover the good agreement with reference solutions supports this assumption.

6.1 Validation example 1 - DIN EN 1991-1-2/NA:2010-12: Anhang CC - Prüfung und Validierung von Rechenprogramm für Brandschutznachweise mittels allgemeiner Rechenverfahren - Beispiel 1)

6.1.1 Description

The geometry examined is a square plate with side length equal to 1 m, as shown in Figure 6.1. The boundary conditions considered are as follows: the left, upper and right edges are assumed to be adiabatic. At the lower edge there is heat transfer by convection with a heat convection coefficient h equation to $1\,\mathrm{Wm^{-2}K^{-1}}$ and an environment temperature equal to 0 °C (see Equation **??**). The initial temperature for the entire plate is 1000 °C. Reference values for the temperature at the middle of the upper edge are supplied to determine performance. The relevant properties of the material making up the plate are its conductivity k, equal to $1\,\mathrm{Wm^{-1}K^{-1}}$, its specific heat c_p, equal to $1\,\mathrm{Jkg^{-1}K^{-1}}$, and its density ρ, set equal to $1000\,\mathrm{kgm^{-3}}$. Table 6.1 summarizes all the information regarding initial and boundary conditions, geometry

and material properties.

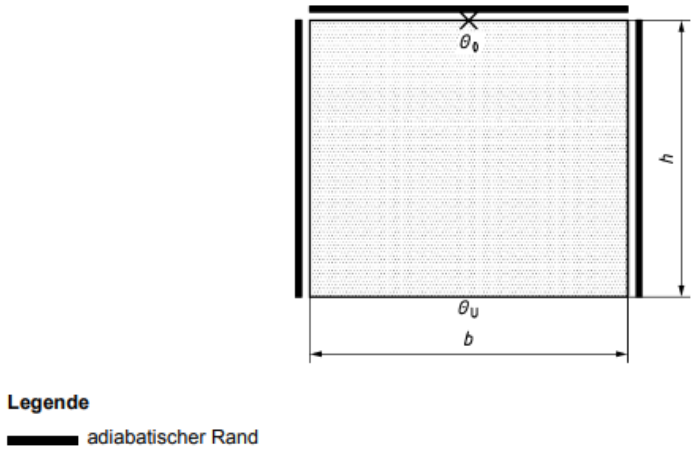

Figure 6.1: Geometry and boundary conditions considered in the validation example 1.

Table 6.1: Material properties, and initial and boundary conditions for validation example 1.

Material Properties		Effective value
Conductivity k	($\mathrm{Wm^{-1}K^{-1}}$)	1
Specific heat c_p	($\mathrm{Jkg^{-1}K^{-1}}$)	1
Density ρ	($\mathrm{kg/m^3}$)	1000
Boundary Conditions		
Dimensions h, b	(m)	1
Heat convection coefficient h	($\mathrm{W/m^2/K}$)	1
Initial Conditions		
Ambient temperature T_{env}	(°C)	0
Temperature in cross-section	(°C)	1000
Reference value		
Temperature T_0 in point X	(°C)	

6.1.2 Results

The numerical solutions obtained using FEM are presented in Table 6.2, as well as, the reference values and the corresponding relative difference. Figure 6.2 presents the same results in graphical form. It can seen that that agreement between the numerical results and the reference solutions is very good, with relative error always smaller than 0.02%. recomends a relative difference ±1% and an absolute difference ±5 °C. Figure 6.3 shows different time instants of the numerical solution using TRI3 elements. The evolution of the temperature field depicted seems reasonable given the description of the problem.

Table 6.2: Reference and computed values for T_0 concerning the validation example 1.

Time (s)	Reference value T_0 (°C)	Element Type	Computed value T_0' (°C)	Relative difference ε (%)
0	1000.0	TRI3	1000.0000	0.00
		TRI6	1000.0000	0.00
		QUAD4	1000.0000	0.00
		QUAD8	1000.0000	0.00
60	999.3	TRI3	999.3436	4.36×10^{-3}
		TRI6	999.2821	1.79×10^{-3}
		QUAD4	999.3434	4.34×10^{-3}
		QUAD8	999.2821	1.79×10^{-3}
300	891.8	TRI3	891.9305	1.46×10^{-2}
		TRI6	891.7957	4.82×10^{-4}
		QUAD4	891.9308	1.47×10^{-2}
		QUAD8	891.7957	4.82×10^{-4}
600	717.7	TRI3	717.7402	5.60×10^{-3}
		TRI6	717.6768	3.23×10^{-3}
		QUAD4	717.7403	5.62×10^{-3}
		QUAD8	717.6768	3.23×10^{-3}
900	574.9	TRI3	574.9004	6.96×10^{-5}
		TRI6	574.8708	5.08×10^{-3}
		QUAD4	574.9005	8.70×10^{-5}
		QUAD8	574.8708	5.08×10^{-3}
1200	460.4	TRI3	460.4098	2.13×10^{-3}
		TRI6	460.4019	4.13×10^{-4}
		QUAD4	460.4098	2.13×10^{-3}
		QUAD8	460.4019	4.13×10^{-4}
1500	368.7	TRI3	368.7175	4.75×10^{-3}
		TRI6	368.7238	6.46×10^{-3}
		QUAD4	368.7175	4.75×10^{-3}
		QUAD8	368.7238	6.46×10^{-3}
1800	295.3	TRI3	295.2860	4.74×10^{-3}
		TRI6	295.3011	3.73×10^{-4}
		QUAD4	295.2860	4.74×10^{-3}
		QUAD8	295.3011	3.73×10^{-4}

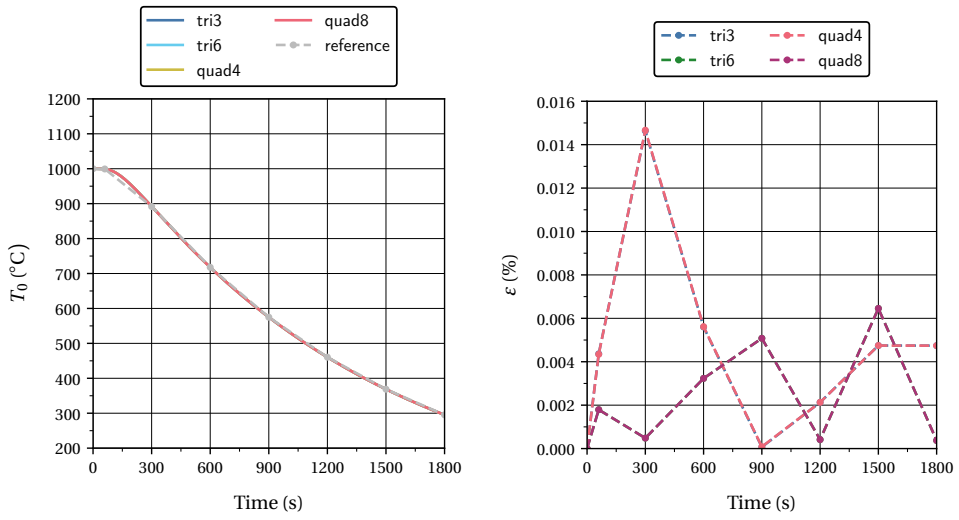

Figure 6.2: Numerical results for the validation example 1. (a) Temperature values at X as a function of time. (b) Relative error in percentage as function of time.

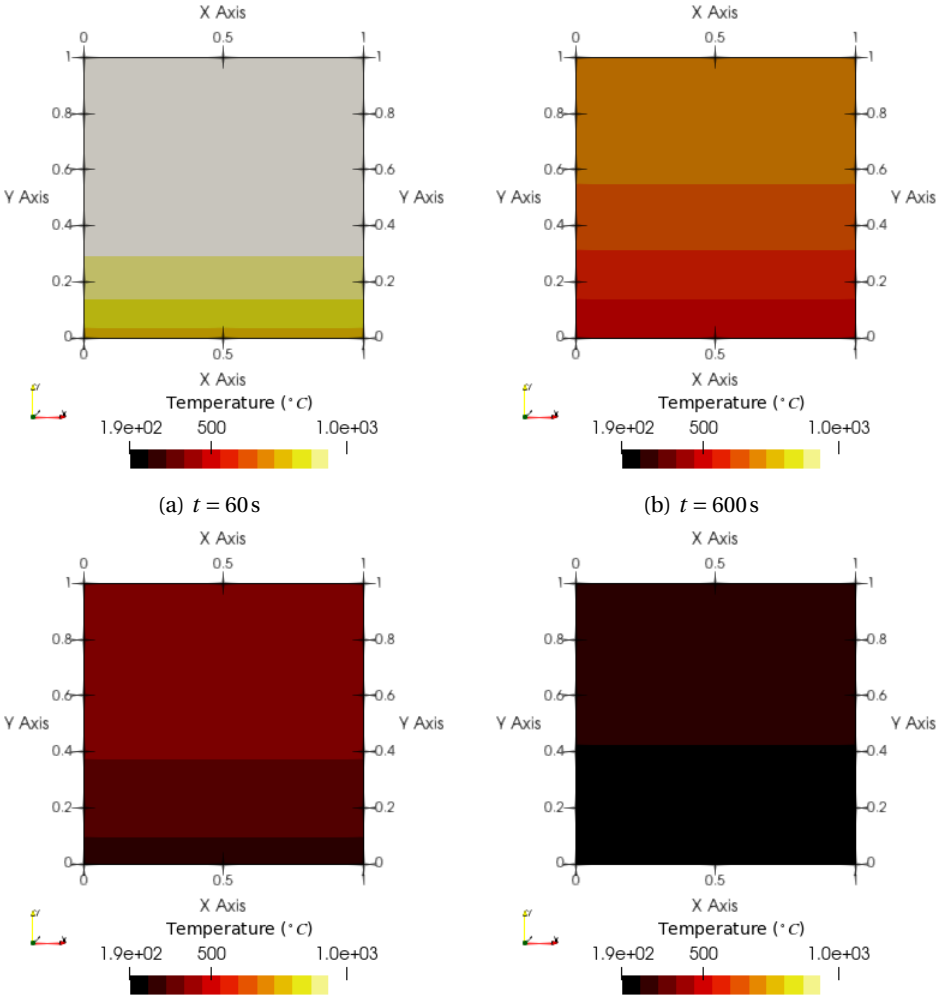

(a) $t = 60\,\mathrm{s}$ (b) $t = 600\,\mathrm{s}$

(c) $t = 1200\,\mathrm{s}$ (d) $t = 1800\,\mathrm{s}$

Figure 6.3: Numerical results for the validation example 1 using a TRI3 mesh.

6.2 Validation example 2 - DIN EN 1991-1-2/NA:2010-12: Anhang CC - Prüfung und Validierung von Rechenprogramm für Brandschutznachweise mittels allgemeiner Rechenverfahren - Beispiel 2)

6.2.1 Description

The geometry examined is a square plate with side length equal to 0.2 m, as shown in Figure 6.4. There is heat transfer by convection along all the edges with a heat convection coefficient h equation to $10\,\mathrm{Wm^{-2}K^{-1}}$ and an environment temperature equal to 1000 °C (see Equation **??**). Thre is also heat transfer through radition, with the emissivity $\varepsilon_{\mathrm{res}}$ equal to 0.8. The initial temperature for the entire plate is 0 °C. Reference values for the temperature in the middle of the plate are supplied to determine performance. The relevant properties of the material making up the plate are its conductivity k, which follows a linear behavior (see Table **??**), its specific heat c_p, equal to $1000\,\mathrm{Jkg^{-1}K^{-1}}$, and its density ρ, set equal to $2400\,\mathrm{kgm^{-3}}$. Table 6.3 summarizes all the information regarding initial and boundary conditions, geometry and material properties.

6.2.2 Results

The numerical solutions obtained using FEM are presented in Table 6.4, as well as, the reference values and the corresponding relative difference. Figure 6.5 presents the same results in graphical form. recomends for $t \leq 60\,\mathrm{min}$ an absolute difference smaller than ±5 °C, and for $t > 60\,\mathrm{min}$, a relative difference smaller than ±2%. It can be seen that that agreement between the numerical results and the reference solutions is acceptable. For $t \leq 60\,\mathrm{min}$ the linear elements do not satisfy the recomendation set forth by . Otherwise the requirements are completly fullfiled. Figure 6.6 shows different time instants of the numerical solution using TRI3 elements. The evolution of the temperature field depicted seems reasonable given the description of the problem.

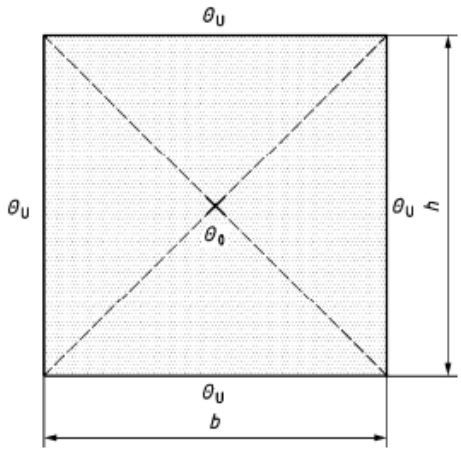

Figure 6.4: Geometry and boundary conditions considered in the validation example 2.

Table 6.3: Material properties, and initial and boundary conditions for validation example 2.

Material Properties		Effective value	
		T	$\lambda(T)$
Conductivity k (Linear behavior)	($\mathrm{W\,m^{-1}\,K^{-1}}$)	0	1.5
		200	0.7
		1000	0.5
Specific heat c_p	($\mathrm{J\,kg^{-1}\,K^{-1}}$)	1000	
Density ρ	($\mathrm{kg/m^3}$)	2400	
Boundary Conditions			
Dimensions h, b	(m)	0.2	
Heat convection coefficient h	($\mathrm{W/m^2/K}$)	10	
Emissivity $\varepsilon_{\mathrm{res}}$		0.8	
Initial Conditions			
Ambient temperature T_{env}	(°C)	1000	
Temperature in cross-section	(°C)	0	
Reference value			
Temperature T_0 in point X	(°C)		

Table 6.4: Reference and computed values for T_0 concerning the validation example 2.

Time (min)	Reference value T_0 (°C)	Element Type	Computed value T_0' (°C)	Relative difference ε (%)
0	0.0	TRI3	0.0000	0.00
		TRI6	0.0000	0.00
		QUAD4	0.0000	0.00
		QUAD8	0.0000	0.00
30	36.9	TRI3	29.7312	1.94×10^{1}
		TRI6	33.5906	8.97
		QUAD4	30.4248	1.75×10^{1}
		QUAD8	33.8503	8.26
60	137.4	TRI3	130.0251	5.37
		TRI6	133.7875	2.63
		QUAD4	131.0145	4.65
		QUAD8	133.8905	2.55
90	244.6	TRI3	240.0627	1.85
		TRI6	242.8709	7.07×10^{-1}
		QUAD4	240.4040	1.72
		QUAD8	242.9500	6.75×10^{-1}
120	361.1	TRI3	362.2362	3.15×10^{-1}
		TRI6	363.4852	6.61×10^{-1}
		QUAD4	361.9427	2.33×10^{-1}
		QUAD8	363.5435	6.77×10^{-1}
150	466.2	TRI3	470.0065	8.16×10^{-1}
		TRI6	470.2503	8.69×10^{-1}
		QUAD4	469.3439	6.74×10^{-1}
		QUAD8	470.2947	8.78×10^{-1}
180	554.8	TRI3	560.5277	1.03
		TRI6	560.1557	9.65×10^{-1}
		QUAD4	559.6558	8.75×10^{-1}
		QUAD8	560.1907	9.72×10^{-1}

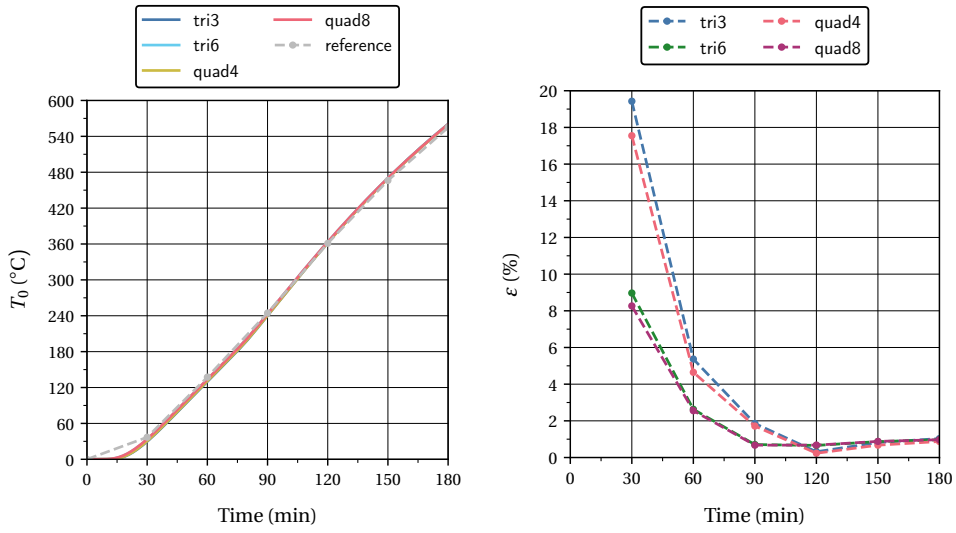

(a) (b)

Figure 6.5: Numerical results for the validation example 2. (a) Temperature values at X as a function of time. (b) Relative error in percentage as function of time.

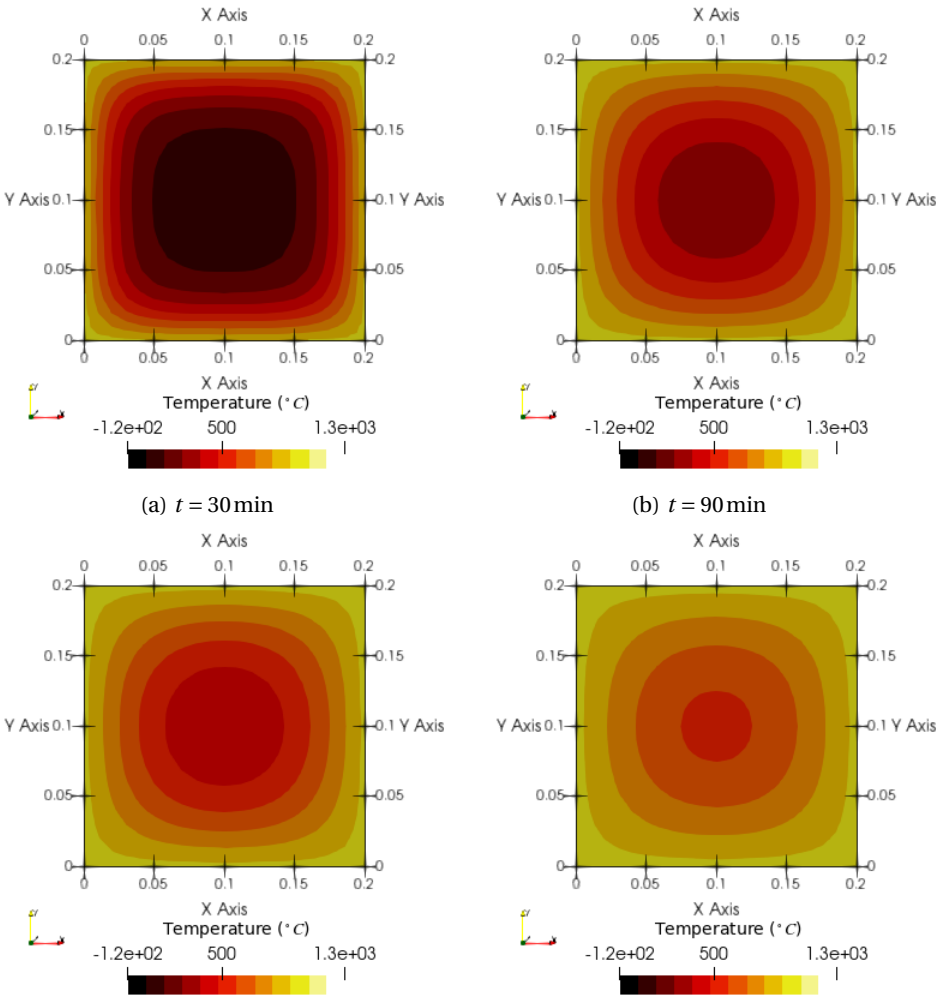

(a) $t = 30\,\text{min}$ (b) $t = 90\,\text{min}$

(c) $t = 120\,\text{min}$ (d) $t = 180\,\text{min}$

Figure 6.6: Numerical results for the validation example 2 using a TRI3 mesh.

6.3 Validation example 3 - The Standard NAFEMS Benchmarks: linear thermo-elastic tests - Two dimensional heat transfer with convection

6.3.1 Description

The geometry examined is a rectangular plate with width equal to 0.6 m and length equal to 1 m, as shown in Figure 6.7. A corresponding three-dimensional geometry is also considered with a thickness equal to 1 m. The boundary conditions considered are as follows: the left edge is assumed to be adiabatic. At the lower edge the temperature is prescribed to be 100 °C and along the upper and right edges there is heat transfer by convection and radiation. The heat convection coefficient h is equal to 70 $Wm^{-2}K^{-1}$, and the ambient temperature is equal to 0 °C (see Equation **??**). The initial temperature for the entire plate is 0 °C. The relevant properties of the material making up the plate are its conductivity k, equal to 52 $Wm^{-1}K^{-1}$, its specific heat c_p, equal to 1 $Jkg^{-1}K^{-1}$, and its density ρ, set equal to 1 kgm^{-3}. Table 6.5 summarizes all the information regarding initial and boundary conditions, geometry and material properties. The expected temperature at E (see Figure 6.7) is 18.3 °C.

6.3.2 Results

The numerical solutions obtained using FEM are presented in Table 6.6 for two dimensions and in Table **??** for three-dimensions, as well as, the reference values and the corresponding relative difference. It can be seen that that agreement between the numerical results and the reference solutions is acceptable. It is below 1% for all elements employed, except for the TETRA4 element. There is no significant difference between the two integrators tested. Figure 6.8 shows the temperature distribution obtained using TRI3 and TETRA10 elements, which is reasonable given the description of the problem.

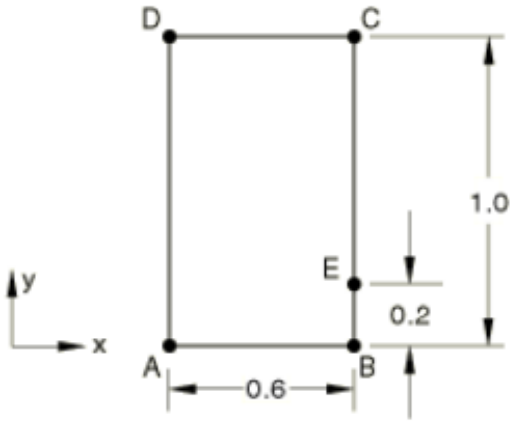

Figure 6.7: Geometry and boundary conditions considered in the validation example 3.

Table 6.5: Material properties, and initial and boundary conditions for validation example 3.

Material Properties		Effective value
Conductivity k	($\mathrm{Wm^{-1}K^{-1}}$)	52
Specific heat c_p	($\mathrm{Jkg^{-1}K^{-1}}$)	1
Density ρ	($\mathrm{kg/m^3}$)	1
Boundary Conditions		
Dimension h	(m)	1
Dimension b	(m)	0.6
Thickness t	(m)	1
Heat convection coefficient h	($\mathrm{W/m^2/K}$)	70
Initial Conditions		
Ambient temperature T_{env}	(°C)	100
Temperature in cross-section	(°C)	0
Reference value		
Temperature T_0 at point E	(°C)	

Table 6.6: Reference and computed values for T_0 concerning the validation example 3 in two-dimensions.

Element	Temperature T_0 at E °C	Relative difference ε (%)
Alpha integrator ($\rho = 1$)		
TRI3	18.1890	6.07×10^{-1}
TRI6	18.2553	2.44×10^{-1}
QUAD4	18.2286	3.90×10^{-1}
QUAD8	18.2532	2.56×10^{-1}
Quasi static integrator		
TRI3	18.1895	6.04×10^{-1}
TRI6	18.2548	2.47×10^{-1}
QUAD4	18.2281	3.93×10^{-1}
QUAD8	18.2536	2.54×10^{-1}

Table 6.7: Reference and computed values for T_0 concerning the validation example 3 in three-dimensions.

Element	Temperature T_0 at E °C	Relative difference ε (%)
Alpha integrator ($\rho = 1$)		
TETRA4	17.9501	1.91
TETRA10	18.2556	2.43×10^{-1}
Quasi static integrator		
TETRA4	17.9497	1.91
TETRA10	18.2548	2.47×10^{-1}

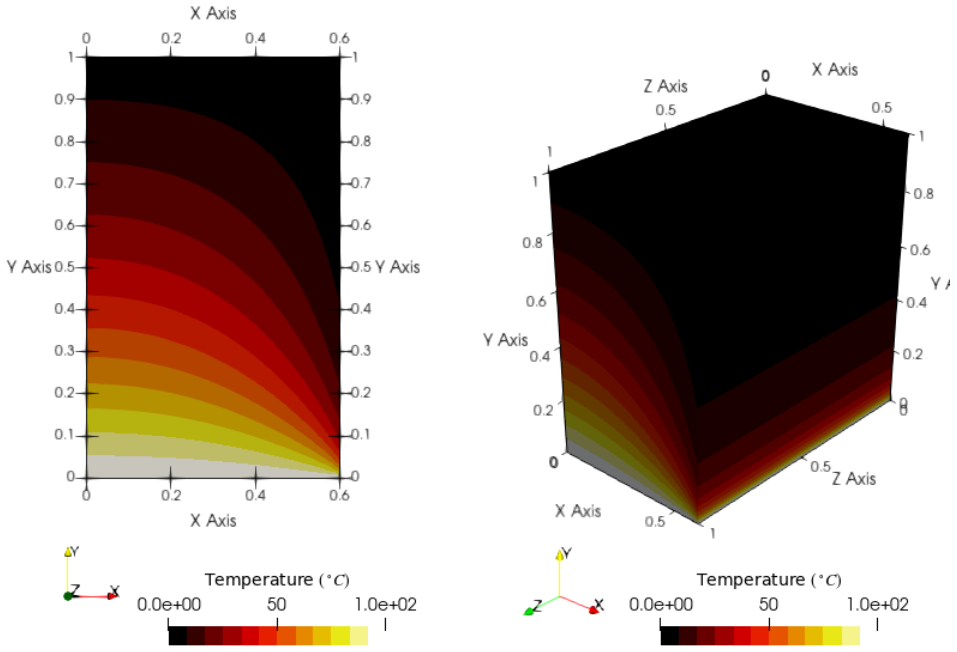

(a) (b)

Figure 6.8

Equations to be solved

$$\mathbf{M}\mathbf{u}_{n+1} + \mathbf{f}_u^{\text{int}}\left(\boldsymbol{\theta}_{n+1}, \mathbf{u}_{n+1}\right) - \mathbf{f}_{u,n+1}^{\text{ext}} = \mathbf{0}$$
$$\mathbf{C}\dot{\boldsymbol{\theta}}_{n+1} + \mathbf{f}_\theta^{\text{int}}\left(\boldsymbol{\theta}_{n+1}, \mathbf{u}_{n+1}\right) - \mathbf{f}_{\theta,n+1}^{\text{ext}} = \mathbf{0}$$

The approach chosen is the strongly coupled approach. To ease the discussion consider

$$\mathscr{R}_u(\boldsymbol{\theta}, \mathbf{u}) = \mathbf{0}, \mathscr{R}_\theta(\boldsymbol{\theta}, \mathbf{u}) = \mathbf{0}.$$

Fixed-point approaches

Consider that the $\boldsymbol{\theta}_n$ and $\mathbf{u}_n$ are both known and that $\boldsymbol{\theta}_{n+1}$ and $\mathbf{u}_{n+1}$ are now to be determined. A superscript k is introduced to denote the iterations concerning the loop of the implicit scheme. To prevent cluttering, the subscripts concerning the timestep are dropped.

There are two basic Schwarz procedures commonly employed in strongly coupled solution procedures. Both originate from domain decomposition.

They are the additive and the parallel Scharwz procedures.

Block Jacobi or Schwarz additive

If both systems of equations (**??**) are solved in parallel the procedure is said to be Schwarz additive or block Jacobi, refering to the similarities with the procedure for the solution of linear systems of equations with the same name i.e.,

$$\text{Solve } \mathscr{R}_u(\boldsymbol{\theta}^k, \mathbf{u}^{k+1}) = \mathbf{0} \text{ for } \mathbf{u}^{k+1} \text{Solve } \mathscr{R}_\theta(\boldsymbol{\theta}^{k+1}, \mathbf{u}^k) = \mathbf{0} \text{ for } \boldsymbol{\theta}^{k+1}$$

which can also be written as

$$\mathbf{u}^{k+1} = \mathscr{U}(\boldsymbol{\theta}^k), \boldsymbol{\theta}^{k+1} = \mathscr{T}(\mathbf{u}^k).$$

Box **??** shows the pseudo-code for the block Jacobi approach.

Block Gauss-Seidel or Schwarz multiplicative

If the systems are solved sequentially, where the output of the first system is used as input when solving the second system, the solution procedure is said to be Scharwz multiplicative or block Gauss-Seidel.

One of the fields must chosen as the first and this may be important (Joosten et al. (2009)).

$$\text{Solve } \mathscr{R}_u(\boldsymbol{\theta}^k, \mathbf{u}^{k+1}) = \mathbf{0} \text{ for } \mathbf{u}^{k+1} \text{Solve } \mathscr{R}_\theta(\boldsymbol{\theta}^{k+1}, \mathbf{u}^{k+1}) = \mathbf{0} \text{ for } \boldsymbol{\theta}^{k+1}$$

or

$$\mathbf{u}^{k+1} = \mathscr{U}(\boldsymbol{\theta}^k), \boldsymbol{\theta}^{k+1} = \mathscr{T}(\mathbf{u}^{k+1}).$$

Box **??** shows the pseudo-code for the block Gauss-Seidel approach.

As from a computational standpoint the block Jacobi and Gauss-Seidel approaches are very similar, the latter is used as the basis for the exposition that follows. Their similarity comes from the fact that the block Jacobi method can be regard as the computation of two simultaneous decoupled block Gauss-Seidel iterations.

Convergence criteria

For an iterative method to be useful, there must be reasonable criteria to determine its convergence.

With this in view, each full iteration of the strongly coupled scheme is written in a fixed-point notation as

$$\tilde{\boldsymbol{\theta}}^{k+1} = \mathscr{T}\left(\mathscr{U}(\boldsymbol{\theta}^k)\right),$$

where $\tilde{\bullet}$ denotes a solution coming directly from the solver, whereas the same symbol without the tilde represents the quantity after post-processing.

The sequence of system solvers can also be inverted, i.e.,

$$\tilde{\mathbf{u}}^{k+1} = \mathscr{U}\left(\mathscr{T}(\mathbf{u}^k)\right).$$

The iteration residual is defined as

$$\mathbf{r}^{k+1} = \mathscr{T}\left(\mathscr{U}(\boldsymbol{\theta}^k)\right) - \boldsymbol{\theta}^k = \tilde{\boldsymbol{\theta}}^{k+1} - \boldsymbol{\theta}^k.$$

It is equal to zero when the fixed-point $\boldsymbol{\theta}$ is reached, i.e.,

$$\mathbf{r} = \mathscr{T}\left(\mathscr{U}(\boldsymbol{\theta})\right) - \boldsymbol{\theta} = \mathbf{0},$$

and hence, a reasonable convergence measure for the fixed-point iteration.

The discrete L^2-norm can be used to obtain a scalar representative of the vectorial residual $r = \left(r^1, \ldots, r^m\right)^T$ as

$$\left\|\mathbf{r}^{k+1}\right\|_{L^2} = \sqrt{\sum_i \left(r^{k+1,i}\right)^2} = \sqrt{\sum_i \left(\tilde{\theta}^{k+1,i} - \theta^{k,i}\right)^2}$$

Directly using (**??**) yields an absolute convergence criterion

$$\left\|\boldsymbol{r}^{k+1}\right\|_{L^2} < \epsilon_{\text{abs}}$$

with $\epsilon_{\text{abs}} > 0$ as absolute convergence limit and convergence being obtained when the above condition renders valid. However, since the absolute value of r can change by orders of magnitude during one simulation, an absolute measure is not appropriate in all situations. A relative measure solves this problem by setting the residual in relation with the current coupling iterate values as

$$\frac{\left\|\mathbf{r}^{k+1}\right\|_{L^2}}{\left\|\tilde{\boldsymbol{\theta}}^{k+1}\right\|_{L^2}} < \epsilon_{\text{rel}}.$$

Since a relative convergence measure can fail to work properly when the coupling iterate values are close to zero and rounding errors come into play, a combination of absolute and relative measure, where the absolute measure takes care of close to zero cases and the relative handles all other cases, is often a good choice.

Acceleration techniques

Newton-Raphson schemes

Newton-Raphson schemes, in the following denoted as Newton schemes, can be applied to the partitioned coupled fields either by considering the chained overall fixed-point notation (Equation (**??**)) or by writing up a blocked system consisting of coupled structural and fluid fixed-point iterations.

To apply a Newton scheme to the overall chained fixed-point iteration (Equation (**??**)), the residual operator from (Equation (**??**)) is defined as

$$\mathscr{R} \equiv \mathscr{U} \circ \mathscr{T} - \boldsymbol{I},$$

where $\boldsymbol{I}$ is the identity matrix of suitable size.

The Newton scheme tries to find the root $\boldsymbol{\theta}$ such that $\mathscr{R}(\boldsymbol{\theta}) = 0$, assuming a linear behavior of $\mathscr{R}$ described by its Jacobi matrix $J_{\mathscr{R}}(\boldsymbol{\theta})$.

An iterative scheme, consisting of repeatedly solving

$$J_{\mathscr{R}}\left(\boldsymbol{\theta}^k\right)\Delta\boldsymbol{\theta}^k = -\mathscr{R}\left(\boldsymbol{\theta}^k\right)$$

for $\Delta\boldsymbol{\theta}^k$ and updating the iterate

$$\boldsymbol{\theta}^{k+1} = \boldsymbol{\theta}^k + \Delta\boldsymbol{\theta}^k$$

is performed. In case of writing up a separate fixed-point iteration for the different fields, a thermal residual operator $\mathscr{R}_u(\mathbf{u},\boldsymbol{\theta})$ and, in addition, a mechanical residual operator $\mathscr{R}_u(\mathbf{u},\boldsymbol{\theta})$ are obtained

$$\mathscr{R}_u(\mathbf{u},\boldsymbol{\theta}) = \mathbf{u} - \mathscr{U}(\boldsymbol{\theta}) = 0 \mathscr{R}_\theta(\mathbf{u},\boldsymbol{\theta}) = \boldsymbol{\theta} - \mathscr{T}(\mathbf{u}) = 0$$

From this, a block Newton iteration can be written as

$$\begin{bmatrix} J_{\mathscr{R}_u}\left(\mathbf{u}^k\right) & J_{\mathscr{R}_u}\left(\boldsymbol{\theta}^k\right) \\ J_{\mathscr{R}_\theta}\left(\mathbf{u}^k\right) & J_{\mathscr{R}_\theta}\left(\boldsymbol{\theta}^k\right) \end{bmatrix} \begin{Bmatrix} \Delta \boldsymbol{f}k \\ \Delta \boldsymbol{s}k \end{Bmatrix} = - \begin{Bmatrix} \mathscr{R}_u\left(\mathbf{u}^k,\boldsymbol{\theta}^k\right) \\ \mathscr{R}_\theta\left(\mathbf{u}^k,\boldsymbol{\theta}^k\right) \end{Bmatrix}$$

and the update of the iteration variables reads

$$\begin{Bmatrix} \mathbf{u}^{k+1} \\ \boldsymbol{\theta}^{k+1} \end{Bmatrix} = \begin{Bmatrix} \mathbf{u}^k \\ \boldsymbol{\theta}^k \end{Bmatrix} + \begin{Bmatrix} \Delta\mathbf{u}^k \\ \Delta\boldsymbol{\theta}^k \end{Bmatrix}$$

Every iteration of the Newton scheme involves at least one invocation of the thermal and mechanical solvers when computing $\mathscr{R}\left(\mathbf{u}^k\right)$ or both $\mathscr{R}_u\left(\mathbf{u}^k,\boldsymbol{\theta}^k\right)$ and $\mathscr{R}_\theta\left(\mathbf{u}^k,\boldsymbol{\theta}^k\right)$.

While in (**??**) the flow and structure solvers have to be executed sequentially, (**??**) allows for interfield-parallelism, i.e., the solvers can be executed at the same time.

The critical point for black box equation coupling is how to obtain the derivative information in the Jacobi matrices in (**??**) or (**??**). In the following, methods are presented which find approximations for the required Jacobian times vector products in different ways.

Single residual

GMRES-inspired approach

In **?**, a Krylov-subspace method is proposed in the context of FSI. In the present work, it approximates the solution $\Delta\boldsymbol{\theta}^k$ of system (**??**), which results in a Newton-Krylov solver for the partitioned thermo-mechanical system. This particular nomenclature is however debatable. **?** argues that the correct this approach should be instead name a "Krylov-based vector extrapolation" method.

A review of Newton-Krylov methods in general is given in [93].

For the GMRES-inspired approach, the Krylov-based subspace of order m is written as

$$\mathscr{K}_m := \operatorname{span}\left\{\boldsymbol{\theta}_i^* - \boldsymbol{\theta}^k\right\}_{i=1}^m = \operatorname{span}\left\{\Delta\boldsymbol{\theta}_i^*\right\}_{i=1}^m$$

where $\Delta\boldsymbol{\theta}_i^* := \boldsymbol{\theta}_i^* - \boldsymbol{\theta}^k$ and the $\boldsymbol{\theta}_i^*$ are generated during the Krylov iterations as $\boldsymbol{\theta}_{i+1}^* = \mathscr{T} \circ \mathscr{U}\left(\boldsymbol{\theta}_i^*\right)$. $\boldsymbol{\theta}^k$ is associated to the outer Newton iteration and fixed during the Krylov iterations.

Residual for the m^{th} Krylov iteration can be written as

$$J_{\mathscr{R}}(\boldsymbol{\theta}^k)\Delta\boldsymbol{\theta}_m^* - \mathscr{R}(\boldsymbol{\theta}^k).$$

It is desirable that the L_2-norm of this residual be as small as possible. Approximating $\Delta\boldsymbol{\theta}_i^*$ using $\mathscr{K}_m$, as $\sum_{i=1}^m \alpha_i \Delta\boldsymbol{\theta}_i^*$, the coefficients α_i are thus found as

$$\tilde{\boldsymbol{\alpha}} = \arg\min_{\boldsymbol{\alpha}} \left\| J_{\mathscr{R}}(\boldsymbol{\theta}^k) \sum_{i=1}^{m} \alpha_i \Delta\boldsymbol{\theta}^i - \mathscr{R}(\boldsymbol{\theta}^k) \right\|.$$

Since the Jacobian matrix $J_{\mathscr{R}}$ is assumed not to be accessible, a finite-difference approach

$$J_{\mathscr{R}}\left(\boldsymbol{\theta}^k\right)\Delta\boldsymbol{\theta}_i^* \approx \mathscr{R}\left(\boldsymbol{\theta}_i^*\right) - \mathscr{R}\left(\boldsymbol{\theta}^k\right)$$

is employed.

Using the notation

$$\mathbf{r}_i^* = \mathscr{R}(\boldsymbol{\theta}_i^*), \quad \mathbf{r}^k \equiv \mathscr{R}(\boldsymbol{\theta}^k), \quad \Delta\mathbf{r}_i^* \equiv \mathbf{r}_i^* - \mathbf{r}^k,$$

Equation (**??**) can be rewritten in a more compact form as

$$\tilde{\boldsymbol{\alpha}} = \arg\min_{\boldsymbol{\alpha}} \left\| \mathbf{r}^k + \sum_{i=1}^{m} \alpha_i \Delta\mathbf{r}_i^* \right\|,$$

with the α_i determined in a least-squares sense. The quality of the approximation is determined from the norm of the residual

$$\xi = \left\| \boldsymbol{r}^k + \sum_{i=1}^{m} \tilde{\alpha}_i \Delta\boldsymbol{r}_i^* \right\|$$

Orthogonalizing a new Krylov-vector $\Delta\boldsymbol{\theta}_m^*$ with respect to all previous ones using the Arnoldi process, as shown in Box **??**, completes the connection to the generalized minimal residual method (GMRES). Furthermore, to stabilize the solver subiterations when setting up the Krylov-subspace approximation, constant underrelaxation by ω can be employed as

$$\Delta\boldsymbol{\theta}_m^* = \omega\Delta\boldsymbol{\theta}_m^*.$$

Box **??** puts all parts of the GMRES-inpired method for one coupling timestep in proper order. The Krylov-vectors can be reused between different coupling iterations k or even between different timesteps n.

Quasi-Newton Method

An interface quasi-Newton method based on (2.151) and (2.152) is presented in [43]. The method is called interface quasi Newton with approximation of the inverse of the interface Jacobian matrix by least squares (IQN-ILS). Its origin, the IBQN-LS method presented in [172], is derived from the block Newton method (2.154) and uses two reduced order models for fluid and structure to approximate their interface Jacobians directly.

In contrast, the IQN-ILS method provides one reduced order model for the inverse of the overall interface Jacobian matrix of the Newton system (2.151) applied to the right-hand side vector.

The following elaborations are based on the description of the method in **?** and adapted to the thermo-mechanical problem.

The input and output deltas are used to construct a reduced order model. In the interface residual formulation (Equation (**??**)) of the chained solvers, the input is given by the structural coupling values $\boldsymbol{\theta}$ and the output by the interface residual $\boldsymbol{r}$. Input and output deltas are defined by

$$\Delta \boldsymbol{r}_k = \boldsymbol{r}_{k+1} - \boldsymbol{r}_k \Delta \tilde{\boldsymbol{\theta}}_k = \tilde{\boldsymbol{\theta}}_{k+1} - \tilde{\boldsymbol{\theta}}_k$$

i.e., not the actual input deltas $\Delta\boldsymbol{\theta}$ are gathered, but the intermediate chained solver outputs $\tilde{\boldsymbol{\theta}}$ are used to construct the $\Delta\tilde{\boldsymbol{\theta}}$. This enables to approximate the inverse of the Jacobian applied to the right-hand side vector of the Newton system, as we will see later.

The deltas are collected in matrices

$$\boldsymbol{V}_k = \left(\Delta \boldsymbol{r}_k, \Delta \boldsymbol{r}_{k-1}, \ldots, \Delta \boldsymbol{r}_1, \boldsymbol{V}^{n-1}, \ldots, \boldsymbol{V}^{n-l}\right)$$
$$\boldsymbol{W}k = \left(\Delta \tilde{\boldsymbol{s}}k, \Delta \tilde{\boldsymbol{s}}k-1, \ldots, \Delta \tilde{\boldsymbol{s}}1, \boldsymbol{W}^{n-1}, \ldots, \boldsymbol{W}^{n-l}\right)$$

with inversed ordering of the columns compared to the original IBQN-LS method. The matrices $\boldsymbol{V}^{n-1}, \ldots, \boldsymbol{V}^{n-l}$ and $\boldsymbol{W}^{n-1}, \ldots, \boldsymbol{W}^{n-l}$ represent the (optional) reuse of columns

Partitioned residual

Block Quasi-Newton Method

Linear reduced order models for the fluid solver and the structure solver are used in [172] to speed up the convergence of the FSI coupling iterations. As important feature, the reduced order models are set up from solver input and output deltas (or sensitivities) during the coupling iterations. The resulting method for two black box solvers is called interface block quasi-Newton method with least-squares approximation (IBQN-LS) in [42].

It application to a thermo-mechanical solver is detailed in what follows based on the version of the method for FSI presented in **?**.

In this method, the block Newton system (Equation (**??**)) is approximated by

$$\begin{bmatrix} \widehat{\boldsymbol{U}'} & -\boldsymbol{I} \\ -\boldsymbol{I} & \widehat{\boldsymbol{T}'} \end{bmatrix} \begin{Bmatrix} \Delta\hat{\mathbf{u}}_k \\ \Delta\hat{\boldsymbol{\theta}}_k \end{Bmatrix} = \begin{Bmatrix} \mathscr{R}_u(\mathbf{u}_k, \boldsymbol{\theta}_k) \\ \mathscr{R}_\theta(\mathbf{u}_k, \boldsymbol{\theta}_k) \end{Bmatrix}$$

where $\widehat{\boldsymbol{U}'}$ and $\widehat{\boldsymbol{T}}'$ are linear reduced order models for the Jacobians of the mechanical and thermal solvers.

Solving Equation (**??**), $\Delta\hat{\mathbf{u}}$ and $\Delta\hat{\boldsymbol{\theta}}$ are found to be

$$\left(\boldsymbol{I} - \widehat{\boldsymbol{T}}'\widehat{\boldsymbol{U}}'\right)\Delta\hat{\mathbf{u}}_k = -\mathscr{R}_\theta\left(\mathbf{u}_k, \boldsymbol{\theta}_k\right) - \widehat{\boldsymbol{T}}'\mathscr{R}_u\left(\mathbf{u}_k, \boldsymbol{\theta}_k\right) \quad \left(\boldsymbol{I} - \widehat{\boldsymbol{U}}'\widehat{\boldsymbol{T}}'\right)\Delta\hat{\boldsymbol{\theta}}_k = -\mathscr{R}_u\left(\mathbf{u}_k, \boldsymbol{\theta}_k\right) - \widehat{\boldsymbol{U}}'\mathscr{R}_\theta\left(\mathbf{u}_k, \boldsymbol{\theta}_k\right)$$

Since neither $\hat{\mathbf{U}}'$ nor $\hat{\mathbf{T}}'$ are known they must be approximated. A Gauss-Seidel like scheme will be employed, in the sense that the equations are solved one after the other with the most up to date values for $\mathbf{u}$ and $\boldsymbol{\theta}$ being used for the approximations. Thus

assuming that $\mathbf{u}_k$ and $\boldsymbol{\theta}_k$ are known, they are used to compute the approximations $\hat{\mathbf{U}}_k$ and $\hat{\mathbf{T}}_k$ and $\mathbf{u}_{k+1}$ is found from

$$\left(\boldsymbol{I} - \widehat{\boldsymbol{T}}'_k \widehat{\boldsymbol{U}}'_k\right) \Delta\hat{\mathbf{u}}_k = -\mathscr{R}_\theta\left(\mathbf{u}_k, \boldsymbol{\theta}_k\right) - \widehat{\boldsymbol{T}}'_k \mathscr{R}_u\left(\mathbf{u}_k, \boldsymbol{\theta}_k\right) \mathbf{u}_{k+1} = \mathbf{u}_k + \Delta\hat{\mathbf{u}}_k$$

Now, $\mathbf{u}_{k+1}$ can be used to improve the approximation of $\hat{\mathbf{U}}$, denoted $\hat{\mathbf{U}}_{k+1}$. Thus, $\boldsymbol{\theta}_{k+1}$ can now be found from

$$\left(\boldsymbol{I} - \widehat{\boldsymbol{U}}'_{k+1} \widehat{\boldsymbol{T}}'_k\right) \Delta\hat{\boldsymbol{\theta}} = -\mathscr{R}_u\left(\mathbf{u}_k, \boldsymbol{\theta}_k\right) - \widehat{\boldsymbol{U}}'_{k+1} \mathscr{R}_\theta\left(\mathbf{u}_k, \boldsymbol{\theta}_k\right)$$

and the approximation to the thermal Jacobian updated to $\hat{\mathbf{T}}_{k+1}$.

It finally remains to precise how are $\hat{\mathbf{U}}$ and $\hat{\mathbf{T}}$ approximated. To achieve this consider the intermediate values for $\mathbf{u}$ and $\boldsymbol{\theta}$ computed as

$$\begin{aligned} \tilde{\mathbf{u}}_i &= \mathscr{U}(\boldsymbol{\theta}_i) \\ \tilde{\boldsymbol{\theta}}_i &= \mathscr{T}(\mathbf{u}_i) \end{aligned} \quad \text{for } i = 1, \ldots, k,$$

Firstly, to approximate $\hat{\mathbf{U}}$, consider the matrices defined as

$$\mathbf{V}_U \equiv \{\Delta\boldsymbol{\theta}_1, \Delta\boldsymbol{\theta}_2, \ldots, \Delta\boldsymbol{\theta}_k\}, \mathbf{W}_U \equiv \{\Delta\tilde{\mathbf{u}}_1, \Delta\tilde{\mathbf{u}}_2, \ldots, \Delta\tilde{\mathbf{u}}_k\}$$

where the deltas $\Delta\boldsymbol{\theta}_i = \boldsymbol{\theta}_{i+1} - \boldsymbol{\theta}_i$ and $\Delta\tilde{\mathbf{u}}_i = \tilde{\mathbf{u}}_{i+1} - \tilde{\mathbf{u}}_i$ are collected into columns.

A new temperature input delta $\Delta\boldsymbol{\theta}$ can be approximated by a linear combination of the columns of $\mathbf{V}_U$ as

$$\mathbf{V}_U \mathbf{c}_U \approx \Delta\boldsymbol{\theta}$$

and a corresponding output delta $\Delta\mathbf{u}$ can then be constructed by using the computed coefficients $\mathbf{c}_U$to linearly combine the columns of $\mathbf{W}_U$ as

$$\Delta\mathbf{u} = \mathbf{W}_U \mathbf{c}_U$$

The $\mathbf{c}_F$ are determined from a minimization

$$\mathbf{c}_U = \arg\min_{\tilde{\mathbf{c}}} \|\Delta\boldsymbol{\theta} - \mathbf{V}_U \tilde{\mathbf{c}}\|$$

which is a least-squares problem, solved in **?** by the normal equations and in using the economy-size QR-decomposition. The action of $\hat{\mathbf{U}}'$ on a vector can then be written as

$$\hat{\mathbf{U}}' \Delta\boldsymbol{\theta} = \mathbf{W}_U \mathbf{c}_U$$

Following **?**, the solution for the least-squares problem is

$$\mathbf{c}_U = (\mathbf{V}_U^T \mathbf{V}_U)^{-1} \mathbf{V}_U \Delta\boldsymbol{\theta}$$

Thus, $\hat{\mathbf{U}}'$ is found to be

$$\hat{\mathbf{U}}' = \mathbf{W}_U (\mathbf{V}_U^T \mathbf{V}_U)^{-1} \mathbf{V}_U$$

The process to set up the reduced order model for the Jacobian of the thermal solver $\hat{\mathbf{T}}$ is analogous to that described for the mechanical solver. Input deltas $\Delta\mathbf{u}_k \equiv \mathbf{u}_{k+1} - \mathbf{u}_k$ and output deltas $\Delta\tilde{\boldsymbol{\theta}} \equiv \tilde{\boldsymbol{\theta}}_{k+1} - \tilde{\boldsymbol{\theta}}_k$ are collected in matrices $\mathbf{V}_T$ and $\mathbf{W}_T$. After solving a

corresponding least-squares problem to find the optimal coefficients $\mathbf{c}_T$, the action of $\hat{\mathbf{T}}'$ on a vector is written as

$$\hat{\mathbf{S}}\Delta\mathbf{u} = \mathbf{W}_T\mathbf{c}_T$$

Box **??** shows this method for one timestep. Initially, a prediction $\boldsymbol{\theta}_p$ is computed by extrapolation from old timesteps and two block Gauss-Seidel iterations are performed using constant underrelaxation. Then, the initial reduced order models for mechanical and thermal systems are set up and the main coupling iteration loop with computation steps as described above starts.

Quasi-Newton methods

- Vierendeels et al. (2007) - Degroote et al. (2008) - Haelterman et al. (2009) - Erbst and Düster (2012) - Gatzhammer (2014) - Erbts et al. (2015) - Wendt et al. (2015)

Newton-Krylov methods

- Michler et al. (2005) - Küttler and Wall (2009) - Gatzhammer (2014) - König et al. (2016) - Scheufele (2018)

GMRES

Applying the GMRES to the thermo-mechanical problem, the Krylov-subspace of order m is written as

$$\mathcal{K}_m := \text{span}\left\{\boldsymbol{s}_i - \boldsymbol{s}_k\right\}_{i=1}^{m} = \text{span}\left\{\Delta\boldsymbol{s}_i\right\}_{i=1}^{m},$$

—

1. $n = 0$ 2. Solve for

Andersen Acceleration

- Uekermann (2016)

Generalized Broyden

- Uekermann (2016)

Filtering

Multi-Scale

Mechanical prediction

- Erbts and Düster (2012) - Erbts et al. (2015) - Wendt et al. (2015)

A very efficient way to increase the chances of stability and reduce computation time is to predict the optimal initial values at the beginning of every time step. This actually means that we take the results of the mechanical field of the converged solution at the end of the last two or more time increments and predict the new solution by polynomial extrapolation. The predicted values can then be used as an improved initial configuration for the electrical and thermal field. This method is based on polynomial vector extrapolation which is quite easy to implement, and the extra computational input involved is negligible.

Here, the maximum polynomial under consideration is of the order two, i.e., we extrapolate the new solution from the results from the last three time steps. Assuming our time increment will be constant over the whole simulation, the mechanical predictors $\mathbf{U}^*$ *for the order $p = 1$ and $p = 2$ read:*

$$p = 1 : \mathbf{U}^*_{n+1} = 2\mathbf{U}_n - \mathbf{U}_{n-1}$$
$$p = 2 : \mathbf{U}^*_{n+1} = 3\mathbf{U}_n - 3\mathbf{U}_{n-1} + \mathbf{U}_{n-2}$$

The subscript n denotes the time step. Where the time increment is adaptive, we refer to [22], since the predictor has to be constructed in an adaptive manner as well.

Acceleration/Stabilization techniques

Constant Underrelaxation
- Gatzhammer (2014)

$$\boldsymbol{s}_{k+1} = (1-\omega)\boldsymbol{s}_k + \omega\tilde{\boldsymbol{s}}_{k+1} = \boldsymbol{s}_k + \omega\boldsymbol{r}_{k+1}$$

Numerical relaxation - Aitken Δ^2-method
- Küttler and Wall (2008) - Irons and Tuck (1969) - Joosten et al. (2009) - Küttler and Wall (2009) - Erbts et al. (2015) - Wendt et al. (2015)

To improve the coupling algorithm, we apply Aitken's Δ^2-method to accelerate the convergence of series.

Aitken's delta-squared process is a method of acceleration of convergence, and a particular case of a nonlinear sequence transformation.

In the one-dimensional case, this method resembles the secant method, which can be used to solve nonlinear equations without differentiation.

$\{x_n\}\, n \in \mathbb{N}$ *will converge linearly to ℓ if there exists a number $\mu \in (0,1)$ such that*

$$\lim n \to \infty \frac{\left|x_{n+1} - \ell\right|}{\left|x_n - \ell\right|} = \mu.$$

The formula for the one-dimensional case is

$$AX_n = \frac{x_n x_{n+2} - x_{n+1}^2}{x_n - 2x_{n+1} + x_{n+2}}$$

or

$$AX_n = x_{n+2} - \frac{x_{n+2} - x_{n+1}}{x_n + x_{n+2} - 2x_{n+1}}(x_{n+1} - x_{n+2})$$

Aitken's method will accelerate the sequence x_n if $\lim_{n\to\infty} \frac{(Ax)_n - \ell}{x_n - \ell} = 0$. A is not a linear operator, but a constant term drops out, viz: $A[x-\ell] = Ax - \ell$, if ℓ is a constant. This is clear from the expression of Ax in terms of the finite difference operator Δ. Although the new process does not in general converge quadratically, it can be shown that for a fixed point process, that is, for an iterated function sequence $x_{n+1} = f\left(x_n\right)$ for some function f, converging to a fixed point, the convergence is quadratic. In this case, the technique is known as Steffensen's method.

Empirically, the A-operation eliminates the "most important error term". One can check this by considering a sequence of the form $x_n = \ell + a^n + b^n$, where $0 < b < a < 1$: The sequence Ax will then go to the limit like b^n goes to zero.

Geometrically, the graph of an exponential function $f(t)$ that satisfies $f(n) = x_n, f(n+1) = x_{n+1}$ and $f(n+2) = x_{n+2}$ has an horizontal asymptote at $\frac{x_n x_{n+2} - x_{n+1}^2}{x_n - 2x_{n+1} + x_{n+2}}$ (if $x_n - 2x_{n+1} + x_{n+2} \neq 0$).

If you want to fit $ae^{bx} + c$ to 3 points, $\left(x_i, y_i\right) * i = 1^3$, you want $y * i = ae^{bx_i} + c$. Subtracting the first two, $y_2 - y_1 = a\left(e^{bx_2} - e^{bx_1}\right) = ae^{bx_1}\left(e^{b(x_2-x_1)} - 1\right)$ and, similarly, $y_3 - y_2 = a\left(e^{bx_3} - e^{bx_2}\right) = ae^{bx_2}\left(e^{b(x_3-x_2)} - 1\right)$. If $x_3 - x_2 = x_2 - x_1 = d$, so the data are equally spaced and $e^{b(x_2-x_1)} - 1 = e^{b(x_3-x_2)} - 1$, we can divide these to get $\frac{y_3-y_2}{y_2-y_1} = e^{bx_2-bx_1} = e^{b(x_2-x_1)} = e^{bd}$ Taking logs, and letting $r = \frac{y_3-y_2}{y_2-y_1}$, $\ln(r) = bd$ so $b = \frac{\ln(r)}{d}$. From this, $e^b = r^{1/d}$. Note that this requires that $r > 0$, so the points are monotonic. Then

$$\begin{aligned} y_2 - y_1 &= a\left(e^{bx_2} - e^{bx_1}\right) \\ &= a\left(r^{x_2/d} - r^{x_1/d}\right) \end{aligned}$$

so that

$$a = \frac{y_2 - y_1}{r^{x_2/d} - r^{x_1/d}}$$

We also get

$$a = \frac{y_3 - y_2}{r^{x_3/d} - r^{x_2/d}} = \frac{y_3 - y_1}{r^{x_3/d} - r^{x_1/d}}$$

Finally, $c = y_i - ae^{bx_i}$ for any i.

![Untitled](https://s3-us-west-2.amazonaws.com/secure.notion-static.com/def2fba4-2bd4-4a98-8216-4d44881db9ff/Untitled.png)

One can also show that if x goes to its limit ℓ at a rate strictly greater than 1, Ax does not have a better rate of convergence. (In practice, one rarely has e.g. quadratic convergence which would mean over 30 resp. 100 correct decimal places after 5 resp. 7 iterations (starting with 1 correct digit); usually no acceleration is needed in that case.)

Thus, after rearranging,

$$c = \frac{ab^* - a^* b}{\left(a - a^+\right) - \left(b - b^+\right)}$$

This can be rewritten as

$$c = \left(1 - \beta_b\right) b^* + \beta_b b \quad \text{with } \beta_b = \frac{b^* - a^+}{\left(a - a^+\right) - \left(b - b^+\right)}$$

The difference $b^* - a^*$ is computationally inconvenient. Anticipating the next iteration step,

$$d = \left(1 - \beta_c\right) c^* + \beta_c c \quad \text{with } \beta_c = \frac{c^* - b^*}{\left(b - b^*\right) - (c - c^*)}$$

a convenient expression for updating the relaxation factor may be found, i.e.

$$\beta_c = \beta_b + \left(\beta_b - 1\right) \frac{c - c^*}{\left(b - b^+\right) - \left(c - c^+\right)}$$

This expression is used in step 4 of Box 2 .

In practice, Ax converges much faster to the limit than x does, as demonstrated by the example calculations below. Usually, it is much cheaper to calculate Ax (involving only calculation of differences, one multiplication and one division) than to calculate many more terms of the sequence x. Care must be taken, however, to avoid introducing errors due to insufficient precision when calculating the differences in the numerator and denominator of the expression.

We scrutinize the multi-dimensional case in [38], which forms the basis for the algorithm utilized in many problems, in particular in the field of strongly coupled FSI, see [44] for instance.

The objective is to improve the iteration process so that as few iterations as possible are required to attain a electro-thermo-mechanical problems converged solution.

We now introduce a general vector $\mathbf{D}$, which can either stand for the solution vector of the displacement or the temperature, respectively. The next step is to work out the solution to the current iteration from the outcome of the previous iteration $\mathbf{D}^{(k)}$ plus a new increment $\Delta\mathbf{D}^{(k)}$

$$\mathbf{D}^{(k+1)} = \mathbf{D}^{(k)} + \Delta\mathbf{D}^{(k)}$$

The increment reads

$$\Delta\mathbf{D}^{(k)} = \omega^{(k)}\left(\tilde{\mathbf{D}}^{(k+1)} - \mathbf{D}^{(k)}\right) = \omega^{(k)}\mathbf{R}^{(k)}$$

with $\omega^{(k)}$ being the relaxation coefficient. From now on, all unmodified values are written with a tilde, like $\tilde{\mathbf{D}}^{(k+1)}$ standing for the unmodified values of the displacement or temperature vector, respectively. The efficiency of this method is mainly due to the relaxation parameter ω. A constant parameter $0 < \omega < 2$ yields static relaxation (SR), whereas an adaptive parameter results in a dynamic relaxation (DR).

For the dynamic case, we follow [44] where the relaxation coefficient is updated in every iteration cycle as a function of two previous residuals:

$$\omega^{(k)} = -\omega^{(k-1)}\frac{\left(\mathbf{R}^{(k)} - \mathbf{R}^{(k-1)}\right)^{\mathrm{T}}\mathbf{R}^{(k-1)}}{\left(\mathbf{R}^{(k)} - \mathbf{R}^{(k-1)}\right)^{2}}$$

Dynamic relaxation is also easy to implement and the additional computational input is acceptable, since only inner vector products have to be performed. Several variations on this method can be found in the literature: A comprehensive study was presented in [47], for instance.

Vector Extrapolation

$$\hat{\boldsymbol{s}}_{k+m} = \boldsymbol{s}_{k+1} + \sum_{i=1}^{m-1}\omega_i\left(\boldsymbol{s}_{k+i+1} - \boldsymbol{s}_{k+i}\right) = \boldsymbol{s}_{k+1} + \sum_{i=1}^{m-1}\omega_i\Delta\boldsymbol{s}_{k+i+1}$$

$$\Delta\hat{\boldsymbol{s}}_{k+m} = \sum_{i=0}^{m-1}\gamma_i\Delta\boldsymbol{s}_{k+i+1}$$

$$\sum_{i=0}^{m-1}\gamma_i = 1$$

$$A\gamma = 0$$

factors γ_i. The difference between th f the system matrix $\boldsymbol{A}$. This is done

$$a_{ij} = \Delta s_{k+i}\cdot\Delta s_{k+j}$$

extrapolation (MPE) method, as

$$a_{ij} = \left(\Delta s_{k+i} - \Delta s_{k+i-1}\right)\cdot\Delta s_{k+j}$$

lation (RRE) method, and as

$$a_{ij} = \boldsymbol{y}^{i}\cdot\Delta\boldsymbol{s}_{k+j}$$

Steepest Descent Relaxation

Bibliography

Adam, L. and J.-P. Ponthot
2002a. Numerical simulation of viscoplastic and frictional heating during finite deformation of metal. Part I: Theory. *Journal of engineering mechanics*, 128(11):1215–1221. Publisher: American Society of Civil Engineers.

Adam, L. and J.-P. Ponthot
2002b. Numerical simulation of viscoplastic and frictional heating during finite deformation of metal. Part II: Applications. *Journal of engineering mechanics*, 128(11):1222–1232. Publisher: American Society of Civil Engineers.

Agelet de Saracibar, C.
1998. Numerical analysis of coupled thermomechanical frictional contact problems. Computational model and applications. *Archives of Computational Methods in Engineering*, 5(3):243–301.

Agelet de Saracibar, C., M. Cervera, and M. Chiumenti
1999. On the formulation of coupled thermoplastic problems with phase-change. *International Journal of Plasticity*, 15(1):1–34.

Argyris, J. H. and J. S. Doltsinis
1981. On the natural formulation and analysis of large deformation coupled thermomechanical problems. *Computer Methods in Applied Mechanics and Engineering*, 25(2):195–253.

Armero, F.
1999. Formulation and finite element implementation of a multiplicative model of coupled poro-plasticity at finite strains under fully saturated conditions. *Computer Methods in Applied Mechanics and Engineering*, 171:205–241.

Armero, F. and J. C. Simo
1992. A new unconditionally stable fractional step method for non-linear coupled thermomechanical problems. *International Journal for Numerical Methods in Engineering*, 35(4):737–766. _eprint: https://onlinelibrary.wiley.com/doi/pdf/10.1002/nme.1620350408.

Armero, F. and J. C. Simo
1993. A priori stability estimates and unconditionally stable product formula algorithms for nonlinear coupled thermoplasticity. *International Journal of Plasticity*, 9(6):749–782.

Badia, S., A. F. Martín, and R. Planas
2014. Block recursive LU preconditioners for the thermally coupled incompressible inductionless MHD problem. *Journal of Computational Physics*, 274:562–591.

Belytschko, T. and R. Mullen
1976. Mesh partitions of explicit-implicit time integration. *Formulations and computational algorithms in finite element analysis*, Pp. 673–690. Publisher: MIT Press: New York.

Belytschko, T. and R. Mullen
1978. Stability of explicit-implicit mesh partitions in time integration. *International Journal for Numerical Methods in Engineering*, 12(10):1575–1586. Publisher: Wiley Online Library.

Belytschko, T., H.-J. Yen, and R. Mullen
1979. Mixed methods for time integration. *Computer Methods in Applied Mechanics and Engineering*, 17:259–275. Publisher: Elsevier.

Blom, D.
2017. *Efficient numerical methods for partitioned fluid-structure interaction simulations*. Ph.D., Delft University of Technology, Netherlands.

Blom, F. J.
1998. A monolithical fluid-structure interaction algorithm applied to the piston problem. *Computer methods in applied mechanics and engineering*, 167(3-4):369–391. Publisher: Elsevier.

Borja, R., C. Tamagnini, and E. Alarćon
1998. Elastoplastic consolidation at finite strain part 2: finite element implementation and numerical examples. *Computer Methods in Applied Mechanics and Engineering*, 159:103–122.

Carter, J. P. and J. R. Booker
1989. Finite element analysis of coupled thermoelasticity. *Computers & Structures*, 31(1):73–80.

Causin, P., J.-F. Gerbeau, and F. Nobile
2005. Added-mass effect in the design of partitioned algorithms for fluid–structure problems. *Computer methods in applied mechanics and engineering*, 194(42-44):4506–4527. Publisher: Elsevier.

Cervera, M., R. Codina, and M. Galindo
1996. On the computational efficiency and implementation of block-iterative algorithms for nonlinear coupled problems. *Engineering Computations*, 13(6):4–30. Publisher: MCB UP Ltd.

Chen, K.
2005. *Matrix Preconditioning Techniques and Applications*, Cambridge Monographs on Applie. Cambridge University Press.

Combescure, A. and A. Gravouil
2002. A numerical scheme to couple subdomains with different time-steps for predominantly linear transient analysis. *Computer Methods in Applied Mechanics and Engineering*, 191(11):1129–1157.

Danowski, C.
2014. *Computational Modelling of Thermo-Structure Interaction with Application to Rocket Nozzles*. Ph.D., Technische Universität München, Germany.

Danowski, C., V. Gravemeier, L. Yoshihara, and W. A. Wall
2013. A monolithic computational approach to thermo-structure interaction. *International Journal for Numerical Methods in Engineering*, 95(13):1053–1078. _eprint: https://onlinelibrary.wiley.com/doi/pdf/10.1002/nme.4530.

Degroote, J., P. Bruggeman, R. Haelterman, and J. Vierendeels
2008. Stability of a coupling technique for partitioned solvers in FSI applications. *Computers & Structures*, 86(23):2224–2234.

Dettmer, W. and D. Perić
2006. A computational framework for fluid–structure interaction: Finite element formulation and applications. *Computer Methods in Applied Mechanics and Engineering*, 195(41):5754–5779.

Dittmann, M.
2017. *Isogeometric analysis and hierarchical refinement for multi-field contact problems*. Ph.D.

Dittmann, M., M. Franke, I. Temizer, and C. Hesch
2014. Isogeometric Analysis and thermomechanical Mortar contact problems. *Computer Methods in Applied Mechanics and Engineering*, 274:192–212.

Erbts, P. and A. Düster
2012. Accelerated staggered coupling schemes for problems of thermoelasticity at finite strains. *Computers & Mathematics with Applications*, 64(8):2408–2430.

Erbts, P., S. Hartmann, and A. Düster
2015. A partitioned solution approach for electro-thermo-mechanical problems. *Archive of Applied Mechanics*, 85(8):1075–1101.

Farhat, C., P. Geuzaine, and G. Brown
2003. Application of a three-field nonlinear fluid–structure formulation to the prediction of the aeroelastic parameters of an F-16 fighter. *Computers & Fluids*, 32:3–29.

Farhat, C. and M. Lesoinne
2000. Two efficient staggered algorithms for the serial and parallel solution of three-dimensional nonlinear transient aeroelastic problems. *Computer methods in applied mechanics and engineering*, 182(3-4):499–515. Publisher: Elsevier.

Farhat, C., M. Lesoinne, P. Stern, and S. Lanteri
1997. High performance solution of three-dimensional nonlinear aeroelastic problems via parallel partitioned algorithms: methodology and preliminary results. *Advances in Engineering Software*, 28:43–61.

Farhat, C., K. Park, and Y. Dubois-Pelerin
1991. An unconditionally stable staggered algorithm for transient finite element analysis of coupled thermoelastic problems. *Applied Mechanics and Engineering*, 85:349–365.

Farhat, C., A. Rallu, K. G. Wang, and T. Belytschko
2010. Robust and provably second-order explicit-explicit and implicit-explicit staggered time-integrators for highly non-linear compressible fluid-structure interaction problems. *International Journal for Numerical Methods in Engineering*, 84:73–107.

Farhat, C., K. Zee, and P. Geuzaine
2006. Provably second-order time-accurate loosely-coupled solution algorithms for transient nonlinear computational aeroelasticity. *Computer Methods in Applied Mechanics and Engineering*, 195:1973–2001.

Felder, S., N. Kopic-Osmanovic, H. Holthusen, T. Brepols, and S. Reese
2021. Thermo-mechanically coupled gradient-extended damage-plasticity modeling of metallic materials at finite strains. *International Journal of Plasticity*, P. 103142.

Felippa, C. and T. L. Geers
1988. Partitioned analysis for coupled mechanical systems. *Engineering Computations*, 5:123–133.

Felippa, C. A. and K. C. Park
1980. Staggered transient analysis procedures for coupled mechanical systems: Formulation. *Computer Methods in Applied Mechanics and Engineering*, 24(1):61–111.

Felippa, C. A., K. C. Park, and C. Farhat
2001. Partitioned analysis of coupled mechanical systems. *Computer Methods in Applied Mechanics and Engineering*, 190(24):3247–3270.

Fernández, M. A., J.-F. Gerbeau, and C. Grandmont
2006. A projection semi-implicit scheme for the coupling of an elasticstructure with an incompressible fluid. *International Journal for Numerical Methods in Engineering*.

Förster, C.
2007. Robust methods for fluid-structure interaction with stabilised finite elements.

Förster, C., W. A. Wall, and E. Ramm
2007. Artificial added mass instabilities in sequential staggered coupling of nonlinear structures and incompressible viscous flows. *Computer methods in applied mechanics and engineering*, 196(7):1278–1293. Publisher: Elsevier.

Gee, M. W., U. Küttler, and W. A. Wall
2011. Truly monolithic algebraic multigrid for fluid–structure interaction. *International Journal for Numerical Methods in Engineering*, 85(8):987–1016. _eprint: https://onlinelibrary.wiley.com/doi/pdf/10.1002/nme.3001.

Gillard, J.
2019. *An Efficient Partitioned Coupling Scheme for Tire Hydroplaning Analysis*. Ph.D., Technishcen Universität München, München.

Gitterle, M.
2012. *A dual mortar formulation for finite deformation frictional contact problems including wear and thermal coupling*. Ph.D., Technische Universität München.

Glaser, S.
1992. *Gekoppelte thermomechanische Berechnung duennwandiger Strukturen mit der Methode der Finiten Elemente*. Ph.D., Institute fuer Statik und Dynamik der Luft- und Raumfahrtkonstruktionen, University of Stuttgart.

Hansen, G.
2011. A Jacobian-free Newton Krylov method for mortar-discretized thermomechanical contact problems. *Journal of Computational Physics*, 230(17):6546–6562.

Hübner, B., E. Walhorn, and D. Dinkler
2004. A monolithic approach to fluid–structure interaction using space–time finite elements. *Computer Methods in Applied Mechanics and Engineering*, 193(23):2087–2104.

Hüeber, S. and B. I. Wohlmuth
2009. Thermo-mechanical contact problems on non-matching meshes. *Computer Methods in Applied Mechanics and Engineering*, 198(15):1338–1350.

Heil, M.
2004. An efficient solver for the fully coupled solution of large-displacement fluid–structure interaction problems. *Computer Methods in Applied Mechanics and Engineering*, 193(1):1–23.

Hesch, C. and P. Betsch
2011. Energy-momentum consistent algorithms for dynamic thermomechanical problems—Application to mortar domain decomposition problems. *International Journal for Numerical Methods in Engineering*, 86(11):1277–1302. _eprint: https://onlinelibrary.wiley.com/doi/pdf/10.1002/nme.3095.

Holt, M. and N. Yanenko
2012. *The Method of Fractional Steps: The Solution of Problems of Mathematical Physics in Several Variables*. Springer Berlin Heidelberg.

Holzapfel, G. A. and J. C. Simo
1996. Entropy elasticity of isotropic rubber-like solids at finite strains. *Computer Methods in Applied Mechanics and Engineering*, 132(1):17–44.

Hron, J. and S. Turek
2006. A Monolithic FEM/Multigrid Solver for an ALE Formulation of Fluid-Structure Interaction with Applications in Biomechanics. In *Fluid-Structure Interaction.*, Lecture Notes in Computational Science and Engineering, vol 53.

Hughes, T. J. and W. Liu
1978. Implicit-explicit finite elements in transient analysis: stability theory.

Ibrahimbegovic, A. and L. Chorfi
2002. Covariant principal axis formulation of associated coupled thermoplasticity at finite strains and its numerical implementation. *International Journal of Solids and Structures*, 39(2):499–528.

Irons, B. M. and R. C. Tuck
1969. A version of the Aitken accelerator for computer iteration. *International*

Journal for Numerical Methods in Engineering, 1(3):275–277. _eprint: https://onlinelibrary.wiley.com/doi/pdf/10.1002/nme.1620010306.

Jha, B. and R. Juanes
2007. A locally conservative finite element framework for the simulation of coupled flow and reservoir geomechanics. *Acta Geotechnica*, 2:139–153.

Johansson, L. and A. Klarbring
1993. Thermoelastic frictional contact problems: Modelling, finite element approximation and numerical realization. *Computer Methods in Applied Mechanics and Engineering*, 105(2):181–210.

Joosten, M. M., W. G. Dettmer, and D. Perić
2009. Analysis of the block Gauss–Seidel solution procedure for a strongly coupled model problem with reference to fluid–structure interaction. *International Journal for Numerical Methods in Engineering*, 78(7):757–778. _eprint: https://onlinelibrary.wiley.com/doi/pdf/10.1002/nme.2503.

Kim, J., H. Tchelepi, and R. Juanes
2011a. Stability and convergence of sequential methods for coupled flow and geomechanics: Drained and undrained splits. *Computer Methods in Applied Mechanics and Engineering*, 200:2094–2116.

Kim, J., H. Tchelepi, and R. Juanes
2011b. Stability and convergence of sequential methods for coupled flow and geomechanics: Fixed-stress and fixed-strain splits. *Computer Methods in Applied Mechanics and Engineering*, 200:1591–1606.

Klöppel, T., A. Popp, U. Küttler, and W. A. Wall
2011. Fluid–structure interaction for non-conforming interfaces based on a dual mortar formulation. *Computer Methods in Applied Mechanics and Engineering*, 200(45):3111–3126.

Küttler, U., M. Gee, C. Förster, A. Comerford, and W. A. Wall
2010. Coupling strategies for biomedical fluid–structure interaction problems. *International Journal for Numerical Methods in Biomedical Engineering*, 26(3-4):305–321. _eprint: https://onlinelibrary.wiley.com/doi/pdf/10.1002/cnm.1281.

Küttler, U. and W. A. Wall
2008. Fixed-point fluid–structure interaction solvers with dynamic relaxation. *Computational Mechanics*, 43(1):61–72.

Küttler, U. and W. A. Wall
2009. Vector Extrapolation for Strong Coupling Fluid-Structure Interaction Solvers. *Journal of Applied Mechanics*, 76(2).

Lenarda, P. and M. Paggi
2016. A geometrical multi-scale numerical method for coupled hygro-thermo-mechanical problems in photovoltaic laminates. *Computational Mechanics*, 57(6):947–963.

Lewis, R. and Y. Sukirman
1993. Finite element modelling of three-phase flow in deforming saturated

oil reservoirs. *International Journal for Numerical and Analytical Methods in Geomechanics*, 17(8):577–598. Publisher: Wiley Online Library.

Lin, P. T., J. N. Shadid, R. S. Tuminaro, M. Sala, G. L. Hennigan, and R. P. Pawlowski
2010. A parallel fully coupled algebraic multilevel preconditioner applied to multiphysics PDE applications: Drift-diffusion, flow/transport/reaction, resistive MHD. *International Journal for Numerical Methods in Fluids*, 64(10-12):1148–1179. tex.eprint: https://onlinelibrary.wiley.com/doi/pdf/10.1002/fld.2402.

Matthies, H. and J. Steindorf
2003a. Partitioned Strong Coupling Algorithms for Fluid-Structure-Interaction. *Computers & Structures*, 81:805–812.

Matthies, H. and J. Steindorf
2003b. Strong Coupling Methods.

Mayr, M., T. Klöppel, W. A. Wall, and M. W. Gee
2015. A Temporal Consistent Monolithic Approach to Fluid-Structure Interaction Enabling Single Field Predictors. *SIAM Journal on Scientific Computing*, 37(1):B30–B59. Publisher: Society for Industrial and Applied Mathematics.

Mayr, M., M. H. Noll, and M. W. Gee
2020. A hybrid interface preconditioner for monolithic fluid–structure interaction solvers. *Advanced Modeling and Simulation in Engineering Sciences*, 7(1):15.

Michler, C.
2005. *Efficient numerical methods for fluid-structure interaction*. Ph.D., Delft University of Technology, Netherlands. ISBN: 90-9019533-5.

Michler, C., E. H. v. Brummelen, S. J. Hulshoff, and R. d. Borst
2003. The relevance of conservation for stability and accuracy of numerical methods for fluid–structure interaction. *Computer Methods in Applied Mechanics and Engineering*, 192(37):4195–4215.

Michler, C., S. Hulshoff, E. Van Brummelen, and R. De Borst
2004. A monolithic approach to fluid–structure interaction. *Computers & fluids*, 33(5-6):839–848. Publisher: Elsevier.

Michler, C., E. H. van Brummelen, and R. de Borst
2005. An interface Newton–Krylov solver for fluid–structure interaction. *International Journal for Numerical Methods in Fluids*, 47(10-11):1189–1195. _eprint: https://onlinelibrary.wiley.com/doi/pdf/10.1002/fld.850.

Miehe, C.
1995a. Entropic thermoelasticity at finite strains. Aspects of the formulation and numerical implementation. *Computer Methods in Applied Mechanics and Engineering*, 120(3):243–269.

Miehe, C.
1995b. A theory of large-strain isotropic thermoplasticity based on metric transformation tensors. *Archive of Applied Mechanics*, 66(1):45–64.

Mikelić, A. and M. F. Wheeler
2013. Convergence of iterative coupling for coupled flow and geomechanics. *Computational Geosciences*, 17(3):455–461. Publisher: Springer.

Miller, B. A.
2015. *Loosely Coupled Time Integration of Fluid- Thermal-Structural Interactions in Hypersonic Flows*. Ph.D., Ohio State University.

Neishlos, H.
1983. Finite-Element Mesh Partitioning for Time Integration of Transient Problems. In *Numerical Solution of Partial Differential Equations: Theory, Tools and Case Studies: Summer Seminar Series Held at CSIR, Pretoria, February 8–10, 1982*, D. P. Laurie, ed., Pp. 225–245. Basel: Birkhäuser Basel.

Netz, T.
2013. *High-order space and time discretization scheme applied to problems of finite thermo-viscoelasticity*. Ph.D., Institute of Applied Mechanics, Clausthal University of Technology.

Novascone, S. R., B. W. Spencer, J. D. Hales, and R. L. Williamson
2015. Evaluation of coupling approaches for thermomechanical simulations. *Nuclear Engineering and Design*, 295:910–921.

Oancea, V. G. and T. A. Laursen
1997. A finite element formulation of thermomechanical rate-dependent frictional sliding. *International Journal for Numerical Methods in Engineering*, 40(23):4275–4311. _eprint: https://onlinelibrary.wiley.com/doi/pdf/10.1002/%28SICI%291097-0207%2819971215%2940%3A23%3C4275%3A%3AAID-NME257%3E3.0.CO%3B2-K.

Pantuso, D., K.-J. Bathe, and P. A. Bouzinov
2000. A finite element procedure for the analysis of thermo-mechanical solids in contact. *Computers & Structures*, 75(6):551–573.

Park, K.
1983. Stabilization of partitioned solution procedure for pore fluid-soil interaction analysis. *International Journal for Numerical Methods in Engineering*, 19:1669–1673.

Park, K., C. Felippa, and J. DeRuntz
1977. Stabilization of staggered solution procedures for fluid-structure interaction analysis. *Computational methods for fluid-structure interaction problems*, 26(94-124):51. Publisher: ASME New York.

Piperno, S.
1997. Explicit/implicit fluid/structure staggered procedures with a structural predictor and fluid subcycling for 2D inviscid aeroelastic simulations. *International Journal for Numerical Methods in Fluids*, 25:1207–1226.

Piperno, S. and C. Farhat
2001. Partitioned procedures for the transient solution of coupled aeroelastic problems–Part II: energy transfer analysis and three-dimensional applications. *Computer methods in applied mechanics and engineering*, 190(24-25):3147–3170. Publisher: Elsevier.

Piperno, S., C. Farhat, and B. Larrouturou
1995. Partitioned procedures for the transient solution of coupled aroelastic problems Part I: Model problem, theory and two-dimensional application. *Computer Methods in Applied Mechanics and Engineering*, 124:79–112.

Rothe, S., P. Erbts, A. Düster, and S. Hartmann
2015. Monolithic and partitioned coupling schemes for thermo-viscoplasticity. *Computer Methods in Applied Mechanics and Engineering*, 293:375–410.

Saetta, A. and R. Vitaliani
1992. Unconditionally convergent partitioned solution procedure for dynamic coupled mechanical systems. *International Journal for Numerical Methods in Engineering*, 33:1975–1996.

Seitz, A.
2019. *Computational Methods for Thermo-Elasto-Plastic Contact*. Ph.D., Technische Universität München, Germany.

Seitz, A., W. A. Wall, and A. Popp
2018. A computational approach for thermo-elasto-plastic frictional contact based on a monolithic formulation using non-smooth nonlinear complementarity functions. *Advanced Modeling and Simulation in Engineering Sciences*, 5(1):5.

Shadid, J., R. Pawlowski, J. Banks, L. Chacón, P. Lin, and R. Tuminaro
2010. Towards a scalable fully-implicit fully-coupled resistive MHD formulation with stabilized FE methods. *Journal of Computational Physics*, 229(20):7649–7671.

Simo, J. C. and F. Armero
1992. Recent Advances in the Numerical Analysis and Simulation of Thermoplasticity at Finite Strains.

Simo, J. C. and C. Miehe
1992. Associative coupled thermoplasticity at finite strains: Formulation, numerical analysis and implementation. *Computer Methods in Applied Mechanics and Engineering*, 98(1):41–104.

Smith, B., P. Bjorstad, and W. Gropp
2004. *Domain Decomposition: Parallel Multilevel Methods for Elliptic Partial Differential Equations*. Cambridge University Press.

Tezduyar, T. E., S. Sathe, R. Keedy, and K. Stein
2006. Space–time finite element techniques for computation of fluid–structure interactions. *Computer methods in applied mechanics and engineering*, 195(17-18):2002–2027. Publisher: Elsevier.

Torii, R., M. Oshima, T. Kobayashi, K. Takagi, and T. E. Tezduyar
2006. Computer modeling of cardiovascular fluid–structure interactions with the deforming-spatial-domain/stabilized space–time formulation. *Computer Methods in Applied Mechanics and Engineering*, 195(13-16):1885–1895. Publisher: Elsevier.

Verdugo, F. and W. A. Wall
2016. Unified computational framework for the efficient solution of n-field coupled problems with monolithic schemes. *Computer Methods in Applied Mechanics and Engineering*, 310:335–366.

Vierendeels, J., L. Lanoye, J. Degroote, and P. Verdonck
2007. Implicit coupling of partitioned fluid–structure interaction problems with reduced order models. *Computers & structures*, 85(11-14):970–976. Publisher: Elsevier.

Wall, W. A., S. Genkinger, and E. Ramm
2007. A strong coupling partitioned approach for fluid–structure interaction with free surfaces. *Computers & Fluids*, 36(1):169–183.

Wendt, G., P. Erbts, and A. Düster
2015. Partitioned coupling strategies for multi-physically coupled radiative heat transfer problems. *Journal of Computational Physics*, 300:327–351.

White, J. A. and R. Borja
2008. Stabilized low-order finite elements for coupled solid-deformation/fluid-diffusion and their application to fault zone transients. *Computer Methods in Applied Mechanics and Engineering*, 197:4353–4366.

Wriggers, P., C. Miehe, M. Kleiber, and J. C. Simo
1992. On the coupled thermomechanical treatment of necking problems via finite element methods. *International Journal for Numerical Methods in Engineering*, 33(4):869–883. _eprint: https://onlinelibrary.wiley.com/doi/pdf/10.1002/nme.1620330413.

Zavarise, G., P. Wriggers, E. Stein, and B. A. Schrefler
1992. Real contact mechanisms and finite element formulation—a coupled thermomechanical approach. *International Journal for Numerical Methods in Engineering*, 35(4):767–785. _eprint: https://onlinelibrary.wiley.com/doi/pdf/10.1002/nme.1620350409.

Zhang, Q. and T. Hisada
2004. Studies of the strong coupling and weak coupling methods in FSI analysis. *International Journal for Numerical Methods in Engineering*, 60(12):2013–2029. _eprint: https://onlinelibrary.wiley.com/doi/pdf/10.1002/nme.1034.

Zienkiewicz, O., D. K. Paul, and A. Chan
1988. Unconditionally stable staggered solution procedure for soil-pore fluid interaction problems. *International Journal for Numerical Methods in Engineering*, 26:1039–1055.